

Acta Technologica Agriculturae 3  
Nitra, Slovaca Universitas Agriculturae Nitriae, 2020, pp. 105–110

## EFFECTIVE PRE-TREATMENTS FOR ENHANCEMENT OF BIODEGRADATION OF AGRICULTURAL LIGNOCELLULOSIC WASTES IN ANAEROBIC DIGESTION – A REVIEW

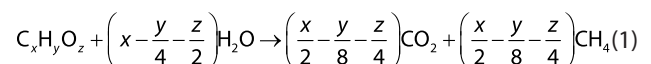
Fatemeh RAHIMI-AJDADI\*, Masoomeh ESMAILI

University of Guilan, Rasht, Iran

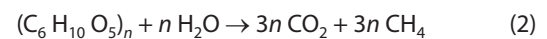
Agricultural crop residues like stems, straws and leaves are valuable resources for biofuel production, especially methane, due to anaerobic digestion. Biogas from agricultural lignocellulosic wastes is capable of attaining sustainable energy yields without environmental pollution. Farmers in many developing countries burn these wastes throughout their fields, imposing environmental hazard due to emission of greenhouse gases. The main problem in this field is the recalcitrance of the agricultural lignocellulose waste that limits its enzymatic degradation and hydrolysis efficiency and consequently decreases biogas production. Therefore, efficient pre-treatments prior to anaerobic digestion are essential. Various pre-treatment methods are used for increasing the anaerobic digestibility of lignocellulose biomass, such as physical (mechanical, thermal, etc.), chemical, biological and combined pre-treatments. This paper reviews different pre-treatments used in anaerobic digestion for the agricultural lignocellulosic wastes and explains the advantages and disadvantages of each. The most frequently used pre-treatments for main agricultural wastes in process of biogas production are also introduced.

**Keywords:** biogas; hydrolysis; lignin; methane

Currently, the most used energy supply in the world is fossil fuel that has some disadvantages, such as limited resources, growing price trends and environmental pollution. The issue of waste management is one of the main environmental challenges (Hlinka et al., 2019). Consequently, global attention is concentrated on finding the alternative energy resources, which would be both economically and environmentally acceptable (Zilouei and Taherdanak, 2015). Biofuels predominantly produced from biomass have the potential to be the reliable alternate energy resource that is considered the fourth largest energy resource in the world (Rajput and Visvanathan, 2018). Lignocellulosic biomass is more acceptable, because it has no nutritional value for humans. Biogas made of lignocellulosic biomass has many other advantages, such as low-cost feedstock and its abundance. In addition, it represents a way to manage the large amounts of agricultural and forest residues that are annually produced. In many developing countries, farmers burn these wastes in their fields, which results in environmental pollution due to emission of greenhouse gases. Biogas from lignocellulosic biomass is capable of attaining the sustainable energy yields without damaging the environment only when it is generated through anaerobic digestion and recovered properly (Chojnacka et al., 2015). Additionally, it is highly recommended to add crop residues to livestock excrement for purposes of digestion process (Kažimírová et al., 2018). The general equation for anaerobic digestion is given in Eq. 1:



Eq. 2 is specifically for cellulose (Rai, 1986)



The problem is that there is a main limitation in degradation phase of lignocellulosic biomass. Due to the recalcitrant nature of lignocellulosic biomass in terms of anaerobic digestion, it is essential to seek different types of pre-treatment methods for more efficient and economic anaerobic digestion. Pre-treatments can solve the issue of low digestibility of substrates and make them degrade more efficiently in biogas process. The relative amount of lignocellulosic compounds varies in different types of agricultural biomass. Consequently, the available substrates have different properties and usage of a specific pre-treatment is of extreme importance in order to increase digestibility and biogas production (Venturin et al., 2019). The purpose of this paper is to present the major types of pre-treatment for lignocellulosic wastes of agricultural crops.

### Mechanical pre-treatments

The most basic method for physical pre-treatment is mechanical pre-treatment. It reduces the biomass particle size and is always applied prior to other pre-treatment methods to enhance their effect. It includes milling; grinding; chipping; etc. Reduction of the lignocellulosic

biomass particle size increases the accessible surface area, reduces the degree of cellulose crystallinity, and decreases the degree of cellulose polymerization (Yuan et al., 2014). The main disadvantage of mechanical pre-treatment is that, if the biomass moisture content is high, the energy consumption necessary to exercise it, is also very high (Tu and Hallett, 2019). However, such pre-treatments are more advantageous specially than chemical pre-treatments, because they produce neither toxic or inhibitory materials nor complex molecules that are difficult to digest (Venturin et al., 2019). Extrusion is also one of the efficient mechanical pre-treatment methods for lignocellulosic materials that results in a lower bulk density, higher specific porosity, higher water-holding capacity and better biodegradability (Gu et al., 2015). Substrate can be placed under a pressure of up to 300 bars at temperatures from 60 to 300 °C, depending on the final consistency required (Montgomery and Bochmann, 2014). High shear force results in efficient mixing that can effectively enhance the anaerobic digestion efficiency (Gu et al., 2015), making this method more efficient than other physical pre-treatment methods. Panepinto and Genon (2016) showed that extruder utilization can lead to an improvement of up to 15% in biogas yield and also an improvement in terms of energy consumption of up to 6.5%. Menardo et al. (2015) reported that by means of extrusion, organic matter degradation was enhanced and methane production was significantly increased by as much as 16%. Hjorth et al. (2011) reported that the methane production increased significantly by 18–70% using extrusion as a pre-treatment for five types of agricultural wastes. However, several disadvantages of the extrusion lie in high energy consumption, high maintenance costs due to abrasion of screws and high sensitivity to stones (Montgomery and Bochmann, 2014).

Thermal pre-treatment uses thermal energy to increase the molecular agitation with the aim to promote the hydrolysis and, consequently, increases the methanogenic production in a shorter period of time. In terms of thermal pre-treatment, lignocellulosic biomass is subjected to heat ranging from 50 to 240 °C at a certain pressure. Thermal pre-treatment at temperatures of 160 °C and higher results in the solubilisation of hemicellulose and lignin (Xie et al., 2011). The disadvantage of higher temperatures (exceeding 160 °C) is that produced phenolic compounds have inhibitory or toxic effects on methanogenic bacteria (Xie et al., 2011). Thermal pre-treatments dependent on the type of heating method can be named as hydrothermal

pre-treatment and steam explosion. In this review, thermal pre-treatment methods are understood as physical pre-treatments, while hydrothermal and steam explosion are considered physiochemical pre-treatments. Ultrasonic pre-treatment increases the total hydrolysis yield of the lignocellulosic biomass through increasing the surface area and reducing the degree of polymerization. The effect of ultrasonics is based on monolithic cavitation beyond the human audio range. The breakdown of cavitation bubbles during the sonication changes the chemical structure by the creation of free radicals (Grönroos et al., 2004). However, the higher sonication power level has adverse effect on the pre-treatment process (Karuppiyah and Azariah, 2019). In their study on ultrasonic pre-treatment of rice hulls, Yu et al. (2009) obtained the net yields of total soluble sugar of 31.8% and glucose of 32.2% in contrast to control group values of 6.9% and 7.6%.

In recent years, microwave-assisted pre-treatment methods have been demonstrated as one of the most effective and promising methods for biomass conversion due to cleavage of β-1,4-glucan bonds, increasing the accessible surface area and reducing the crystallinity of cellulose (Chandra et al., 2012a). There are several disadvantages related to ultrasound and microwave methods, such as production of inhibiting by-products (Li et al., 2013); high energy consumption (Zeynali et al., 2017); and complex operation procedures. Table 1 shows the researches performed on several physical pre-treatments of main agricultural crops.

### Chemical pre-treatments

Chemical pre-treatment is the most utilized method for pre-treating of lignocellulosic substrates. The main function of the majority of chemical pre-treatments lies in the destruction of rigid or complex structures of lignocellulosic biomass (Venturin et al., 2019). In comparison to other pre-treatment methods, chemical pre-treatments are advantageous because of their easiness, fastness, and effectiveness. They mainly include dilute-acid; alkaline; ionic liquids; and ozone pre-treatments.

Strong concentrated acids can hydrolyse the hemicellulose and solubilize lignin; nevertheless, their use is limited because they produce undesirable by-products, such as furfural as well as its derivatives that inhibit the anaerobic digestion process (Mussoline et al., 2013). In addition, there are certain other disadvantages – chemicals used are extremely corrosive and high-cost materials are

**Table 1** Mechanical pre-treatments used for biogas production from certain agricultural substrates by means of anaerobic digestion

| Crop    | Category   | Pre-treatments                                 | Methane/biogas (mL·gVS <sup>-1</sup> ) | Increased (%) | References             |
|---------|------------|--|--|---------------|------------------------|
| Rice    | milling    | 5–10 mm; 6% NaOH; 20 °C; 21 day                | 520                                    | 44            | He et al., 2008        |
| Corn    | milling    | 5–10 mm; 2% NaOH; 10, 20 °C; 3 day; SLR* 1 : 9 | 207.9; 233.0                           | 56; 75        | Zheng et al., 2010     |
| Wheat   | thermal    | 40, 100, 160 °C; 30 min                        | 201; 199; 224                          | 0; 0; 10      | Sambusiti et al., 2013 |
| Sorghum | thermal    | 40; 100; 160 °C; 30 min                        | 242; 282; 273                          | 0; 5; 2       | Sambusiti et al., 2013 |
| Maize   | ultrasound | Machine J.P Selecta Ultrasons 110 W, 3 min     | 710                                    | 41            | Wang et al., 2011      |

\* – solid loading rate

necessary for building of the reactor when using this type of pre-treatment (Zheng et al., 2014). Simultaneously, dilute acids (4% w-w<sup>-1</sup>) are commonly used in applications and researches. The main mechanism of dilute acid pre-treatment lies in the solubilization of hemicellulose (Montgomery and Bochmann, 2014) by breaking ether bonds in lignin/phenolics-carbohydrates complexes without dissolving lignin, which helps to increase the biogas production. Frequently used acids for lignocellulosic biomass are H<sub>2</sub>SO<sub>4</sub>, HNO<sub>3</sub> and H<sub>3</sub>PO<sub>4</sub>. Antonopoulou and Lyberatos (2013) reported that the combination of acids with thermal pre-treatment caused an increase in soluble carbohydrate's concentration. Alkaline pre-treatment is one of the most commonly used pre-treatment methods that usually uses NaOH, Ca(OH)<sub>2</sub>, KOH, and ammonia. An important aspect of alkaline pre-treatment is that the substrate itself consumes some of the alkali (Chen et al., 2014). Alkaline pre-treatments are more effective than acidic ones because they change the structure of lignin and increase the accessibility to holocelluloses (Sambusiti et al., 2013). However, there are also several disadvantages – high alkali concentration in digester and high cost of chemical material. Alkaline pre-treatments are performed by bases such as sodium; potassium; calcium; and ammonium hydroxides. Literature review shows that sodium hydroxide (Salehian et al., 2013) and calcium hydroxide are the two most frequently utilized alkalis in alkaline pre-treatment. However, their utilization consumes much more time (order of hours or days) than acid pre-treatment (minutes or seconds) (Sambusiti et al., 2013). Calcium hydroxide may be preferable than sodium and potassium hydroxides because it is a much cheaper reagent, safer, more environmentally friendly, and more easily recovered (Singh et al., 2015). In addition, Ca<sup>2+</sup> has no inhibitory effect on anaerobic digestion (Chen et al., 2008). Nevertheless, it may not improve the biomass digestion significantly alone because it is known as a weak alkali (Ji et al., 2017). Generally, alkaline pre-treatments are used along with other pre-treatments like thermal, hydrothermal, etc.

Ionic liquids are salts that are in the liquid phase at a temperature as low as room temperature (Venturin et al., 2019). In fact, using ionic liquid pre-treatment results in producing much less crystalline cellulose, causing it to facilitate and accelerate enzymatic hydrolysis (Zhao et al., 2009). Ionic liquids can be applied under mild conditions and their reactions result in negligible vapour pressures; therefore, they can be recovered and reused after the process (Tu and Hallett, 2019). Ozone is a strong oxidant and the ozonation process can break cell wall, what leads to more

soluble and easily biodegradable lignocellulosic biomass (Karuppiah and Azariah, 2019). Consequently, substrates can be easily accessed and assimilated by anaerobic microorganisms, resulting in improved efficiency of hydrolysis and, in turn, anaerobic digestion. The advantage of ozone pre-treatment is that it can be carried out at room temperature and atmospheric pressure. However, this process requires large amounts of ozone, resulting in high cost. Table 2 shows the studies on different chemical pre-treatments of several agricultural crop wastes processed by means of anaerobic digestion.

### Combined pre-treatments

Results of previous studies show that the combination of pre-treatments can result in much better biogas yield and the effect of pre-treatment alone is limited (Gu et al., 2015). Hydrothermal pre-treatment – as one of the most efficient physicochemical pre-treatments – is performed in hot compressed water. It is widely recognized as a green method without potential utilization of chemicals and resulting pollution and thus gains high importance in the 21<sup>st</sup> century (Chandra et al., 2012a). Its process allows water molecules to penetrate lignocellulose network, removes most of the hemicellulose and part of lignin in biomass via degrading them into soluble fractions, and loosens the recalcitrant structure. One of the advantages of hydrothermal pre-treatment is that it performs a selective hydrolysis of hemicellulosic fraction by using a cheap reagent. Simo et al. (2016) studied the effect of hydrothermal pre-treatment on sugarcane bagasse. They found that the hydrothermal pre-treatment showed hydrolysis yield of 42.86%, increasing the amount of lignin from 22% to 47% of dry matter without degradation of cellulose. Wang et al. (2018) performed hydrothermal pre-treatment on rice straw and examined the temperatures of 90, 150, 180 and 210 °C for 15 min (heating rate of 10 °C·min<sup>-1</sup>). Their results showed a reduction of 30% in biogas yield at 210 °C. According to their results, hydrothermal pre-treatment was not technically recommended for biomethane production, especially at higher temperatures; however, lower temperatures were potentially suggested. Costa et al. (2014) compared the effect of hydrothermal, acid and alkaline pre-treatments on sugarcane bagasse and found that the best values of biochemical methane production were obtained for hydrothermal pre-treatment. Liquid hot water or steam pre-treatment is a hydrothermal pre-treatment in which water is used instead of steam. Pressure is provided to keep the water in the liquid state at elevated temperatures (200–240 °C)

**Table 2** Chemical pre-treatments used for biogas production from certain agricultural substrates by means of anaerobic digestion

| Crop        | Type     | Pre-treatments                              | Methane/biogas (mL·gV <sup>-1</sup> ) | Increased (%) | References            |
|-------------|----------|---|---------------------------------------|---------------|-----------------------|
| Rice straw  | alkaline | 5 g NaOH·100 g <sup>-1</sup> ; 200 °C       | 133                                   | 122           | Chandra et al., 2012b |
| Corn stover | alkaline | 2.5% Ca(OH) <sub>2</sub>                    | 260.7                                 | –             | Ji et al., 2017       |
| Wheat straw | chemical | ammonia, 0.70%; 105 °C                      | 538.1 mL·g <sup>-1</sup>              | 31.9          | Wang et al., 2019     |
| Sunflower   | alkaline | 55 °C; 24 h; 4 g NaOH·100 gTS <sup>-1</sup> | 191 ±3                                | 26            | Menardo et al., 2015  |
| Barley      | alkaline | 30 g NaOH·100 g <sup>-1</sup> ; 25 °C       | 222                                   | 792           | Neves et al., 2006    |

for few minutes (Kumar et al., 2009). This method does not require rapid decompression. Considering the microwave method (steam explosion), a high temperature – from 160 to 260 °C at pressure ranging from 1 to 7 MPa – is used to penetrate the substrate structure for a few minutes. Then, in an explosive manner, the pressure is suddenly released to allow the water molecules to escape (Sambusiti, 2013). On the other hand, hemicellulose and lignin solubilize and decompose into lightweight compounds and the secondary explosion aids structural breakdown of the residual biomass leading to finer particles (Paudel et al., 2017). In steam explosion, a quick depressurization and cooling down of the lignocelulosic material take place after the steam explosion, which do not occur in steam pre-treatment (Hendriks and Zeeman, 2009). Oxidative pre-treatment, including wet oxidation, hydrogen peroxide and ozone, can enhance biogas production thanks to delignification mechanism; moreover, oxidative treatment attack the hemicellulose complex (Venturin et al., 2019). Wet oxidation is one of the methods used for hydrothermal processing, which has been used as a pre-treatment for lignocelulosic materials in anaerobic digestion. The inhibitory materials of microorganisms, such as lignin (phenolics) and sugars (furans) – produced as a result of a degradation phase – can be oxidized to carboxylic acid (Klinke et al., 2002). Hydrogen is a strong oxidant and it rarely remains in secondary residues (Yu et al., 2019). It increases biodegradability of

lignin, cellulose and hemicellulose. Since hydrogen peroxide promotes a non-selective oxidation process, inhibitors might be generated as lignin is oxidized to form of soluble aromatic compounds (Hendriks and Zeeman, 2009). Table 3 shows selected researches in which the combination of the pre-treatments was observed.

**Biological pre-treatments**

Biological pre-treatment by means of microorganisms is considered an efficient method for biodegradation promotion of lignocelulosic material (Zhao et al., 2019). There are various types of biological pre-treatments – fungal, enzymatic, ensilaging and microbial consortium – which use commercial enzymes or fungi to reduce the degree of polymerization of cellulose and partial hydrolysis of hemicellulose. Microbial consortium increases lignin degradation and methane thanks to fermentation of volatile fatty acids (Ali et al., 2017). This process is environmentally friendly because one avoids the formation of by-products and chemical-free processes by using it. It has other considerable advantages, such as the possibility to be used under mild conditions, potential methane inhibition (Howard et al., 2003), low energy consumption, and low initial investment requirements. However, this type of pre-treatment is time consuming and its application is limited. In a research, stover was pre-treated via microbial consortium by Zhao et al. (2019). The methane production increased by 62.85% and

**Table 3** Combined pre-treatments used for biogas production from certain agricultural substrates by means of anaerobic digestion

| Crop              | Category                              | Pre-treatment  | Produced methane/ biogas (mL·gVS <sup>-1</sup> )                     | Increased (%)                     | References                    |
|-------------------|---------------------------------------|--|--|-----------------------------------|-------------------------------|
| Rice straw        | chemical plus thermal                 | 0.25; 0.5 M Ca(OH) <sub>2</sub> ; 90, 110, 130 °C; 1, 2, 3 h | max: 0.5 M Ca(OH) <sub>2</sub> ; 110 °C; 2 h; 292 mL·g <sup>-1</sup> | 125                               | Dehghani et al., 2015         |
| Wheat straw       | chemical plus autoclaving             | 1.5% HCl; autoclaved; 121 °C; 60 min                         | 0  | NP* slurry = 0<br>NP solid = 0.36 | Bolado-Rodríguez et al., 2016 |
| Sugarcane bagasse | hydrothermal plus Ca(OH) <sub>2</sub> | 160, 180, 200, 220 °C  | max: 318 (180 °C; 8.5%)  | 47                                | Mustafa et al., 2018          |
| Maize stalks      | liq hot water                         | 120 °C; 1 h  | 267  | 9                                 | Menardo et al., 2012          |
| Barley straw      | liq hot water                         | 90 °C; 1 h   | 340  | 42                                | Menardo et al., 2012          |

\* – normalized methane production

**Table 4** The optimum pre-treatments for some important agricultural crops

| Crop (straw)      | Category                 | Pre-treatments   | Methane/biogas (mL·gVS <sup>-1</sup> ) | Increased (%) | References             |
|-------------------|--------------------------|--|--|---------------|------------------------|
| Rice              | chemical plus thermal    | 0.5 M Ca(OH) <sub>2</sub> ; 110 °C; 2 h  | 292                                    | 125           | Dehghani et al., 2015  |
| Wheat             | alkaline                 | 4% NaOH; 37 °C; 120 h  | 165.9                                  | 111.6         | Chandra et al., 2012c  |
| Corn              | alkaline                 | 8 g NaOH 100 g <sup>-1</sup> substrate; 15 °C; 20 days   | 472                                    | 207           | Zhong et al., 2011     |
| Ensiled sorghum   | alkaline plus thermal    | 10% g NaOH g <sup>-1</sup> TS; 1 h   | 356                                    | 32            | Sambusiti et al., 2013 |
| Safflower         | hydrothermal             | 120 °C; 1 h  | 148.4                                  | 98.5%         | Hashemi et al., 2019   |
| Sugarcane bagasse | chemical plus biological | 2% H <sub>2</sub> SO <sub>4</sub> (g L <sup>-1</sup> ); 121 °C; 15 min plus enzyme (cellulase, hemicelluloses and β-glucosidase) | 200                                    | 208           | Badshah et al., 2012   |

the activity of *Methanosaeta* increased from 2.0 to 10.1%, indicating significant enhancement of the community ability to capture the acetic acid and reduce CO<sub>2</sub> to methane.

Considering all kinds of aforementioned pre-treatments, a major achievement of previous studies lies in extraction of optimal pre-treatments for certain important agricultural crops, e.g. for rice straw, the highest increase in biogas production (125%) was obtained when combined pre-treatment including chemical plus thermal pre-treatments was used (Dehghani et al., 2015). The physiochemical pre-treatment including chemical plus thermal pre-treatments (3% C<sub>2</sub>H<sub>5</sub>OH and 100 °C during 60 min) showed an increase by 122% in biogas production (Olugbemide et al., 2019). The combined pre-treatment including chemical plus thermal pre-treatments that used 5% NaOH and 200 °C for 10 min showed similar increase in biogas production (Chandra et al., 2012c). For wheat straw, alkaline pre-treatment with 4% NaOH resulted in an increase by 111.6% in biogas production. Optimal pre-treatments for selected important agricultural crops are given in Table 4.

### Conclusion

Due to recalcitrant nature of agricultural lignocellulosic wastes, it is essential to use efficient pre-treatments prior to anaerobic digestion. There are several types of pre-treatments that are used for lignocellulosic materials, such as physical, chemical, biological and combined pre-treatments. The mechanical pre-treatments are commonly utilized for particle size reduction, increasing the surface area and decreasing the technical digestion time. Conducted studies show that the physical pre-treatment combined with other pre-treatments has much better results in terms of degradability of lignocellulosic materials. Thermal or hydrothermal pre-treatments showed good results in terms of increasing anaerobic digestion degradation phase. Alkaline pre-treatments are more effective than acidic ones. Chemical pre-treatments have the advantage of easy usage, fastness, and effectiveness in comparison to other pre-treatment methods. Biological pre-treatments are environmentally friendly because there are no by-products and the process is chemical-free; however, it is time-consuming.

### References

- ALI, S. S. – ABOMOHRA, A. E. – SUN, J. 2017. Effective bio-pretreatment of sawdust waste with a novel microbial consortium for enhanced biomethanation. In *Bioresource Technology*, vol. 238, pp. 425–432.
- ANTONOPOULOU, G. – LYBERATOS, G. 2013. Effect of pretreatment of sweet sorghum biomass on methane generation. In *Waste and Biomass Valorization*, vol. 4, no. 3, pp. 583–591.
- BADSHAH, M. – LAM, D. M. – LIU, J. – MATTIASSON, B. 2012. Use of an automatic methane potential test system for evaluating the biomethane potential of sugarcane bagasse after different treatments. In *Bioresource Technology*, vol. 114, pp. 262–269.
- BOLADO-RODRIGUEZ, S. – TOQUERO, C. – MARTIN-JUAREZ, J. – TRAVAINI, R. GARCIA-ENCINA, P. A. 2016. Effect of thermal, acid, alkaline and alkaline-peroxide pretreatments on the biochemical methane potential and kinetics of the anaerobic digestion of wheat straw and sugarcane bagasse. In *Bioresource Technology*, vol. 201, pp. 182–190.
- CHANDRA, R. – TAKEUCHI, H. – HASEGAWA, T. 2012a. Methane production from lignocellulosic agricultural crop wastes: A review in context to second generation of biofuel production. In *Renewable and Sustainable Energy Reviews*, vol. 16, no. 3, pp. 1462–1476.
- CHANDRA, R. – TAKEUCHI, H. – HASEGAWA, T. 2012b. Hydrothermal pretreatment of rice straw biomass: A potential and promising method for enhanced methane production. In *Applied Energy*, vol. 94, pp. 129–140.
- CHANDRA, R. – TAKEUCHI, H. – HASEGAWA, T. – KUMAR, R. 2012c. Improving biodegradability and biogas production of wheat straw substrates using sodium hydroxide and hydrothermal pretreatments. In *Energy*, vol. 43, no. 1, pp. 273–282.
- CHEN, X. – GU, Y. – ZHOU, X. – ZHANG, Y. 2014. Asparagus stem as a new lignocellulosic biomass feedstock for anaerobic digestion: Increasing hydrolysis rate, methane production and biodegradability by alkaline pretreatment. In *Bioresource Technology*, vol. 164, pp. 78–85.
- CHEN, Y. – CHENG, J. J. – CREAMER, K. S. 2008. Inhibition of anaerobic digestion process: A review. In *Bioresource Technology*, vol. 99, no. 10, pp. 4044–4064.
- CHOJNACKA, A. – SZCZĘSNY, P. – BŁASZCZYK, M. K. – ZIELENKIEWICZ, U. – DETMAN, A. – SALAMON, A. – SIKORA, A. 2015. Noteworthy facts about a methane-producing microbial community processing acidic effluent from sugar beet molasses fermentation. In *PLoS One*, vol. 10, no. 5, pp. e0128008.
- COSTA, A. – PINHEIRO, G. – PINHEIRO, F. – DOS SANTOS, A. – SANTAELLA, S. – LEITÃO, R. 2014. The use of thermochemical pretreatments to improve the anaerobic biodegradability and biochemical methane potential of the sugarcane bagasse. In *Chemical Engineering Journal*, vol. 248, pp. 363–372.
- DEHGHANI, M. – KARIMI, K. – SADEGHI, M. 2015. Pretreatment of rice straw for the improvement of biogas production. In *Energy & Fuels*, vol. 29, no. 6, pp. 3770–3775.
- GRÖNROOS, A. – PIKONEN, P. – RUPPERT, O. 2004. Ultrasonic depolymerization of aqueous carboxymethylcellulose. In *Ultrasonics Sonochemistry*, vol. 11, no. 1, pp. 9–12.
- GU, Y. – ZHANG, Y. – ZHOU, X. 2015. Effect of Ca(OH)<sub>2</sub> pretreatment on extruded rice straw anaerobic digestion. In *Bioresource Technology*, vol. 196, pp. 116–122.
- HASHEMI, S. S. – KARIMI, K. – MIRMOHAMADSADEGHI, S. 2019. Hydrothermal pretreatment of safflower straw to enhance biogas production. In *Energy*, vol. 172, pp. 545–554.
- HE, Y. – PANG, Y. – LIU, Y. – LI, X. – WANG, K. 2008. Physicochemical characterization of rice straw pretreated with sodium hydroxide in the solid state for enhancing biogas production. In *Energy & Fuels*, vol. 22, no. 4, pp. 2775–2781.
- HENDRIKS, A. – ZEEMAN, G. 2009. Pretreatments to enhance the digestibility of lignocellulosic biomass. In *Bioresource Technology*, vol. 100, no. 1, pp. 10–18.
- HJORTH, M. – GRÄNITZ, K. – ADAMSEN, A. P. – MØLLER, H. B. 2011. Extrusion as a pretreatment to increase biogas production. In *Bioresource Technology*, vol. 102, no. 8, pp. 4989–4994.
- HLINKA, P. – KARANDUŠOVSKÁ, I. – MIHINA, Š. 2019. Monitoring of gas production during the biowaste composting. In *Acta Technologica Agriculturae*, vol. 22, no. 3, pp. 75–79.
- HOWARD, R. – ABOTSI, E. – VAN RENSBURG, E. J. – HOWARD, S. 2003. Lignocellulose biotechnology: Issues of bioconversion and enzyme production. In *African Journal of Biotechnology*, vol. 2, no. 12, pp. 602–619.
- Ji, J. – ZHANG, J. – YANG, L. – HE, Y. – ZHANG, R. – LIU, – G. CHEN, C. 2017. Impact of co-pretreatment of calcium hydroxide and steam explosion on anaerobic digestion efficiency with corn stover. In *Environmental Technology*, vol. 38, no. 12, pp. 1465–1473.
- KARUPPIAH, T. – AZARIAH, V. E. 2019. Biomass pretreatment for

- enhancement of biogas production. In *Anaerobic Digestion*. IntechOpen CY – Rijeka.
- KAŽIMÍROVÁ, V. – GADUŠ, J. – GIERTL, T. 2018. Verification of suitability of substrate composition for production and quality of biogas. In *Acta Technologica Agriculturae*, vol. 21, no. 3, pp. 115–118.
- KLINKE, H. B. – AHRING, B. K. – SCHMIDT, A. S. – THOMSEN, A. B. 2002. Characterization of degradation products from alkaline wet oxidation of wheat straw. In *Bioresource Technology*, vol. 82, no. 1, pp. 15–26.
- KUMAR, P. – BARRETT, D. M. – DELWICHE, M. J. – STROEVE, P. 2009. Methods for pretreatment of lignocellulosic biomass for efficient hydrolysis and biofuel production. In *Industrial & Engineering Chemistry Research*, vol. 48, no. 8, pp. 3713–3729.
- LI, C. – CHAMPAGNE, P. – ANDERSON, B. C. 2013. Effects of ultrasonic and thermo-chemical pre-treatments on methane production from fat, oil and grease (FOG) and synthetic kitchen waste (KW) in anaerobic co-digestion. In *Bioresource Technology*, vol. 130, pp. 187–197.
- MENARDO, S. – AIROLDI, G. – BALSARI, P. 2012. The effect of particle size and thermal pre-treatment on the methane yield of four agricultural by-products. In *Bioresource Technology*, vol. 104, pp. 708–714.
- MENARDO, S. – CACCIATORE, V. – BALSARI, P. 2015. Batch and continuous biogas production arising from feed varying in rice straw volumes following pre-treatment with extrusion. In *Bioresource Technology*, vol. 180, pp. 154–161.
- MONTGOMERY, L. F. – BOCHMANN, G. 2014. Pretreatment of feedstock for enhanced biogas production. IEA Bioenergy Ireland.
- MUSSOLINE, W. – ESPOSITO, G. – GIORDANO, A. – LENS, P. 2013. The anaerobic digestion of rice straw: A review. In *Critical Reviews in Environmental Science and Technology*, vol. 43, no. 9, pp. 895–915.
- MUSTAFA, A. M. – LI, H. – RADWAN, A. A. – SHENG, K. – CHEN, X. 2018. Effect of hydrothermal and  $\text{Ca}(\text{OH})_2$  pretreatments on anaerobic digestion of sugarcane bagasse for biogas production. In *Bioresource Technology*, vol. 259, pp. 54–60.
- NEVES, L. – RIBEIRO, R. – OLIVEIRA, R. – ALVES, M. 2006. Enhancement of methane production from barley waste. In *Biomass and Bioenergy*, vol. 30, no. 6, pp. 599–603.
- OLUGBEMIDE, A. D. – LAJIDE, L. – ADEBAYO, A. – OWOLABI, B. J. 2019. Enhanced biogas production from rice husk through solid-state chemical pretreatments. In *Waste and Biomass Valorization*, pp. 1–11.
- PANEPINTO, D. – GENON, G. 2016. Analysis of the extrusion as a pretreatment for the anaerobic digestion process. In *Industrial Crops and Products*, vol. 83, pp. 206–212.
- PAUDEL, S. R. – BANJARA, S. P. – CHOI, O. K. – PARK, K. Y. – KIM, Y. M. – LEE, J. W. 2017. Pretreatment of agricultural biomass for anaerobic digestion: Current state and challenges. In *Bioresource Technology*, vol. 245, pp. 1194–1205.
- RAI, G. 1986. *Non-Conventional Energy Sources*. Delhi: Khanna Publishers, 696 pp. ISBN 9788174090737.
- RAJPUT, A. A. – VISVANATHAN, C. 2018. Effect of thermal pretreatment on chemical composition, physical structure and biogas production kinetics of wheat straw. In *Journal of Environmental Management*, vol. 221, pp. 45–52.
- SALEHIAN, P. – KARIMI, K. – ZILOUEI, H. – JEIHANIPOUR, A. 2013. Improvement of biogas production from pine wood by alkali pretreatment. In *Fuel*, vol. 106, pp. 484–489.
- SAMBUSITI, C. 2013. Physical, chemical and biological pretreatments to enhance biogas production from lignocellulosic substrates. Doctoral dissertation, 209 pp., Polytechnic University of Milan.
- SAMBUSITI, C. – MONLAU, F. – FICARA, E. – CARRÈRE, H. – MALPEI, F. 2013. A comparison of different pre-treatments to increase methane production from two agricultural substrates. In *Applied Energy*, vol. 104, pp. 62–70.
- SIMO, W. S. F. – JONG, E. N. – KAPSEU, C. 2016. Improving biogas production of sugarcane bagasse by hydrothermal pretreatment. In *Chemical and Biomolecular Engineering*, vol. 1, no. 3, 21–25.
- SINGH, J. – SUHAG, M. – DHAKA, A. 2015. Augmented digestion of lignocellulose by steam explosion, acid and alkaline pretreatment methods: A review. In *Carbohydrate Polymers*, vol. 117, pp. 624–631.
- TU, W. C. – HALLETT, J. P. 2019. Recent advances in the pretreatment of lignocellulosic biomass. In *Current Opinion in Green and Sustainable Chemistry*, vol. 20, pp. 11–17.
- VENTURIN, B. – BONATTO, C. – DAMACENO, F. M. – MULINARI, J. – FONGARO, G. – TREICHEL, H. 2019. Physical, chemical, and biological substrate pretreatments to enhance biogas yield. In *Improving Biogas Production*. Springer, pp. 25–44.
- WANG, D. SHEN, F. – YANG, G. – ZHANG, Y. – DENG, S. – ZHANG, J. – ZENG, Y. – LUO, T. – MEI, Z. 2018. Can hydrothermal pretreatment improve anaerobic digestion for biogas from lignocellulosic biomass. In *Bioresource Technology*, vol. 249, pp. 117–124.
- WANG, D. – XIN, Y. – SHI, H. – AI, P. – YU, L. – LI, X. – CHEN, S. 2019. Closing ammonia loop in efficient biogas production: Recycling ammonia pretreatment of wheat straw. In *Biosystems Engineering*, vol. 180, pp. 182–190.
- WANG, L. – MATSSON, M. – RUNDSTEDT, J. – KARLSSON, N. 2011. Different pretreatments to enhance biogas production. Master of Science thesis, Halmstad University.
- XIE, S. – FROST, J. P. – LAWLOR, P. G. – WU, G. – ZHAN, X. 2011. Effects of thermo-chemical pre-treatment of grass silage on methane production by anaerobic digestion. In *Bioresource Technology*, vol. 102, no. 19, pp. 8748–8755.
- YU, Q. – LIU, R. – LI, K. – MA, R. 2019. A review of crop straw pretreatment methods for biogas production by anaerobic digestion in China. In *Renewable and Sustainable Energy Reviews*, vol. 107, pp. 51–58.
- YU, J. – ZHANG, J. – HE, J. – LIU, Z. – YU, Z. 2009. Combinations of mild physical or chemical pretreatment with biological pretreatment for enzymatic hydrolysis of rice hull. In *Bioresource Technology*, vol. 100, no. 2, pp. 903–908.
- YUAN, X. – WEN, B. – MA, X. – ZHU, W. – WANG, X. – CHEN, S. – CUI, Z. 2014. Enhancing the anaerobic digestion of lignocellulose of municipal solid waste using a microbial pretreatment method. In *Bioresource Technology*, vol. 154, pp. 1–9.
- ZEYNALI, R. – KHOJASTEHPOUR, M. – EBRAHIMI-NIK, M. 2017. Effect of ultrasonic pre-treatment on biogas yield and specific energy in anaerobic digestion of fruit and vegetable wholesale market wastes. In *Sustainable Environment Research*, vol. 27, no. 6, pp. 259–264.
- ZHAO, H. – JONES, C. L. – BAKER, G. A. – XIA, S. – OLUBAJO, O. – PERSON, V. N. 2009. Regenerating cellulose from ionic liquids for an accelerated enzymatic hydrolysis. In *Journal of Biotechnology*, vol. 139, no. 1, pp. 47–54.
- ZHAO, Y. – XU, C. – AI, S. – WANG, H. – GAO, Y. – YAN, L. – MEI, Z. – WANG, W. 2019. Biological pretreatment enhances the activity of functional microorganisms and the ability of methanogenesis during anaerobic digestion. In *Bioresource Technology*, pp. 121660.
- ZHENG, M. – LI, L. – LI, X. – XIONG, J. – MEI, T. – CHEN, G. 2010. The effects of alkaline pretreatment parameters on anaerobic biogasification of corn stover. In *Energy Sources, Part A: Recovery, Utilization, and Environmental Effects*, vol. 32, no. 20, pp. 1918–1925.
- ZHENG, Y. – ZHAO, J. – XU, F. – LI, Y. 2014. Pretreatment of lignocellulosic biomass for enhanced biogas production. In *Progress in Energy and Combustion Science*, vol. 42, pp. 35–53.
- ZHONG, W. – ZHANG, Z. – QIAO, W. – FU, P. – LIU, M. 2011. RETRACTED: Comparison of chemical and biological pretreatment of corn straw for biogas production by anaerobic digestion. In *Renewable Energy*, vol. 36, no. 6, pp. 1875–1879.
- ZILOUEI, H. – TAHERDANAK, M. 2015. Biohydrogen from lignocellulosic wastes. In *Lignocellulose-based bioproducts*. Springer, pp. 253–288.



Acta Technologica Agriculturae 3  
Nitra, Slovaca Universitas Agriculturae Nitriae, 2020, pp. 111–117

## EFFECT OF FIRES ON CERTAIN PROPERTIES OF FOREST SOILS IN WESTERN ALGERIA

Ayoub ALLAM<sup>1\*</sup>, Amine Habib BORSALI<sup>1</sup>, Abdelkrim KEFIFA<sup>1</sup>, Mohamed ZOUIDI<sup>1</sup>, Raphael GROS<sup>2</sup>

<sup>1</sup>University of Dr Moulay Tahar, Saïda, Algeria

<sup>2</sup>Aix-Marseille University, Marseille Cedex, France

Natural disturbances, such as forest fires, cause significant changes in the structure and functioning of semi-arid ecosystems. After such disturbances, the impact on the soil ecosystem in its entirety is misunderstood. In this study, two years after the last fire, changes in the physicochemical and biological properties of Aleppo pine forest soils in the semi-arid zone were observed. Among all physical properties analysed, only the soil moisture remained significantly lower in the burnt zone in contrast to control zone. Considering the chemical properties, the only negatively affected parameter is the rate of organic matter. In terms of biological properties, results showed that the fire caused a significant decrease in soil microorganisms by decreasing basal respiration and microbial biomass. Conversely, the metabolic quotient recorded higher values in the fire zone than in the control zone. These results indicate that microbial communities in semi-arid soils, already stressed by climatic hazards, are very sensitive to the passage of even low-intensity fires.

**Keywords:** degradation; organic matter; microbial biomass; semi-arid regions

The forest ecosystems of the Mediterranean basin contain remarkable biodiversity, providing important economic resources in terms of silvo-pastoral production, as well as tourism and leisure areas. Furthermore, they also provide essential ecosystem services, e.g. water erosion reduction by the retention of water in the soil (Eamus et al., 2005). Drought is one of the most unfavourable and most common constraints in arid and semi-arid regions (Sabaghnia and Janmohammadi, 2014), and the presence of pyrophyte species in these regions, such as *Cistus* (*Cistus ladaniferus*) or Aleppo Pine (*Pinus halepensis* Mill), can promote fires (Borsali, 2013). Soil degradation by any means represents one of the most significant issues in terms of maintaining the soil quality (Nouraein et al., 2020).

Numerous authors confirm that the origins of fire are mainly related to humans and directly depend on imprudence and insouciance of people, especially in terms of the agricultural and pastoral utilization of land (Meddour, 2014). According to the statistics provided by the Direction General of Forests, Algeria is seriously affected by fires, especially the north of the country. In 2017, the total area burnt by fires was 51,908 ha. Due to the significant evolution of this disaster and observed damage on the forest ecosystem, it is highly recommendable to investigate the changes in properties of these burnt soils.

Certini (2005) synthesizes the effects of fire on the properties of forest soils and shows that the main factor is the severity of fire, which depends on the environmental factors involved in the combustion processes: quantity; nature and moisture of the dead and living combustible;

wind speed; and site topography. This severity depends on two factors: the intensity and duration of the fire. High intensity combined with a long duration of fire would cause the greatest damage to vegetation and soil. The decline in soil protection leads to lower stability and, as a result, increased vulnerability to erosion risk (Hart et al., 2005).

The increase in the number of fires and their frequency have reduced the time between the two successive fires to less than 20 years (Vennetier et al., 2008). Their effects on soil biology are both direct – instantaneous destruction of organisms living on the surface – and indirect – environment modification (soil, vegetation cover) (Uroz et al., 2014). In addition to their effect on physicochemical parameters, fires also directly or indirectly affect the soil organisms. Direct effects induce short-term changes that modify species composition and abundance of taxonomic groups (Gongalsky et al., 2012).

Algerian soils are naturally vulnerable, sometimes highly degraded, especially in the semi-arid zone. These soils are highly affected by the issue of forest fires and their impact on soils is not very investigated by scientists. In addition, the difficulty of returning to an optimal performance level after fire must be enlightened by an objective evaluation of the short-term return dynamics of these soil properties. In order to answer the most significant questions related to the state of Algerian post-fire soils, a comparative study of selected physicochemical and biological parameters of a soil after two years of the last fire and a control soil that did not undergo fire for twenty years was carried out.

## Material and methods

### Study area

The study area is in the semi-arid bioclimatic stage of Ouled Khaled Saïda. This private forest, known as Keroua, is located between (34° 54' 55.00' N 0° 7' 29.14" E). It covers an area of 760 ha (Fig. 1).

This bioclimatic domain receives 345.16 mm of precipitation with a seasonal rainfall regime of winter, spring, summer and autumn (WSSA). According to the Saïda Meteorological Station (SMS, 2017), the maximum average temperature is 24.6 °C; the minimum average temperature is 11 °C and the thermal average amplitude is 19.9 °C. In the observed area, the number of fires for the period from 1999 to 2016 is 190 in total, which destroyed a total forest area of 3,355.25 ha. This corresponds to an annual average of 10.56 fires and 186.40 ha of burnt area. The number of fires varies from year to year – in 2007, fires burnt the smallest area of 9 ha, and in 1999 an absolute

maximum of 1,160.5 ha, while in 2015, only a small number of fires (9) was recorded, yet a total forest area of 720.75 ha was destroyed as a result.

The plots used for control measurements are in the same area but were not affected by fires for at least twenty years. This zone is characteristic with good density of vegetal cover dominated mainly by the Aleppo Pine and different plant strata.

### Methodology and soil sampling

The study of the fire effects on the soil properties required determination of an appropriate methodology with the thematic, for that, the following criteria were respected:

1. the forest cover in observed zone was to predominantly compose of a monospecific population of Aleppo pine;
2. the control zone must be at least by 50 m away from the fire border;
3. the analysis is conducted two years after the fire that was recorded in 2015. Thus, the plots were visited in

spring of 2017 for the collection of soil samples.

In each zone (burnt and control), five plots were randomly selected. Soil samples were taken from the first horizon with a depth of 0–10 cm, sieved to particle size of 2 mm at maximum and conditioned in cold for biological analysis.

### Physical analysis

Soil moisture content (d.b.) was determined by weighing a certain amount of soil before and after drying in an oven at 105 °C for 24 h. The soil mass loss represents the mass of water evaporated during drying (Mathieu and Pieltain, 1998). The soil moisture content was determined as follows:

$$u = \left( \frac{m_{B2} - m_{B3}}{m_{B3} - m_{B1}} \right) 100 \text{ (\%)} \quad (1)$$

where:

*u* – soil moisture content (%); *m*<sub>B1</sub> – mass of empty breaker (g); *m*<sub>B2</sub> – mass of breaker + fresh soil (5 g); *m*<sub>B3</sub> – mass of breaker + dried soil (g)

Soil permeability is given by the height of water measured per centimetre of infiltration per unit of time (Mathieu and Pieltain, 1998).

The samples were placed in graduated cylinders up to 100 ml, which are then filled with distilled water up to 200 ml. Subsequently, it is left resting for 12 h, and after it, the water height is measured. Permeability is defined as follows:

$$K = 0.857 \cdot h \quad (2)$$

where:

*K* – permeability (cm·h<sup>-1</sup>); *h* – water height (cm)

The soil sample is moistened for 12 h by capillary rise in a sintered glass Buchner filter. Then, the filter is placed on a vacuum flask connected to a water pump to remove water in pores with a diameter less than 8 μm. The retention capacity (*RC*) is defined as the water content remaining in the soil after 24 h (Saetre, 1998). It was calculated according to the following formula:

$$RC = \left[ \frac{(m_{B2} - m_{B1}) - (m_{B3} - m_{B1})}{(m_{B3} - m_{B1})} \right] 100 \text{ (\%)} \quad (3)$$

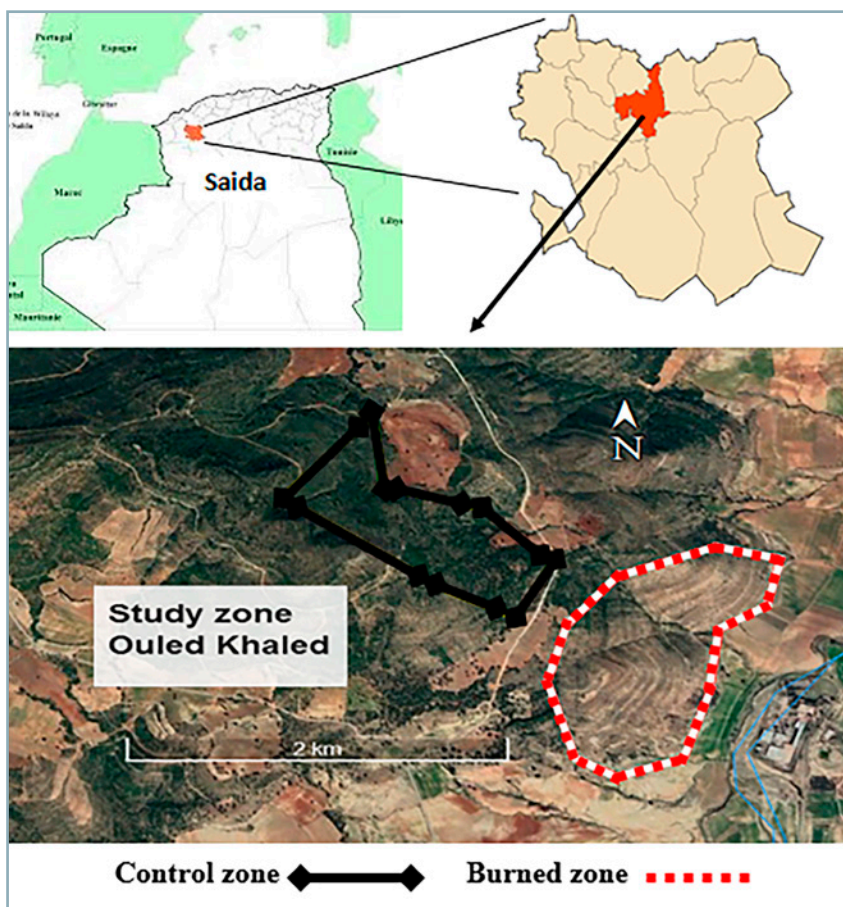


Fig. 1 Location of the observed zone

where:

$RC$  – retention capacity (%);  $m_{B1}$  – empty filter mass (g);  $m_{B2}$  – filter mass with moistened soil for 12 h (g);  $m_{B3}$  – mass of (filter + moist soil) after drying for 24 h at 105 °C (g)

The bulk density ( $\rho_V$ ) corresponds to the dry mass of a soil volume, the structure of which has not been disturbed, knowing the constant dry mass of the sample at 105 °C and the volume of the cylinders used (Blake and Hartge, 1986). Bulk density was calculated according to the following formula:

$$\rho_V = \frac{m_B}{V} \quad (4)$$

where:

$\rho_V$  – bulk density ( $\text{g}\cdot\text{cm}^{-3}$ );  $m_B$  – dry soil mass (g);  $V$  – cylinder volume ( $\text{cm}^3$ )

$$V = \pi \cdot r^2 \cdot h$$

where:

$\pi$  – 3.14;  $r$  – cylinder radius (cm);  $h$  – cylinder height (cm)

The measurement of the real density ( $\rho$ ) was determined by the pycnometer method, which consists of determining the volume of benzene displaced by the solid phase of sample with a known mass in a known volume (Pétard, 1993). The real density was obtained as follows:

$$\rho = \frac{m_B}{V} \quad (5)$$

$$V = \frac{(m_{B1} + m_B) - m_{B2}}{\rho_B} \quad (6)$$

where:

$\rho$  – real density ( $\text{g}\cdot\text{cm}^{-3}$ );  $m_B$  – 10 g of soil dried in oven at 105 °C (g);  $V$  – volume of used soil ( $\text{cm}^3$ );  $m_{B1}$  – mass of pycnometer filled with benzene up to the mark (g);  $m_{B2}$  – mass of pycnometer with 10g of soil filled with benzene up to the mark after the disappearance of air bubbles (g);  $\rho_B$  – benzene density ( $\text{g}\cdot\text{cm}^{-3}$ )

The porosity was determined by the following formula:

$$p = \left( \frac{\rho - \rho_V}{\rho} \right) 100 \quad (7)$$

where:

$p$  – porosity;  $\rho$  – real density ( $\text{g}\cdot\text{cm}^{-3}$ );  $\rho_V$  – bulk density ( $\text{g}\cdot\text{cm}^{-3}$ )

The soil electrical conductivity measurement was performed by a conductivity meter HI2300, (HANNA Instruments, Italy) using a ratio of 20 g of dried fine soil in the open air and 50 ml of distilled water (Paycheng, 1980).

## Chemical analysis

The measurement of the  $\text{pH}_{\text{H}_2\text{O}}$  and  $\text{pH}_{\text{KCl}}$  of the soil is an empirical measurement. For the measurement of  $\text{pH}_{\text{H}_2\text{O}}$ , 20 g of fine soil dried in the open air were mixed in a beaker with 50 ml of distilled water. For the measurement of  $\text{pH}_{\text{KCl}}$ , 20 g of soil and 50 ml of potassium chloride were mixed in separate beaker (Paycheng, 1980). The measurements were conducted using a pH meter HI2210 (HANNA Instruments, Italy).

Total limestone ( $\text{CaCO}_3$ ) was estimated by the Bernard calcimeter. This method allows the measurement of the volume of  $\text{CO}_2$  released by the soil samples under the action of hydrochloric acid (HCl). The total limestone was calculated using the following expression:

$$TL = \left[ \left( \frac{V_1}{m_{B1}} \right) \left( \frac{m_B}{V} \right) \right] 100 \quad (8)$$

where:

$TL$  – total limestone (%);  $m_B$  – reference sample mass ( $\text{CaCO}_3 = 1$  g);  $m_{B1}$  – mass of soil samples (1 g);  $V$  – volume generated by reference sample ( $V = 225 \text{ cm}^3$ );  $V_1$  – volume generated by soil samples ( $\text{cm}^3$ )

The organic matter (OR) was determined by mass loss of dry sample after the calcination at 550 °C for 16 h. It was calculated using the following formula:

$$OR = \left[ \frac{(m_{B1} - m_B) - (m_{B2} - m_B)}{(m_{B1} - m_B)} \right] 100 \quad (9)$$

where:

$OR$  – organic matter (%);  $m_B$  – empty breaker mass (g);  $m_{B1}$  – breaker mass with dried soil (g);  $m_{B2}$  – breaker mass with calcined soil (g)

## Biological analysis

Basal respiration (BR) was measured according to the protocol described by Anderson and Domsch (1978) to assess the physiological status of soil microbial communities. Ten grams (dry equivalent) of fresh soil kept at 4 °C were weighted in a glass phial (117 ml). The phials were hermetically sealed with a plug immediately after the replacement (4 min) of their internal atmosphere by a stable  $\text{CO}_2$  concentration atmosphere and incubated for 4 h at 25 °C. After incubation, an aliquot of phial atmosphere (1 ml) was injected using a syringe into a gas chromatograph (Chrompack CHROM3 – CP 9001). Ambient  $\text{CO}_2$  concentrations were subtracted from the  $\text{CO}_2$  concentrations measured after incubation to obtain the amount of  $\text{CO}_2$  produced by the heterotrophic microorganisms contained in the sample.

Microbial biomass (MB) was estimated using substrate-induced respiration (SIR) rates (Anderson and Domsch, 1978). Ten grams (dry mass equivalent) of sub-samples were placed in 117 ml glass jars and amended with powdered glucose ( $1,000 \mu\text{g}\cdot\text{g}^{-1}$ ). One millilitre of air was sampled in the head space with a syringe and injected into a gas chromatograph (Chrompack CHROM 3 – CP 9001). SIR rates were converted to microbial biomass value using the equation given by Beare et al. (1990).

The metabolic quotient ( $qCO_2$ ) was calculated as follows (Anderson and Domsch, 1978):

$$qCO_2 = \frac{BR}{MB} \quad (10)$$

where:

$qCO_2$  – metabolic quotient ( $mg\ C-CO_2 \cdot (g\ Cmic)^{-1} \cdot h^{-1}$ );  
 $BR$  – basal respiration ( $\mu g\ C-CO_2 \cdot g^{-1}\ DM \cdot h^{-1}$ );  $MB$  – microbial biomass ( $\mu g\ Cmic \cdot g^{-1}\ DM$ )

### Statistical analysis

Collected data were analysed using the Minitab 17 software (Minitab, LLC, company, United States). The 5% threshold comparison test was used to compare the averages (student's test). The thresholds of significance considered are: (\* Significant:  $P < 0.05$ ; \*\* Very significant:  $P < 0.01$ ; \*\*\* Highly significant;  $P < 0.001$ ; NS: Not significant).

## Results and discussion

The results obtained by the chemical properties evaluation show that the organic matter content of burnt soils (7.73%) was significantly lower compared to the control zone (16.08%) ( $P < 0.001$ ). However, the statistical tests of the other properties do not indicate a significant difference, only a slight decrease was noticed for total limestone in the burnt soil in contrast to control zone. The average values of  $pH_{H_2O}$  and  $pH_{KCl}$  approach each other in both zones.

The fire did not significantly affect the physical parameters except soil moisture. Here, a decrease of 4.89% between the burnt zone and its control zone ( $P < 0.05$ ) was observed. In terms of permeability, retention capacity, porosity and electrical conductivity, a slight decrease was observed in burnt soils compared to control zone. Considering the bulk density and real density, an increase in both parameters was observed in the burnt zone in contrast to control zone (Table 1).

The results obtained for the biological analyses show that the basal respiration and microbial biomass were significantly lower in burnt area than in control zone ( $P < 0.001$ ) despite the passing of two years since the fire. decrease was approx.  $1.09\ (\mu g\ C-CO_2 \cdot g^{-1}\ DM \cdot h^{-1})$  for basal respiration and  $0.19\ (\mu g\ Cmic \cdot g^{-1}\ DM)$  for microbial biomass.

Considering the metabolic quotient, there was a significant increase ( $P < 0.05$ ) in burnt zone compared to control zone – values  $14.59$  and  $8.02\ (mg\ C-CO_2 \cdot (g\ Cmic)^{-1} \cdot h^{-1})$ , respectively (Fig. 2).

Two years since the fire, results show that organic matter decreased significantly in the burnt soil compared to control zone. According to Verma and Jayakumar (2012), high intensity fires can result in a total loss of soil organic matter. Similarly, Annabi et al. (2009) recorded critical organic carbon values for forest soils in the semi-arid zone eight years after the last fire.

The role of organic matter as a cementing agent for soil aggregates is extremely important after a fire (Granged et al., 2011). Therefore, the higher the organic matter content in soil, the better the cohesion between soil particles, and thus higher resistance to erosion.

This deficit in organic matter is a direct result of the combination of total vegetation burning in this area and the water erosion phenomenon. Van der Werf et al. (2010) and Guenon et al. (2011) reported that fires eliminate large quantities of organic matter from ecosystems by vegetation burning and complete oxidation of soil organic matter. Furthermore, Knicker (2007) concluded that erosion and burning progressively deplete organic matter and nutrients of soil. Wind and water erosion of ash is a significant risk in recently burnt areas. In general, the wind carries them to gullies, where they accumulate and from which they are leached by runoff, causing a net loss of soil fertility (Vennetier et al., 2014).

In terms of the rest of chemical properties, the average values of the two zones (burnt and control) were getting closer, showing the absence of a significant difference. This means that either these soil properties have not been affected by the fire from the beginning, or the impact was

**Table 1** Physicochemical properties of burnt and control soils

| Properties                                    | Burnt | Control | Signification |
|---|-------|---------|---------------|
| <b>Chemical</b>                               |       |         |               |
| $pH_{H_2O}$                                   | 7.64  | 7.64    | NS            |
| $pH_{KCl}$                                    | 7.40  | 7.38    | NS            |
| organic matter (%)                            | 7.73  | 16.08   | ***           |
| total limestone (%)                           | 15.80 | 20.98   | NS            |
| <b>Physical</b>                               |       |         |               |
| bulk density ( $g \cdot cm^{-3}$ )            | 1.23  | 1.05    | NS            |
| real density ( $g \cdot cm^{-3}$ )            | 2.42  | 2.39    | NS            |
| total porosity (%)                            | 49.17 | 56.07   | NS            |
| moisture (%)                                  | 3.33  | 8.22    | *             |
| retention capacity (%)                        | 61.20 | 79      | NS            |
| permeability ( $cm \cdot h^{-1}$ )            | 2.63  | 2.74    | NS            |
| electrical conductivity ( $dS \cdot m^{-1}$ ) | 0.18  | 0.22    | NS            |

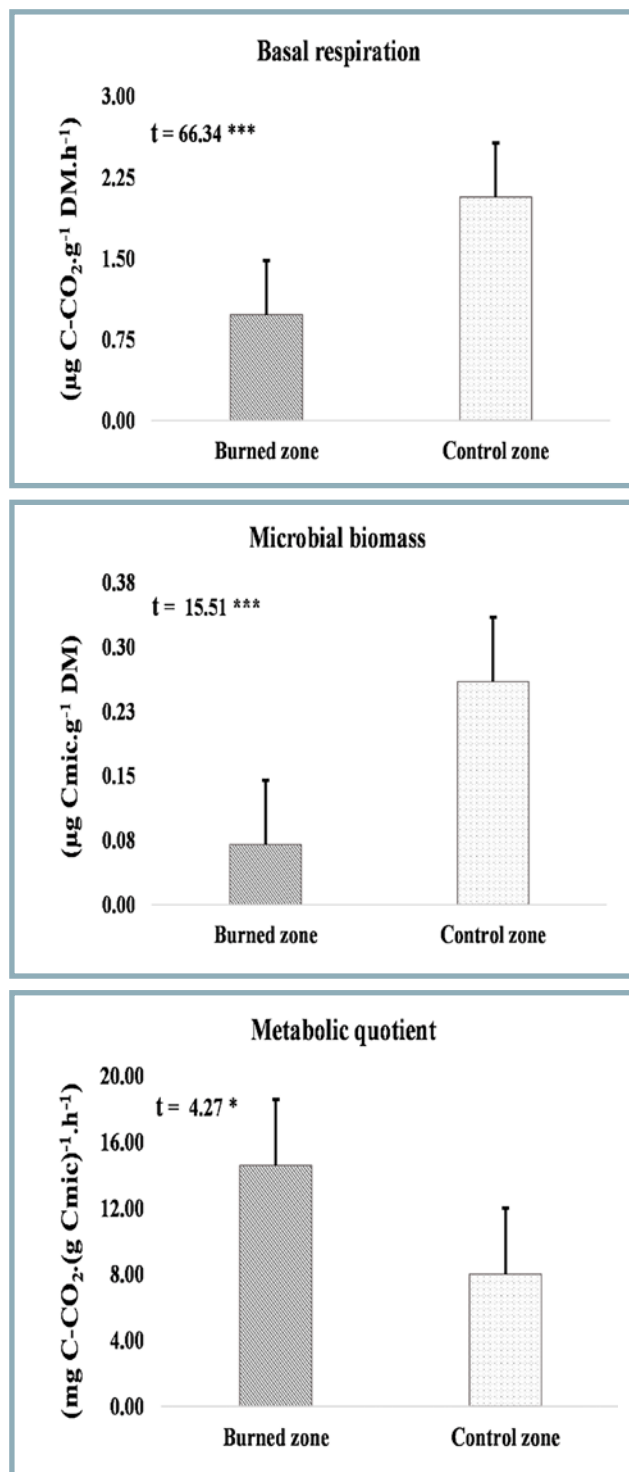


**Fig. 2** Variation in biological properties in burnt and control soils

particularly significant during the first months after the fire, and over time, the differences between the two zones gradually disappeared.

Study results indicate that after two years since the last fire, the physical properties of these soils were not significantly affected with exception of the moisture – there was a decrease in this value in the burnt zone compared to control zone. The results obtained corroborate those obtained by Mabuhay et al. (2006), who reported that after thirteen months, the soil moisture content was significantly higher in the unburnt site in contrast to the burnt site. Moreover, Holden et al. (2013) reported a decrease in soil moisture after the fire.

The decrease in soil moisture is due to absolute destruction of trees protecting the soil against the direct effect of solar radiation, and their replacement by the herbaceous stratum, which increases the use of water in the superficial horizon. This will accentuate evapotranspiration in burnt soils. Mulumba and Lal (2008) demonstrated the relationship between the soil organic matter and moisture: they observed that moisture increases in soils containing higher amount of organic matter, which comes from plant residues.

Considering the other physical properties, there were only slight differences between the two areas, but these were not statistically significant. Bulk density and real density increased in burnt soils in contrast to control zone; this increase in density reduced the porosity, permeability and retention capacity in burnt soils.

After two years since fire, basal respiration and microbial biomass in burnt soils remained lower in all cases compared to the control zone. Therefore, the effect of this constraint on the soil biological properties can persist for multiple years after the fire passage. According to the results obtained by Holden and Treseder (2013), microbial reactions were significantly negative after fires, a reduction in microbial biomass was positively correlated with low values of microbial respiration. After the fires, Smith et al. (2008) observed a reduction in microbial biomass and diversity of microorganisms. Furthermore, Barcenas et al. (2011) reported that soil respiration decreased to lower values in contrast to unburnt reference site thirty-two months after the fire.

This decrease in basal respiration and microbial biomass was due to low rate of organic matter and moisture in these burnt soils, which prevented the rapid maintenance of microbial communities. Papa et al. (2008) suggested that a low moisture and high temperatures can be considered the most important factors affecting soil biological activities in Mediterranean ecosystems.

The metabolic quotient is used as an indicator of the physiological state of soil microorganisms. It shows how efficiently microorganisms use the available carbon in soil for their biosynthesis (Anderson, 2003). Fließbach et al. (2007) suggested that high values of  $q\text{CO}_2$  reflect the growing microbial communities with high energy needs to sustain themselves, while low values of  $q\text{CO}_2$  indicate less disturbed soils, harbouring communities, more diversified communities with more prominent mutual interactions.

Statistical analysis shows that the metabolic quotient in the burnt zone was significantly higher compared to the control zone. Therefore, the fire has a negative impact on the microbial community metabolic efficiency. This confirms our results (decrease of basal respiration and microbial biomass) and shows that the microbial population of these soils is still stressed and affected by the fire even after two years of its passage.

### Conclusion

Forest fires are one of the most widespread factors responsible for the degradation of forest ecosystems in the world, especially their frequency poses a permanent threat to the already fragile biodiversity in the Mediterranean basin. In this study, changes in the physicochemical and biological properties of forest soils after two years since the last fire were evaluated.

The results of the physicochemical properties show that, after two years since the last fire, only the soil organic matter content and soil moisture are significantly affected with lower rates in the burnt area in contrast to control zone. A slight decrease in permeability and water retention capacity is caused by a reduction in porosity resulting from the increase in bulk and real density. Considering the rest of the chemical properties, the recorded values were almost similar, indicating the absence of a significant difference between the two zones.

In terms of biological properties, the burnt zone showed lower rates of basal respiration and microbial biomass compared to unburnt zone. The metabolic quotient was significantly higher in the burnt zone in comparison to control zone, indicating persistent disturbance of the microbial community in these soils.

### Acknowledgement

All thanks are addressed to the team of the two research laboratories (Water Resources and Environment, University of Dr Moulay Tahar, Saida, Algeria, and the Faculty of Sciences and Technologies of Saint-Jerome, Mediterranean Institute of Biodiversity and Ecology, University of Aix-en-Provence, Marseille, France), for the support and contribution to the realization of this study.

### References

- ANDERSON, J. P. E. – DOMSCH, K. H. 1978. A physiological method for the quantitative measurement of microbial biomass in soils. In *Soil Biology and Biochemistry*, vol. 10, no. 3, pp. 215–221.
- ANDERSON, T. H. 2003. Microbial eco-physiological indicators to assess soil quality. In *Agriculture, Ecosystems & Environment*, vol. 98, no. 1–3, pp. 285–293.
- ANNABI, M. – BAHRI, H. – LATIRI, K. 2009. Organic status and microbial respiration of soils in northern Tunisia. In *Biotechnology, Agronomy, Society and Environment*, vol. 13, no. 3, pp. 401–408. (In French: Statut organique et respiration microbienne des sols du nord de la Tunisie).
- BARCENAS, M. G. – GARCIA, O. F. – MATAIX, S. J. – MATAIX, B. J. – BĂĂTH, E. 2011. Soil microbial recolonisation after a fire in a Mediterranean forest. In *Biology and Fertility of Soils*, vol. 47, no. 3, pp. 261–272.
- BEARE, M. H. – NEELY, C. L. – COLEMAN, D. C. – HARGROVE, W. L. 1990. A substrate-induced respiration (SIR) method for measurement of fungal and bacterial biomass on plant residues. In *Soil Biology and Biochemistry*, vol. 22, no. 5, pp. 585–594.
- BLAKE, G. R. – HARTGE, K. H. 1986. Part 1. Bulk density in physical and mineralogical methods. In: KLUTE, A. (2<sup>nd</sup> eds). *Methods of Soil Analysis*. American Society of Agronomy, Soil Science Society of America, Madison, Wisconsin USA, pp. 363–382. doi:10.2136/sssabookser5.1.2ed.c13.
- BORSALI, A. H. 2013. Contribution to the assessment of the impact of fires on forest ecosystems: case of F  nouane Forest, Ain El Hadjer town, Saida Province, Algeria. Doctoral dissertation, University of Aix-Marseille, 200 pp. (In French: Contribution    l'  valuation de l'impact des incendies sur les   cosyst  mes forestiers: cas de la For  t de F  nouane, Commune d'Ain El Hadjer, Wilaya de Saida, Alg  rie).
- CERTINI, G. 2005. Effects of fire on properties of forest soils: a review. In *Oecologia*, vol. 143, no. 1, pp. 1–10.
- EAMUS, D. – MACINNIS-NG, C. M. – HOSE, G. C. – ZEPPEL, M. J. – TAYLOR, D. T. – MURRAY, B. R. 2005. Ecosystem services: an ecophysiological examination. In *Australian Journal of Botany*, vol. 53, no. 1, pp. 1–19.
- FLIEBACH, A. – OBERHOLZER, H. R. – GUNST, L. – M  DER, P. 2007. Soil organic matter and biological soil quality indicators after 21 years of organic and conventional farming. *Agriculture, Ecosystems & Environment*, vol. 118, no. 1–4, pp. 273–274.
- GONGALSKY, K. B. – MALMSTR  M, A. – ZAITSEV, A. S. – SHAKHAB, S. V. – BENGTSSON, J. – PERSSON, T. 2012. Do burned areas recover from inside? An experiment with soil fauna in a heterogeneous landscape. In *Applied Soil Ecology*, vol. 59, pp. 73–86.
- GRANGED, A. J. – JORDAN, A. – ZAVALA, L. M. – MU  OZ-ROJAS, M. – MATAIX-SOLERA, J. 2011. Short-term effects of experimental fire for a soil under eucalyptus forest (SE Australia). In *Geoderma*, vol. 167, pp. 125–134.
- GUENON, R. – VENNETIER, M. – DUPUY, N. – ZIARELLI, F. – GROS, R. 2011. Soil organic matter quality and microbial catabolic functions along a gradient of wildfire history in a Mediterranean ecosystem. In *Applied Soil Ecology*, vol. 48, no. 1, pp. 81–93.
- HART, S. C. – DELUCA, T. H. – NEWMAN, G. S. – MACKENZIE, M. D. – BOYLE, S. I. 2005. Post-fire vegetative dynamics as drivers of microbial community structure and function in forest soils. In *Forest Ecology and Management*, vol. 220, no. 1–3, pp. 166–184.
- HOLDEN, S. R. – GUTIERREZ, A. – TRESEDER, K. K. 2013. Changes in soil fungal communities, extracellular enzyme activities, and litter decomposition across a fire chronosequence in Alaskan boreal forests. In *Ecosystems*, vol. 16, no. 1, pp. 34–46.
- HOLDEN, S. R. – TRESEDER, K. K. 2013. A meta-analysis of soil microbial biomass responses to forest disturbances. In *Frontiers in Microbiology*, vol. 4, pp. 163.
- KNICKER, H. 2007. How does fire affect the nature and stability of soil organic nitrogen and carbon? A review. In *Biogeochemistry*, vol. 85, no. 1, pp. 91–118.
- MABUHAY, J. A. – NAKAGOSHI, N. – ISAGI, Y. 2006. Soil microbial biomass, abundance, and diversity in a Japanese red pine forest: first year after fire. In *Journal of Forest Research*, vol. 11, no. 3, pp. 165–173.
- MATHIEU, C. – PIELTAIN, F. 1998. Physical analysis of soils. Selected methods. Montpellier, France: Research Institute for Development, 275 pp. ISBN 2-7430-0283-2. (In French: Analyse physique des sols: m  thodes choisies).
- MEDDOUR, S. O. 2014. Forest fires in Algeria: Risk analysis, study of causes, evaluation of the defense system and management politics. PhD Thesis in Agricultural Sciences, University of Mouloud Mammeri Tizi Ouzou, 256 pp. (In French: Les feux de for  t en Alg  rie: Analyse du risque,   tude des causes,   valuation du dispositif de d  fense et des politiques de gestion).

- MULUMBA, L. N. – LAL, R. 2008. Mulching effects on selected soil physical properties. In *Soil and Tillage Research*, vol. 98, no. 1, pp. 106–111.
- NOURAËIN, M. – KOUCHAK-KHANI, H. – JANMOHAMMADI, M. – MOHAMADZADEH, M. – ION, V. 2020. The effects of tillage and fertilizers on growth characteristics of Kabuli chickpea under Mediterranean conditions. In *Acta Technologica Agriculturae*, vol. 23, no. 1, pp. 18–23.
- PAPA, S. – PELLEGRINO, A. – FIORETTO, A. 2008. Microbial activity and quality changes during decomposition of *Quercus ilex* leaf litter in three Mediterranean woods. In *Applied Soil Ecology*, vol. 40, no. 3, pp. 401–410.
- PAYCHENG, C. 1980. Analytical methods used at the Dakar Laboratory. Nouméa, French: ORSTOM, 109 pp. [http://horizon.documentation.ird.fr/exl-doc/pleins\\_textes/divers10-09/010005303.pdf](http://horizon.documentation.ird.fr/exl-doc/pleins_textes/divers10-09/010005303.pdf) (In French: Méthodes d'analyses utilisées au laboratoire commun de Dakar).
- PÉTARD, J. 1993. Soil analysis: Methods of analysis (volume 1). Nouméa, French: ORSTOM, 192 pp. ISBN 010005303. (In French: Les méthodes d'analyses: tome 1. Analyse de sols).
- SABAGHNIA, N. – JANMOHAMMADI, M. 2014. Evaluation of selection indices for drought tolerance in some chickpea (*Cicer arietinum* L.) genotypes. In *Acta Technologica Agriculturae*, vol. 17, no. 1, pp. 6–12.
- SAETRE, P. 1998. Decomposition, microbial community structure, and earthworm effects along a birch-spruce soil gradient. In *Ecology*, vol. 79, no. 3, pp. 834–846.
- SMITH, N. R. – KISHCHUK, B. E. – MOHN, W. W. 2008. Effects of wildfire and harvest disturbances on forest soil bacterial communities. In *Applied and Environmental Microbiology*, vol. 74, no. 1, pp. 216–224.
- SMS. 2017. Climatic data. Saïda Meteorological Station.
- UROZ, S. – BISPO, A. – BUÉE, M. – CEBRON, A. – CORTET, J. – DECAENS, T. – HEDDE, M. – PERES, G. – VENNETIER, M. – AND VILLENAVE, C. 2014. Overview of advances in the field of forest soil biology. In *French Forest Review*, vol. 66, no. 4, pp. 467–477. (In French: Aperçu des avancées dans le domaine de la biologie des sols forestiers).
- VAN DER WERF, G. R. – RANDERSON, J. T. – GIGLIO, L. – COLLATZ, G. J. – MU, M. – KASIBHATLA, P. S. – VAN LEEUWEN, T. T. 2010. Global fire emissions and the contribution of deforestation, savanna, forest, agricultural, and peat fires (1997–2009). In *Atmospheric Chemistry and Physics*, vol. 10, no. 23, pp. 11707–11735.
- VENNETIER, M. – CECILLON, L. – GUENON, R. – SCHAFFHAUSER, A. – VERGNOUX, A. – BOICHARD, J. L. – MASION, A. – BOTTÉRO, J. Y. – RUY, S. – DOUSSAN, C. – GAUDU, J. C. – RENARD, D. – CURT, T. – FAIVRE, N. – RIPERT, C. – ESTÈVE, R. – MARTIN, W. – MAS, C. – MORGE, D. – BRUN, J. J. – JUVY, B. – CASSAGNE, N. – MERMIN, E. – TARDIF, P. – FAVIER, G. – DE DANIELI, S. – GROS, R. – TATONI, T. – CARRARA, M. – DOUMENQ, P. – GIULIANO, M. – MILLE, G. – MALLERET, L. – LEBARRILLER, S. – ASIA, L. – DOMEIZEL, M. – VASSALO, L. – MASSIANI, C. – THÉRAULAZ, F. – DI ROCCO, R. – CZARNES, S. – CLAYS-JOSSERAND, A. – COMMEAUX, C. – DEGRANGE, V. – GUILLAUMAUD, N. – LE ROUX, X. – POLY, F. – HOEPFFNER, M. – PIGNOT, V. – CHANDIOUX, O. 2008. Study of the impact of repeated forest fires on biodiversity and soils: search for indicators. Final report, CEMAGREF, Ministry of Agriculture and Fisheries, European Union, Aix en Provence, 236 pp. (In French: Etude de l'impact d'incendies de forêt répétés sur la biodiversité et sur les sols: recherche d'indicateurs).
- VENNETIER, M. – LADIER, J. – REY, F. 2014. Control of forest soil erosion by vegetation in the face of global changes. In *French Forest Review*, vol. 66, no. 4, pp. 467–478. (In French: Le contrôle de l'érosion des sols forestiers par la végétation face aux changements globaux).
- VERMA, S. – JAYAKUMAR, S. 2012. Impact of forest fire on physical, chemical and biological properties of soil. In *Review, Proceedings of the International Academy of Ecology and Environmental Sciences*, vol. 2, no. 3, pp. 168–176.



Acta Technologica Agriculturae 3  
Nitra, Slovaca Universitas Agriculturae Nitriae, 2020, pp. 118–125

## PREDICTIONS OF THE APPLE BRUISE VOLUME ON THE BASIS OF IMPACT ENERGY OR MAXIMUM CONTACT FORCE USING ADAPTIVE NEURO-FUZZY INFERENCE SYSTEM (ANFIS)

Farhad FAZEL<sup>1</sup>, Abdollah GOLMOHAMMADI<sup>1\*</sup>, Gholamhossein SHAHGHOLI<sup>1</sup>, Ebrahim AHMADI<sup>2</sup>

<sup>1</sup>University of Mohaghegh Ardabili, Ardabil, Iran

<sup>2</sup>Bu-Ali Sina University, Hamedan, Iran

Fruit quality drops significantly due to physical impacts and contact forces. Stress on the fruit surface during harvesting, transportation and storage operations causes bruising in its tissue and eventually result in fruit failure. Therefore, prediction of the bruise volume caused by impacts can be very important. In this research, adaptive neuro fuzzy inference system (ANFIS) was used to predict the bruise volume caused by the impacts on apples. The input parameters were the maximum contact force or impact energy; curvature radius at the contact point; temperature; and fruit mass. Its response was the bruise volume. The results show that the ANFIS models operated better in the bruise volume prediction than regression models. Between different available ANFIS models, the model based on the grid partitioning showed the best results with a mean squared error of  $MSE = 0.00015941$ , which was less than value showed by the sub-clustering mode. However, its implementation time to reach a fixed error was longer. Eventually, impact energy-based models, in contrast to maximum contact force-based models, were more capable in terms of the apple bruising prediction.

**Keywords:** stress; transport; contact point; curvature radius

Annually, large quantities of agricultural products are degraded due to bruise and other mechanical damage during harvesting, transportation, storage and packaging. One of the most important reasons for deterioration of the quality of fresh fruit market is bruising (Ahmadi et al., 2016). Common mechanical damage during harvesting and transportation of fruits is defined as plastic deformation, surface rupture and tissue destruction due to external forces (Lewis et al., 2008). The factors affecting damage severity are fruit falling height, contact energy, number of contact points, type of contact surface and size and ripeness of the fruit (Roth et al., 2005). Identifying the impact situation, which can cause bruises, is essential to improve methods and equipment for harvesting, transportation and grading process (Van Linden et al., 2006). Three important factors cause fruit damage: impact, vibration and compressive force (Diezma et al., 2006).

In order to provide models for fruit bruise prediction, it is important to determine the fruit physical properties. In recent years, certain types of equipment have been developed to simulate the dynamic impact, from among which the impact table and the pendulum device are the most applicable for impact testing of agricultural products. Since the impact location on the fruit is not controlled in the table, using pendulum to make impact and fruit bruises appears to be more reasonable (Abedi and Ahmadi, 2013). The bruise volume prediction models include main and minor variables, which are considered independent

variables. The main variables depend on the impact characteristics, and include factors such as the maximum contact force, impact energy, impact time, and falling height. The sub-variables are related to the fruit characteristics, such as temperature, stiffness, storage time, harvesting history and curvature radius (Diezma et al., 2006). Among main variables, two variables – impact energy and the maximum contact force – are mostly used for determining the bruise volume (Van Zeebroeck et al., 2007). They have both advantages and disadvantages. A model, in which the maximum contact force is an independent variable, can be generalized to materials with different curvature radius and properties. For example, bruise damage will be greater when an apple falls on a hard plate than on a second apple. But in a case of impact energy as an independent variable, the estimated bruise is the same for both. Disadvantage of the model, in which the maximum contact force is used as an independent variable, lies in the fact that contact force is a function of sub-variables, such as temperature, stiffness, curvature radius, etc. Therefore, without taking these variables into account, the estimated bruise will be inaccurate. However, model based on impact energy criterion does not have these defects (Van Zeebroeck et al., 2007). The bruise volume and dynamic yield pressure are calculated as dependent variables in the bruise prediction models (Menesatti and Paglia, 2001).

In the past, mathematical models were used to find the relationship between inputs and outputs in a process.

**Contact address:** Abdollah Golmohammadi, University of Mohaghegh Ardabili, Ardabil, Iran  
e-mail: [agolmohammadi42@yahoo.com](mailto:agolmohammadi42@yahoo.com)

However, this classical logic approach requires a precise definition of the mathematical model equations described for that phenomenon. Today, it has been proven that in many applications that fuzzy logic (FL) is superior to the classical mathematical procedures for achieving artificial intelligence (AI) solutions goals, since FL is conceptually very simple and flexible. In fact, it is easy to set up a fuzzy system to solve a complex problem using organized if-then rules (Moinfar and Shahgholi, 2019). In recent years, learning techniques have been widely used to develop uncontrolled systems for assessing the food quality (Du and Sun, 2006). In contrast to other learning techniques, ANFIS has higher training speed, effective learning algorithms and software simplicity (Jang and Sun, 1997), as well as faster convergence and better results when used without any prior knowledge (Altug et al., 1999). Hence, ANFIS as a modelling tool has been used in agricultural technology (Zheng et al., 2011); food rheology (Karaman and Kayacier, 2011); food processing (Amiryousefi et al., 2011); performance prediction (Khoshnevisan et al., 2014); and various extractions of plants and vegetables (Jhin and Hwang, 2014). Models of artificial intelligence have various applications, including in apple bruising prediction (Barreiro et al., 1997), fruit grading (Effendi et al., 2010), and apple drying process modelling (Khoshhal et al., 2010). The purpose of this study was to develop the artificial intelligence models for predicting the apple bruising using the impact energy or maximum contact force with fruit properties, such as temperature, density, and curvature radius as independent variables.

## Material and methods

For the purposes of experiment, certain numbers of apples were taken several times in 2014 from the Shend Abad Shabestar gardens. Apple samples were of Golden Delicious variety. To prevent any damage to the fruit, the harvesting was carried out manually and apples were carefully placed in plastic boxes for transportation. The fruits were stored in a refrigerator at a temperature of 3 °C at a relative humidity

of 85%. The fruits were stored at desired temperature for at least 10 hours prior to test (Ahmadi et al., 2010). The maximum duration of test conducted on each fruit was 5 minutes, in order to reduce apple warming. A total number of 58 apples was tested. The curvature radius was measured by means of radius meter on the fruit parts, which were under the test (radius meter by LG with a resolution of 0.01 mm, Fig. 1a). The fruit curvature radius measurement was carried out using Eq. 1 (Mohsenin, 1986; Fig. 1b):

$$\text{Radius} = \frac{(AC)^2}{8(BD)} + \frac{(BD)}{2} \quad (1)$$

where:

AC – distance between A and C bars (mm); BD – curvature between A and C bars (mm)

Since apples cannot be considered completely spherical, the mean of harmonic curvature radius was calculated on the basis of the circumferential and the meridian radius at the impact area.

A pendulum was used to test the fruit; it was equipped with a 57.7 cm long wooden arm, an aluminium impactor, and a place to accommodate acceleration and force sensors. The accelerometer sensor (PCB 320c33, PCB Piezotronics, USA, sensitivity: 105.2 mV·g<sup>-1</sup>) was placed on the rear sensor and then on the potentiometer sensor (PCB 208c02, PCB piezotronics, USA, sensitivity: 10.97 mV·N<sup>-1</sup>), which was on the impactor head. An incremental optical encoder (Autonic E 5058, resolution: 0.018, made in Korea) was also installed on the joint of pendulum bar (Fig. 2). The collision force was directly calculated by potentiometer, displacement rate by an accelerometer and displacement by an encoder, which basically measures the angular position of the impactor. These parameters were analysed by means of four-channel data processing system (ECON, AVANT Lite, model: MI-6004). The description of calculated parameters by the pendulum through the energy method has been described in detail by Abedi and Ahmadi (2013).

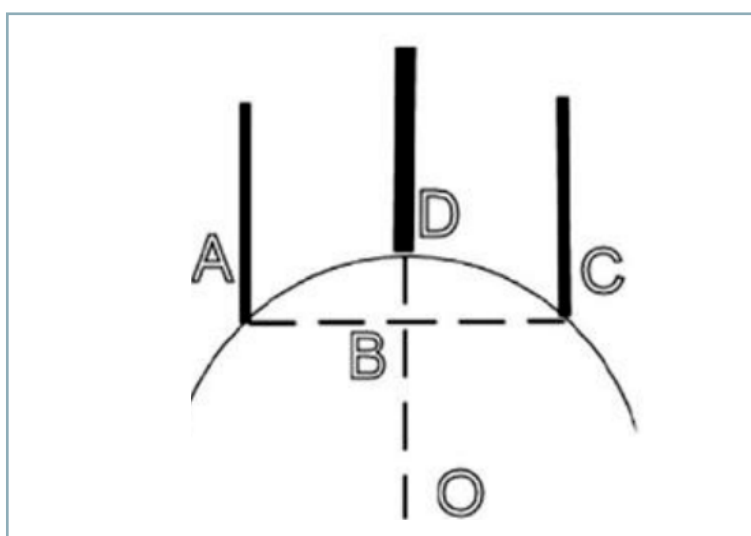
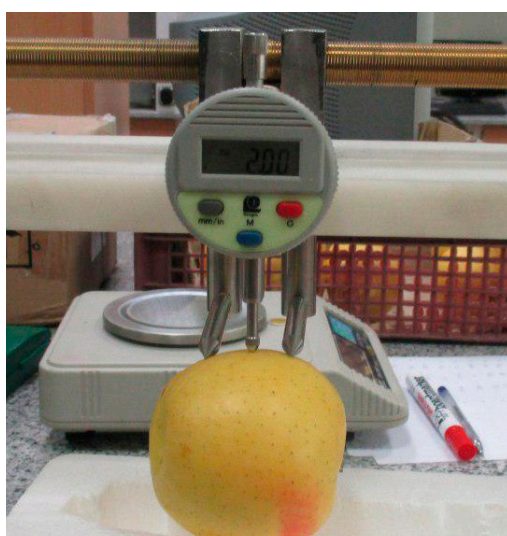


Fig. 1 Curvature radius meter (a); required dimensions to compute the curvature radius (b)

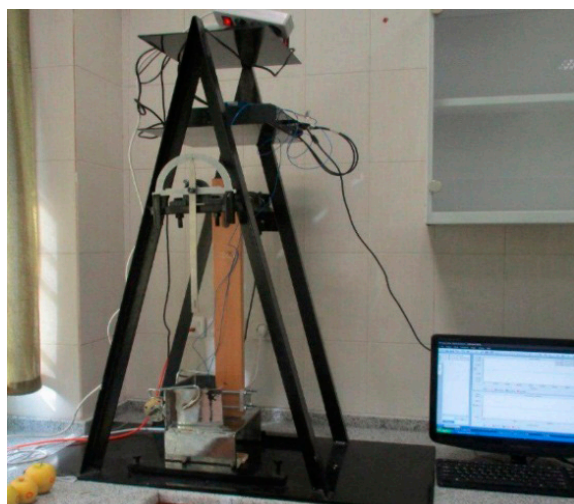


Fig. 2 Pendulum (a); impactor (b)

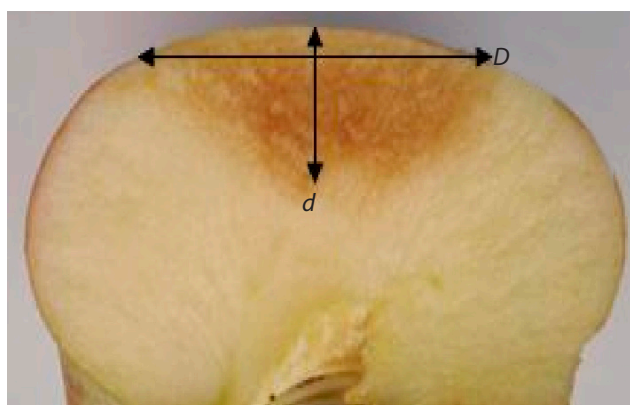


Fig. 3 Measurement of the diameter and depth of the bruise in apple cross section

The bruise volume was used as a dependent variable in bruise prediction models. The apple was observed after twenty-four hours post-impact; the diameter of the impacted bruise surface was measured, and subsequently, the thickness was measured by making a vertical shear perpendicular to the bruise surface (Fig. 3). Finally, the bruise volume was calculated according to the method used by Chen and San (1981):

$$BV = \frac{\pi}{6}dD^2 \quad (2)$$

where:

$BV$  – bruise volume ( $\text{mm}^3$ );  $d$  – bruise depth (mm);  $D$  – bruise diameter (mm)

Bruise prediction models include either impact energy, or maximum contact force at the moment of collision as major independent variables and other input factors are minor independent variables. Independent variables used in the regression and ANFIS models are:  $E$  – impact energy,  $J$ ;  $PF$  – peak force,  $N$ ; two fruit temperatures ( $T$ ) of 3 and 20 °C;  $R$  – curvature radius at the contact location, mm;  $\rho$  – apple density ( $\text{kg}\cdot\text{m}^{-3}$ ).

Multiple stepwise regression was used to form the bruising patterns. This method analyses were carried out in Minitab 18 software.

Adaptive neural network (ANFIS) as a basis for fuzzy inference systems

The principle of ANFIS is based on fuzzy inference system (FIS) input/output data. This system is based on the rules of combination of three components: membership functions of input/output variables (fuzzy), fuzzy rules (rule base), mechanism inference (combination of rules with fuzzy input), and output and system results characteristics (defuzzification) (Krueger et al., 2011). Frequently, ANFIS systems are using Takagi-Sugno-Kang (TSK) fuzzy system (TSK), which is a progressive network structure.

For simplicity, it was assumed that the fuzzy system has two inputs –  $x$  and  $y$  – and an output –  $z$ . The rules are as follows.

$$\text{Rule 1: if } x \text{ is } A_1 \wedge y \text{ is } B_1 \text{ then } f_1 = P_1x + q_1y + r_1 \quad (3)$$

$$\text{Rule 2: if } x \text{ is } A_2 \wedge y \text{ is } B_2 \text{ then } f_2 = P_2x + q_2y + r_2 \quad (4)$$

If the centre method is used for defuzzifying (converting the final system output to a classical number), the output will be as follows:

$$f = \frac{w_1}{w_1 + w_2}f_1 + \frac{w_2}{w_1 + w_2}f_2 = \overline{w_1}f_1 + \overline{w_2}f_2 \quad (5)$$

The ANFIS equivalent structure with five layers will be as follows (Fig. 4).

Layer 1 (input nodes): in this layer, the membership degree of input nodes to different fuzzy intervals is determined using the membership function:

$$O_i^1 = \mu_{A_i}(x) \text{ for } i = 1, 2 \wedge O_i^1 = \mu_{B_i}(y) \text{ for } i = 1, 2 \quad (6)$$

The Gaussian membership function  $\mu_{A_i}(x)$  is expressed in terms of the parameter set  $a_i, c_i$  (initial parameters) and the input  $x$  of the  $i^{\text{th}}$  node.

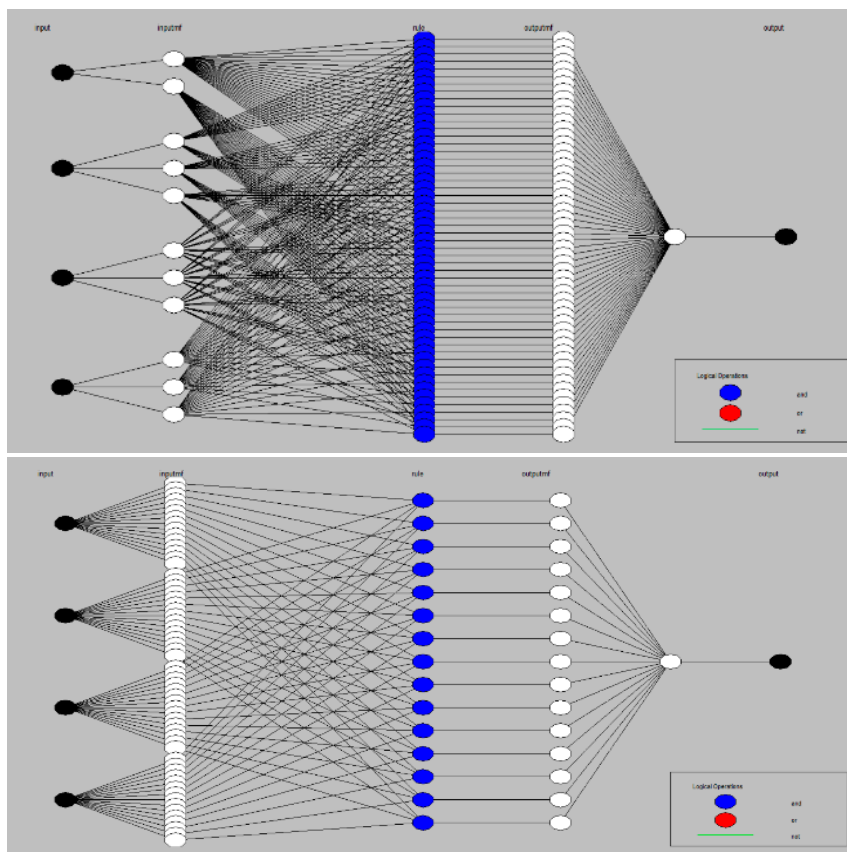


**Fig. 4** The structure of the best ANFIS models for bruising prediction: Inference system using grid partitioning method (a); Inference system using sub-clustering method (b)

$$\mu_{A_i}(x) = \exp\left[-\left(\frac{x - c_i}{a_i}\right)^2\right] \quad (7)$$

Layer 2 (rule nodes): each node in this layer calculates the degree of a rule activity.

$$O_i^2 = w_i = \mu_{A_i}(x) \times \mu_{B_i}(y) \quad (8)$$

$i = 1, 2$

Layer 3: the output of this layer is the normalized to the previous layer:

$$O_i^3 = \bar{w}_i = \frac{w_i}{w_1 + w_2} \quad (9)$$

$i = 1, 2$

Layer 4 (output nodes): in this output layer, each node is equal to:

$$O_i^4 = \bar{w}_i f_i = \bar{w}_i (p | i x + q_i y + r_i) \quad (10)$$

Layer 5 (output nodes): in this layer, each node calculates the final output

value as follows (the number of nodes is equal to the number of outputs):

$$\text{Overall output} = O_i^5 = \sum_i \bar{w}_i f_i = \frac{\sum_i w_i f_i}{\sum_i w_i} \quad (11)$$

The training of these systems means that educational data, the nonlinear parameters related to the fuzzy membership functions in the first layer and the linear parameters of the fourth layer are determined so that the desired output is obtained for the desired input. The hybrid training method is one of the most important methods for teaching the fuzzy inference systems based on the adaptive neural network. In this method, for the first layer, the method of post-propagation error is used, while in the fourth layer, the least squares estimation method is used (Jang and Sun, 1997). In this paper, several models were provided on the basis of preceding parameters in MATLAB software (Version7.12.0) and in Fuzzy Logic Toolbox.

## Results and discussion

Several models were developed on the basis of the ANFIS techniques and stepwise regression to predict the bruise volume value. The first series of models used the maximum contact force as input parameter; the second series used the impact energy for this purpose. Among the developed models, models with a higher coefficient of determination ( $R^2$ ) were presented in Tables 1 and 2 in order to compare their performance. As shown in Tables 1 and 2, ANFIS models have the highest mean squared error (MSE) and determination coefficient ( $R^2$ ); the step-by-step regression models have the lowest determination coefficient ( $R^2$ ).

### Comparison of ANFIS models

Among different ANFIS configurations, grid partitioning-based model had a higher  $R^2$  than the sub-clustering model, but its execution time to get the fixed error took longer. This can be attributed to the number of rules created in each of these models. In a grid partitioning-based model, the space of each input is divided into equal intervals, and a rule is set in each of the multidimensional spaces derived from all different input combinations. As a result, the number of rules increases with increasing inputs. In a sub-clustering model, data mining is first performed on a data set; the spaces, in which there is a higher number of data, are identified for each input, and instead of dividing inputs into equal intervals in areas, in which the number of data is greater, membership functions are created with smaller intervals. Therefore, rules are created only in certain domains and the number of rules decreases. Fig. 4 shows the general structure of the two network separation methods. It also demonstrates different clustering, in which the grid partitioning has 54 rules and the sub-clustering model has 15 rules. The higher the number of rules, the more precise and slower the network execution. Such behaviour has also been reported by Ay and Kisi (2014).

**Table 1** Results of adaptive neuro-fuzzy inference system and stepwise regression for the bruise volume prediction on the basis of maximum contact force (*F*), curvature radius (*R*), temperature (*T*) and mass (*M*)

| Model             | Type of MF                                    |              | Number of MF  |       | Optimization method | RMSE       | R <sup>2</sup> |
|-------------------|---|--------------|---------------|-------|---------------------|------------|----------------|
|                   | input   | output       | input         | epoch |                     |            |                |
| Grid partitioning | trimf   | linear       | 2 3 3 3       | 20    | hybrid              | 0.00017625 | 1              |
| Grid partitioning | gaussmf                                       | linear       | 2 3 3 3       | 20    | hybrid              | 0.00059748 | 1              |
| Grid partitioning | trmf  | linear       | 2 3 3 3       | 20    | hybrid              | 0.00017041 | 1              |
| Grid partitioning | gbellmf                                       | linear       | 2 3 3 3       | 20    | hybrid              | 0.0011199  | 1              |
|                   | reject ratio                                  | accept ratio | squash factor |       | range of influence  | –          |                |
| Sub-clustering    | 0.15  | 0.5          | 1.25          |       | 0.5                 | 0.0020133  | 1              |
| Regression        | $BV = 103.821 + T - 2.595R + 4.037F - 0.334M$ |              |               |       |                     | –          | 0.6842         |

**Table 2** Comparative neural fuzzy inference system and stepwise regression for the bruise volume prediction on the basis of impact energy (*E*), curvature radius (*R*), temperature (*T*), mass (*M*)

| Model             | Type of MF   |              | Number of MF  |       | Optimization method | RMSE       | R <sup>2</sup> |
|-------------------|--|--------------|---------------|-------|---------------------|------------|----------------|
|                   | input  | output       | input         | epoch |                     |            |                |
| Grid partitioning | trimf  | linear       | 2 3 3 3       | 20    | hybrid              | 0.00016625 | 1              |
| Grid partitioning | gaussmf  | linear       | 2 3 3 3       | 20    | hybrid              | 0.00023578 | 1              |
| Grid partitioning | trmf   | linear       | 2 3 3 3       | 20    | hybrid              | 0.00015941 | 1              |
| Grid partitioning | gbellmf  | linear       | 2 3 3 3       | 20    | hybrid              | 0.0011012  | 1              |
|                   | reject ratio   | accept ratio | squash factor |       | range of influence  | –          |                |
| Sub-clustering    | 0.15   | 0.5          | 1.25          |       | 0.5                 | 0.0033166  | 1              |
| Regression        | $BV = 128.143 + 0.854T - 1.459R + 2,559.185E - 0.318M$ |              |               |       |                     | –          | 0.6954         |

**Membership functions comparison**

Four types of the most common fuzzy membership functions were used in this study. These functions include Gaussian, triangular, trapezoidal, and generalized bell functions (Fig. 5). For both models, the trapezoidal membership function showed the maximum contact force, as well as impact energy, having the best performance and

the lowest mean squared error (MSE). The triangular and Gaussian membership functions are ranked the second in terms of performance, respectively. Such functions are also derived from the membership functions in other researches (Taghavifar and Mardani, 2014).

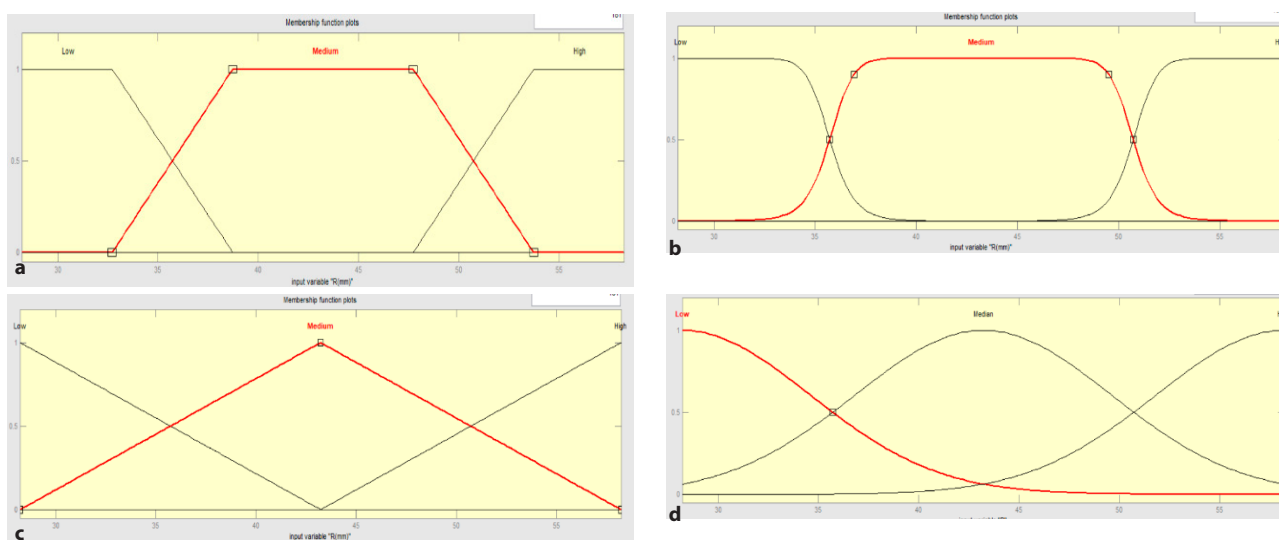


**Fig. 5** Membership functions  
a – trapezoidal; b – generalized bell; c – triangular; d – Gaussian

**Table 3** Statistical characteristics of stepwise regression model for the bruise volume prediction (*BV*) on the basis of maximum force (*F*); curvature radius (*R*); temperature (*T*); mass (*M*)

| Model   | Equation parameters | Unstandardized coefficients |            | Standardized coefficients |        |       |
|---|---------------------|-----------------------------|------------|---------------------------|--------|-------|
|   |                     | B                           | Std. error | Beta                      | t      | sig   |
| $BV = 103.821 + T - 2.595R + 4.037F - 0.334M$ | constant            | 103.821                     | 75.113     |                           | 1.382  | 0.179 |
|   | T                   | 1.000                       | 1.273      | 0.082                     | 0.786  | 0.439 |
|   | R                   | -2.595                      | 2.118      | -0.168                    | -1.225 | 0.232 |
|   | F                   | 4.037                       | 0.524      | 0.801                     | 7.708  | 0.000 |
|   | M                   | -0.334                      | 0.381      | -0.110                    | -0.875 | 0.390 |

**Table 4** Statistical characteristics of stepwise regression model for the bruise volume prediction (*BV*) on the basis of impact energy (*E*); curvature radius (*R*); temperature (*T*); mass (*M*)

| Model  | Equation parameters | Unstandardized coefficients |            | Standardized coefficients |        |       |
|--|---------------------|-----------------------------|------------|---------------------------|--------|-------|
|  |                     | B                           | Std. error | Beta                      | t      | sig   |
| $BV = 128.143 + 0.854T - 1.459R + 2,559.185E - 0.318M$ | constant            | 128.143                     | 74.459     |                           | 1.721  | 0.098 |
|  | T                   | 0.854                       | 1.293      | 0.070                     | 0.666  | 0.515 |
|  | R                   | -1.459                      | 2.210      | -0.094                    | -0.660 | 0.515 |
|  | E                   | 2559.185                    | 339.202    | 0.819                     | 7.545  | 0.000 |
|  | M                   | -0.318                      | 0.387      | -0.105                    | -0.823 | 0.418 |

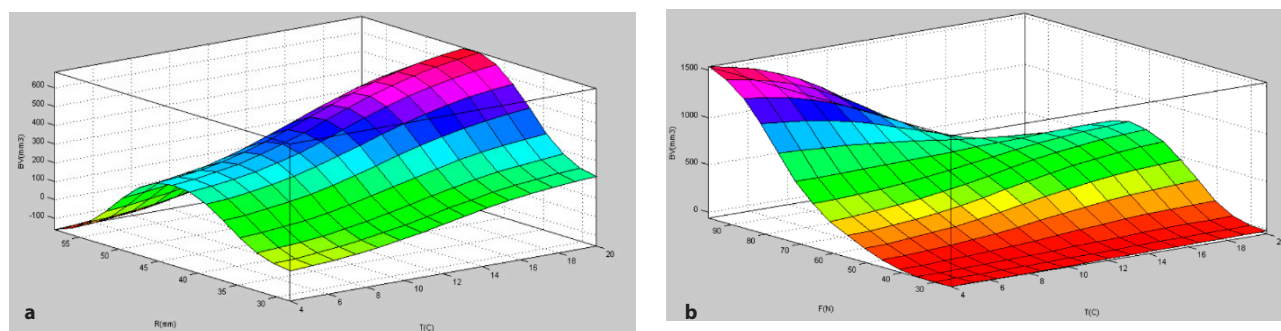
### Comparison of regression models

Two different models were developed to predict the bruise volume. The first model used the maximum contact force as an independent variable and the second model used the impact energy as an independent variable. Both models provided relatively low performance in terms of prediction. Both models showed determination coefficient  $R^2$  of 0.758 and 0.776 for the maximum contact force and impact energy models, respectively. The statistical analysis of data of these models are shown in Tables 3 and 4, respectively. These results can be attributed to the nonlinear behaviour of biological materials under the effect of mechanical changes, which makes it difficult to model such phenomena using regression models. Impact energy-based models, as they have been mentioned by multiple researchers (Ahmadi et al., 2010; Abedi and Ahmadi 2013), are more capable of the bruise volume prediction. The reason is that the maximum

contact force depends on its sub-variables: temperature, stiffness, bending radius, etc.

### Observation of the surface curves

The output results of the ANFIS models are three-dimensional diagrams, which indicate the effect of changes in input parameters on the output (*T*, *R*, *F*, *M* are input variables and *BV* is the model output, Fig. 6A, B). As shown in Fig. 6A, B a, b, d, with an increase in the maximum contact force, the bruise volume also greatly increased, which has been reported in numerous studies (Ahmadi et al. 2010; Van Linden et al., 2006). The fruit bruise from the impact varies on the basis of fruit tissue and environment temperature. At lower temperatures, the force effect on the bruise is considered much more severe. According to Fig. 6A, B a, d, e, it is evident that, in fruits with a smaller curvature radius, more damage occurred due to the impact. The fact is that, at

**Fig. 6A** 3D Curves of the bruise volume versus effects of input factors a – temperature – curvature radius; b – temperature – maximum force

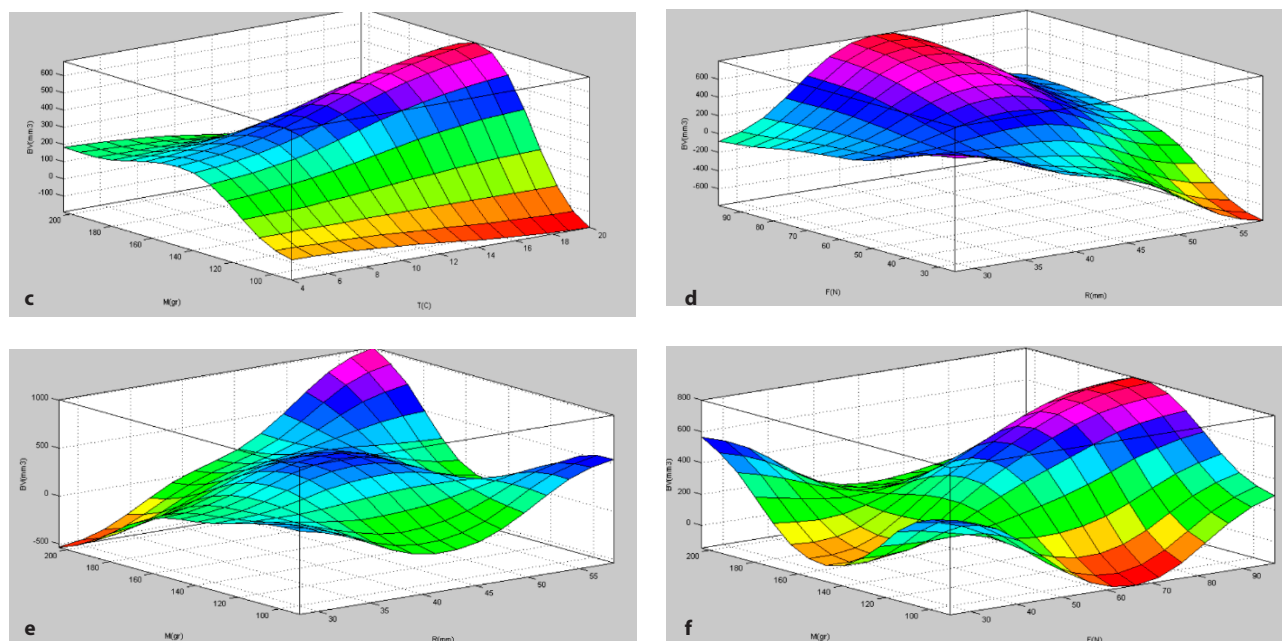


**Fig. 6B** 3D Curves of the bruise volume versus effects of input factors  
 c – temperature – mass; d – curvature radius – maximum force; e – curvature radius – mass; f – maximum force – mass

the point in which the impact occurs, if the curvature radius and area under tension are small, the tension will be greater at this point (Ahmadi et al., 2010). Given the existing forms, it is not possible to give a definitive account of the temperature effect on the bruise volume. In Fig. 6A b, c, the bruise volume decreases with increasing temperature; however, in Fig. 6A a, there is almost a different trend in the temperature effect on the fruit bruise volume. This can be due to other factors involved in this phenomenon, the effect of which cannot be ignored. Therefore, careful examination of the temperature effect on the bruise volume by conduction of special tests and analyses is recommended.

### Conclusion

1. ANFIS models presented a much better performance than regression models in terms of the bruise volume prediction. All ANFIS models showed a coefficient of determination value exceeding 0.95, while regression models reached a coefficient of determination of less than 0.7.
2. Among the ANFIS models, the created models based on the grid partitioning method were more accurate; however, the models based on the sub-clustering mode had faster runtime.
3. Models using impact energy as an independent variable under all ANFIS conditions, as well as regression models, showed better accuracy than the models using maximum contact force models as an independent variable.

### References

ABEDI, G. – AHMADI E. 2013. Design and evaluation a pendulum device to study postharvest mechanical damage in fruits: Bruise modeling of red delicious apple. In *Australian Journal of Crop Science*, vol. 7, no. 7, pp. 962–968.

AHMADI, E. – BARIKLOO, H. – KASHFI, M. 2016. Viscoelastic finite element analysis of the dynamic behavior of apple under impact loading with regard to its different layers. In *Computers and Electronics in Agriculture*, vol. 121, pp. 1–11.

AHMADI, E. – GHASSEMZADEH, H. R. – SADEGHI, M. – MOGHADDAM, M. – ZARIFNESHAT, S. 2010. The effect of impact and fruit properties on the bruising of peach. In *Journal of Food Engineering*, vol. 97, pp. 110–117.

AMIRYOUSEFI, M. R. – MOHEBBI, M. – KHODAIYAN, F. – ASADI, S. 2011. An empowered adaptive neuro-fuzzy inference system using self-organizing map clustering to predict mass transfer kinetics in deep-fat frying of ostrich meat plates. In *Computers and Electronics in Agriculture*, vol. 76, pp. 89–95.

AY, M. – KISI, O. 2014. Modelling of chemical oxygen demand by using ANNs, ANFIS and k-means clustering techniques. In *Journal of Hydrology*, vol. 511, pp. 279–289.

ALTUG, S. – CHOW, M. Y. – TRUSSELL, H. J. 1999. Fuzzy inference systems implemented on neural architectures for motor fault detection and diagnosis. In *IEEE Transactions on Industrial Electronics*, vol. 46, no. 6, pp. 1069–1079.

BARREIRO, P. – STEINMETZ, V. – RUIZ-ALTISENT, M. 1997. Neural bruise prediction models for fruit handling and machinery evaluation. In *Computers and Electronics in Agriculture*, vol. 8, pp. 91–103.

CHEN, P. – SUN, Z. 1981. Impact parameters related to postharvest bruising of apples. ASAE Paper No. 81, pp. 3041, St. Joseph, Michigan.

DIEZMA, B. – VALERO, C. – GARCIA-RAMOS, F. J. – RUIZ-ALTISENT, M. 2006. Monitoring of firmness evolution of peaches during storage by combining acoustic and impact methods. In *Journal of Food Engineering*, vol. 77, pp. 926–935.

DU, C. J. – SUN, D. W. 2006. Learning techniques used in computer vision for food quality evaluation: a review. In *Journal of Food Engineering*, vol. 72, no. 1, pp. 39–55.

EFFENDI, Z. – RAMLI, R. – GHANI, J. A. 2010. A back propagation neural networks for grading *Jatropha curcas* fruits maturity. In *American Journal of Applied Sciences*, vol. 7, no. 3, pp. 390–394.

- JANG, J. S. R. – SUN, C. T. 1997. Neuro-fuzzy modeling and control. In Proceedings of IEEE, vol. 83, no. 3, pp. 378–405.
- JHIN, C. – HWANG, K. T. 2014. Prediction of radical scavenging activities of anthocyanins applying adaptive neuro-fuzzy inference system (ANFIS) with quantum chemical descriptors. In International Journal of Molecular Sciences, vol. 15, pp. 14715–14727.
- KARAMAN, S. – KAYACIER, A. 2011. Effect of temperature on rheological characteristics of molasses: Modeling of apparent viscosity using Adaptive Neuro-Fuzzy Inference System (ANFIS). In LWT–Food Sciences, vol. 44, pp. 1717–1725.
- KHOSHHAL, A. – ALIZADEH, A. – ETEMADI, A. – ZERESHKI, S. 2010. Artificial neural network modeling of apple drying process. In Journal of Food Process Engineering, vol. 33, pp. 298–313.
- KHOSHNEVISAN, B. – RAFIEE, S. – OMID, M. – MOUSAZADEH, H. 2014. Prediction of potato yield based on energy inputs using multi-layer adaptive neuro-fuzzy inference system. In Measurement, vol. 47, pp. 521–530.
- KRUEGER, E. – PRIOR, S. A. – KURTENER, D. – ROGERS, H. H. – RUNION, G. B. 2011. Characterizing root distribution with adaptive neuro-fuzzy analysis. In International Agrophysics, vol. 25, pp. 93–96.
- LEWIS, R. – YOXALL, A. – MARSHALL, M. B. – CANTY, L. A. 2008. Characterising pressure and bruising in apple fruit. In Wear, vol. 264, pp. 37–46.
- MENESATTI, P. – PAGLIA, G. 2001. Development of a drop damage index of fruit resistance to damage. In Journal of Agricultural Engineering Research, vol. 80, pp. 53–64.
- MOHSENIN, N. N. 1986. Physical Properties of Plant and Animal Materials. Gordon and Breach Science Publishers, New York.
- MOINFAR, A. – SHAHGHOLI, G. 2019. The effect of tractor driving system type on its slip and rolling resistance and its modelling using ANFIS. In Acta Technologica Agriculturae, vol. 4, pp. 116–122.
- ROTH, E. – KOVACS, E. – HERTOOG, M. – VANSTREELS, E. – NICOLAI, B. 2005. Relationship between physical and biochemical parameters in apple softening. In Proceedings of the 5<sup>th</sup> International Postharvest Symposium (PS'05), ISHS, pp. 573–578.
- TAGHAVIFAR, H. – MARDANI, A. 2014. On the modeling of energy efficiency indices of agricultural tractor driving wheels applying adaptive neuro-fuzzy inference system. In Journal of Terramechanics, vol. 56, no.1, pp. 37–47.
- VAN LINDEN, V. – SCHEERLINCK, N. – DESMET, M. – DE BAERDEMAEKER, J. 2006. Factors that affect tomato bruise development as a result of mechanical impact. In Postharvest Biology and Technology, vol. 42, pp. 260–270.
- VAN ZEEBROECK, M. – VAN LINDEN, V. – DARIUS, P. – DE KETELAERE, B. – RAMON, H. – TIJSKENS, E. 2007. The effect of fruit factors on the bruise susceptibility of apples. In Postharvest Biology and Technology, vol. 46, pp.10–19.
- ZHENG, H. – FANG, S. S. – LOU, H. Q. – CHEN, Y. – JIANG, L. L. – LU, H. F. 2011. Neural network prediction of ascorbic acid degradation in green asparagus during thermal treatments. In Expert Systems with Applications, vol. 38, pp. 5591–5602.



Acta Technologica Agriculturae 3  
Nitra, Slovaca Universitas Agriculturae Nitriae, 2020, pp. 126–131

## METHANE PRODUCTION POTENTIAL OF AZOLLA UNDER DIFFERENT RATIOS OF C/N, CHEMICAL AND THERMAL PRE-TREATMENT

Majid FARDMANESH, Razieh POURDARBANI\*, Bahman NAJAFI

University of Mohaghegh Ardabili, Ardabil, Iran

Azolla algae currently represent a major threat to the environment and rice cultivation fields. Various studies have shown that one of the practical solutions is to turn this threat into an opportunity for biomass energy production. This research investigates the production potential of methane in Azolla. Test was conducted in a completely randomized design (CRD) with Mini Tap software. Three different C/N ratios, 30, 34 and 38, two levels of thermal pre-treatment (raw and steamed Azolla) and two levels of chemical pre-treatment (NaOH 0% and 9%) were used and effects of each case on the methane production rate was studied. The highest amount of methane ( $247.7 \text{ ml}\cdot\text{g}^{-1}_{\text{vs}}$ ) was produced at C/N ratio of 30 with application of NaOH (9%) and no thermal pre-treatment (raw Azolla). ANOVA analysis showed that interactions of the effective variables were significant, but the trend was not incremental or decreasing; therefore, ANFIS and stepwise regression modelling were used. The results showed that the ANFIS model provides more accurate mapping between the empirical and predicted values than the regression model. Furthermore, among examined models (triangular; trapezoidal; Gaussian; bell-shaped models), the best model for methane production prediction was Gaussian linear membership function ( $R^2 = 0.997$  and  $\varepsilon (\%) = 0.32$ ). According to the regression model, the thermal-chemical factor is the most efficient in prediction of the model ( $b = 35.6$ ).

**Keywords:** Azolla algae; ANFIS; C/N ratio; regression model

Azolla is a floating aquatic fern that grows rapidly in stagnant waters and ponds and covers the water surface. This coating is very dangerous for aquatic organisms by creating a layer at the water level, which prevents the sunlight from reaching other herbaceous grasses, thus preventing their growth. Transfer of Azolla from the Philippines to Iran (Gilan province) had unpleasant consequences over the last few years. It is accessible throughout the year, and although this plant is not native to Iran, it adapted and rapidly expands. Currently, the plant is a major threat to the northern region of Iran, and considerable costs are annually spent on collection of this algae from the environment. However, after its collection, it can be put to some use. Anaerobic digestion of Azolla with cow dung is an alternative for C/N ratio modification in order to increase the gas production – Azolla fixes atmospheric N, thus reducing the necessary amount of cow dung for biogas production (Paudel, 2009). Wilkie (2000) reported that anaerobic digestion is a natural process converting the biomass to energy. Yadava and Hesse (1981) declared that biogas consists of 50–70%  $\text{CH}_4$ ; 30–40%  $\text{CO}_2$ ; 5–10%  $\text{H}_2$ ; 1–2% N and  $\text{H}_2\text{S}$ . Based on the reports, biomass can be considered an energy source with potential to satisfy 14% of global energy demand. In developed countries, this share is estimated to be 40–50% (Anonymous, 2013). Biomass utilization can reduce the greenhouse gas emissions, as it can balance the production and consumption of carbon dioxide. From all alternative sources, biomass represents

the main source for renewable energy production (Adelard et al., 2015). Utilization of biogas technology at micro- and macro-scales has been considered as a promising approach, especially in development planning, organic waste management in urban and rural areas (Abdeshahian et al., 2016; Kažimírová et al., 2018). Research on methane production from Azolla is scarce; Das et al. (1994) studied the biogas production from Azolla – authors mixed Azolla and cow dung in different proportions, namely 1 : 0.2, 1 : 0.4 and 1 : 0.6. They observed that the ratio of 1 : 0.4 showed the highest biogas production. Roy et al. (2016) also found that the amount of produced hydrogen increases when the Azolla is cultivated in a controlled environment with incomplete vacuum and injection of either argon gas or rich carbon dioxide into the cultivation bed. Shilpakar and Shilpakar (2009) reported that, with high C/N ratio, nitrogen was rapidly consumed by methanogens in order to meet the protein requirements, which no longer reacted with leftover C content, resulting in a low gas production. On the other hand, with low C/N ratio, N was accumulated in the form of ammonia, which increased pH. Tasnim et al. (2017) investigated the biogas production by means of an anaerobic digestion of cow manure with kitchen waste and hyacinths. Basri et al. (2010) studied the biogas production from palm leaves. Phetyima et al. (2015) examined the biogas production from vegetable waste with dog and cattle manure.

**Contact address:** Razieh Pourdarbani, University of Mohaghegh Ardabili, Faculty of Agriculture & Natural Sciences, Department of Biosystem Engineering, Ardabil, Iran, 56199-11367, 00989143162785, e-mail: [r\\_pourdarbani@uma.ac.ir](mailto:r_pourdarbani@uma.ac.ir)

All in all, Azolla is considered a threat to Anzali wetland due to the aforementioned disadvantages. One of the practical solutions is to turn this threat into an economically viable opportunity, which would be possible with the construction of biogas production reservoirs. Therefore, this research attempts to identify the variables affecting the production potential of methane from Azolla using ANFIS and regression modelling.

## Material and methods

### Methane production method

Firstly, Azolla was collected from Anzali Lagoon. Subsequently, dung was collected from the dairy; in order to enrich it, an amount of water equivalent to the cow dung weight (1 kg) was added to it. Before mixing Azolla and cow dung, samples of both were sent to the laboratory in order to determine the C/N ratio: 73/26 for cow dung and 65/65 for Azolla. There were examined two levels of chemical pre-treatment (with NaOH content of 9% and 0%); two levels of thermal pre-treatment (steamed Azolla for 60 min, and raw Azolla without thermal pre-treatment) and three C/N ratios of 30, 34, 38.

By determining the amounts of cow dung, Azolla and water (as shown in Table 1), the bottles were loaded. In order to establish the constant temperature of 37 °C, these were placed in a hot water bath (under the conditions of the mesophilic bacteria) and the gas production stage began. For the purposes of the produced gas transfer, a pipe was provided on the doors of the digesters, transferring the produced gas to the bottles outside the heated bath. The useful gas extracted from biogas with high thermal value is methane. Therefore, the method of positive displacement of liquids (water) was used to determine the methane in the biogas. It was examined twice a day and the quantities of gas produced from each digestion were measured. Each digestion lasted for 90 days.

### Data analysis method

The model was based on 4 input factors, including time of thermal pre-treatment (steamed Azolla; raw Azolla), chemical pre-treatment (NaOH 9%; 0%), C/N ratio (33; 34; 38) and number of days (90 days). Four types of membership functions (triangular, trapezoidal, Gaussian, and bell-shaped functions) were considered as membership functions for representing the inputs.

Hybrid optimization method was used for network learning. The number of rules created by the network was 36. Due to the high number of rules created, only a few of

**Table 1** Ratios for each biogas production digester

| Sample | Water   | Azolla  | Cow dung | C/N | NaOH 9% | NaOH 0% | Steamed Azolla | Raw Azolla |
|--------|---------|---------|----------|-----|---------|---------|----------------|------------|
| 1      | 1,107.5 | 59.1    | 333      | 30  |         | *       |                | *          |
| 2      | 1,215.1 | 118.2   | 166.6    | 34  |         | *       |                | *          |
| 3      | 1,322.7 | 177.3   | 0        | 38  |         | *       |                | *          |
| 4      | 1,107.5 | 59.1    | 333      | 30  | *       |         |                | *          |
| 5      | 1,215.1 | 118.3   | 166.6    | 34  | *       |         |                | *          |
| 6      | 1,322.7 | 177.3   | 0        | 38  | *       |         |                | *          |
| 7      | 824.3   | 342.7   | 333      | 30  |         | *       | *              |            |
| 8      | 652.4   | 680.8   | 166.6    | 34  |         | *       | *              |            |
| 9      | 478.7   | 1,021.2 | 0        | 38  |         | *       | *              |            |
| 10     | 824.3   | 342.7   | 333      | 30  | *       |         | *              |            |
| 11     | 652.4   | 680.8   | 166.6    | 34  | *       |         | *              |            |
| 12     | 478.7   | 1,021.2 | 0        | 38  | *       |         | *              |            |

**Table 2** Part of the rules for the methane production model

| Rules | Input variables |      |     |     | Linear output function (methane)                       |
|-------|-----------------|------|-----|-----|--|
|       | thermal         | NAOH | Day | C/N |  |
| 6     | S               | L    | M   | H   | methane = 2,392M + 0N - 15,060D + 18,180 + 478.4       |
| 12    | S               | H    | L   | H   | methane = 2.957M + 5.322N - 1,140D + 22.47C + 0.5913   |
| 18    | S               | H    | H   | H   | methane = 352.8M + 635.1N - 1,156D + 2,681C + 70.56    |
| 24    | R               | L    | M   | H   | methane = 34,230M + 0N - 67,810D + 65,030C + 1,711     |
| 30    | R               | H    | L   | H   | methane = 234.9M + 105.7N - 23,160D + 446.4C + 11.75   |
| 36    | R               | H    | H   | H   | methane = 22,160M + 9,971N - 23,130D + 42,100C + 1,108 |

them are presented in Table 2 in order to better understand ANFIS modelling. These rules are based on a Sugden-Tang-Sugden-Kang fuzzy system or TSK. In this system, the rules of if-then are fuzzy, but the result is non-phase and linear combination of input variables. The space of all inputs is divided into two parts, the low region representing the membership function L and the greater region representing the membership function H.

$$\varepsilon = \frac{100}{N} \sum_{i=1}^N \frac{Y_{measured} - Y_{predicted}}{Y_{measured}} \quad (1)$$

$$R^2 = \frac{\sum_{i=1}^N (Y_{measured} - Y_{predicted})^2}{\sum_{i=1}^N (Y_{measured} - \bar{Y})^2} \quad (2)$$

To evaluate the ability of developed models, two statistical measures of relative error ( $\varepsilon$ ) and coefficient of determination ( $R^2$ ) were used, which are given by the following equations (Carman, 2008):

Models based on stepwise linear regression in SPSS software were developed to obtain more information on the effects of each input variable on methane production.

## Material and methods

Considering the samples with C/N ratio of 30 (1, 4, 7 and 10) methane production was low since the first days until the 20<sup>th</sup> day; however, it began to rise since the 20<sup>th</sup> day onwards. At the start of production, raw Azolla pre-treated with NaOH (0%) showed higher production increase, but eventually, raw Azolla pre-treated with NaOH (9%) showed greater methane production. In fact, chemical pre-treatment accelerates degradation of Azolla lignin and hard substances by destroying the material structure and increases the availability of microorganisms for gaining high production (Zhang et al., 2013). Chemical pre-treatment can manage pH, prevent excessive acidification of digestion by degradation of hard tissues before the hydrolysis and acidification step, and cause the biogas production to be higher in the first peak in contrast to control treatment (Janke et al., 2016).

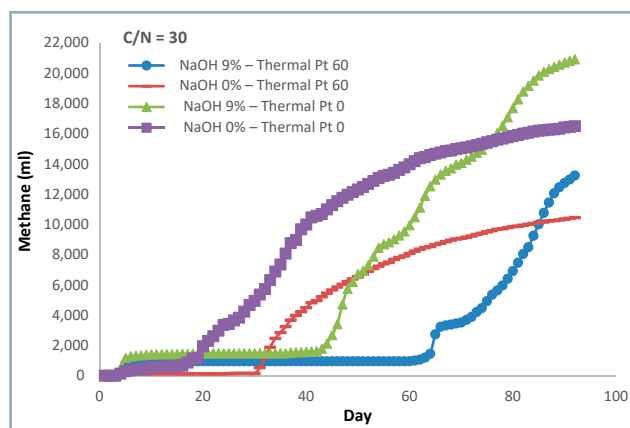


Fig. 1 Cumulative methane production rate of samples 1, 4, 7 and 10 with C/N ratio of 30

Fig. 2 demonstrates that, although steamed Azolla started production of methane faster than raw Azolla, higher methane production was observed in raw Azolla. Furthermore, by addition of NaOH (9%), methane bacteria can be active from the beginning in an alkaline environment, since they feed on acetic acid, and microorganisms must be first activated in the acidic environment. Conversion of conditions should be performed in such a manner that the micro-nutrient bed provides the activity field for methane microorganisms. Process of these chain transitions causes methane production to be delayed or start early. In relation to the C/N ratio of 30, this situation is most pronounced. Regarding C/N ratios of 34 and 38, the higher the carbon-nitrogen ratio, the faster the acidic environment neutralization of these conditions; this is the reason why C/N ratio of 30 showed the highest production (Shilpakar and Shilpakar, 2009).

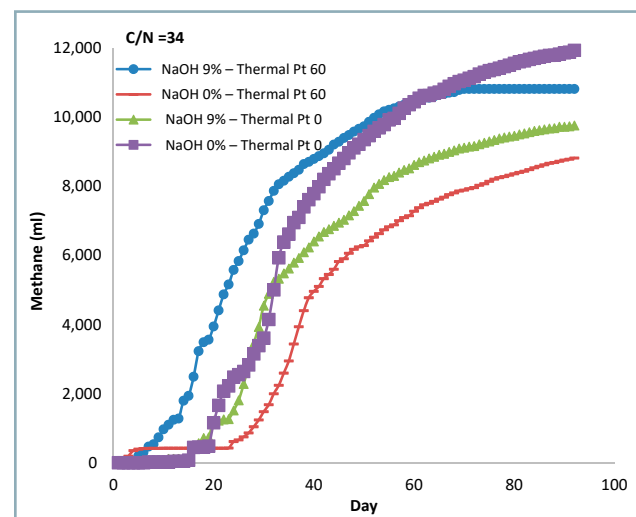


Fig. 2 Cumulative methane production rate of samples 2, 5, 8 and 11 with C/N ratio of 34

Fig. 3 depicts how raw Azolla showed higher methane production in comparison to steamed samples. As it was already mentioned, it was expected that chemical pre-treatment will show greater effect on methane production, but it was neutralized by the environment being more acidic due to high C/N ratio.

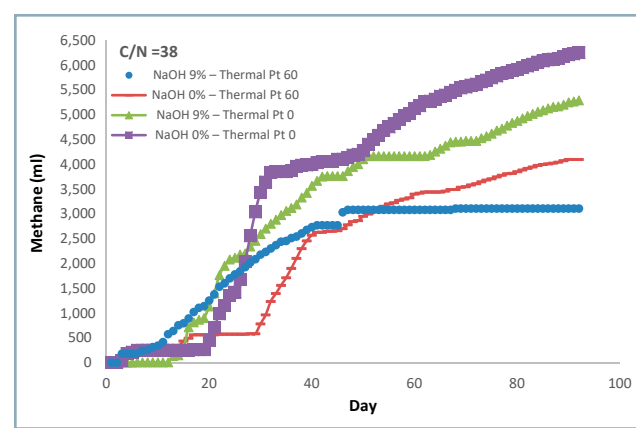


Fig. 3 Cumulative methane production rate of samples 3, 6, 9 and 12 with C/N ratio of 38

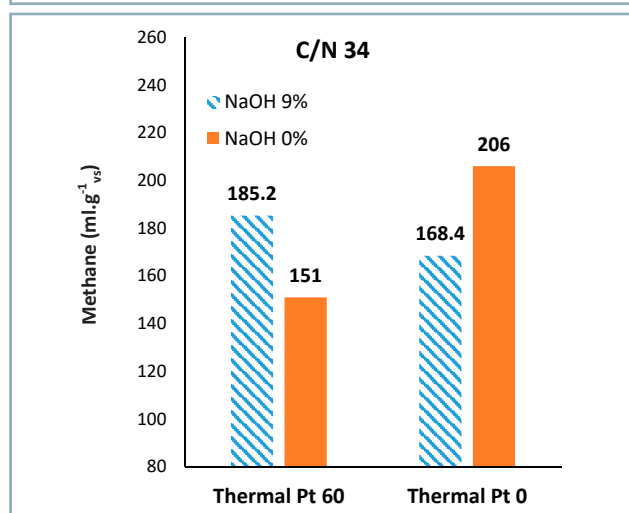
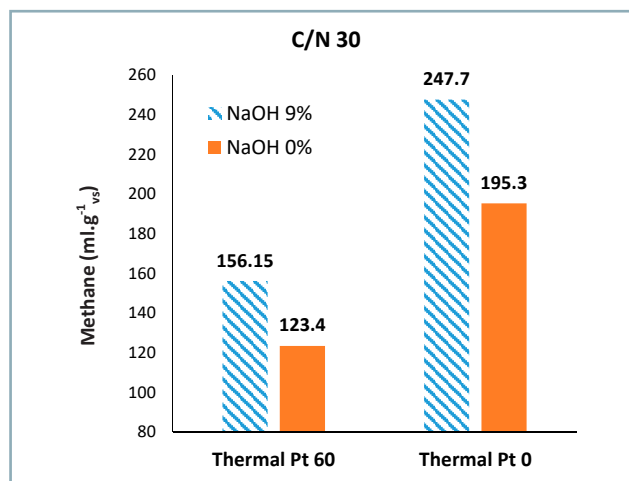


Fig. 4A Cumulative methane production by different samples

The effects of chemical pre-treatment, thermal pre-treatment and C/N ratios on methane production were analysed by means of Minitab software. The results of methane production are presented in Fig. 4 and Table 3. According to Fig. 4, it was observed that the highest methane production level ( $247.7 \text{ ml}\cdot\text{g}^{-1}\cdot\text{vs}$ ) was obtained for raw Azolla with C/N ratio and no thermal pre-treatment (raw

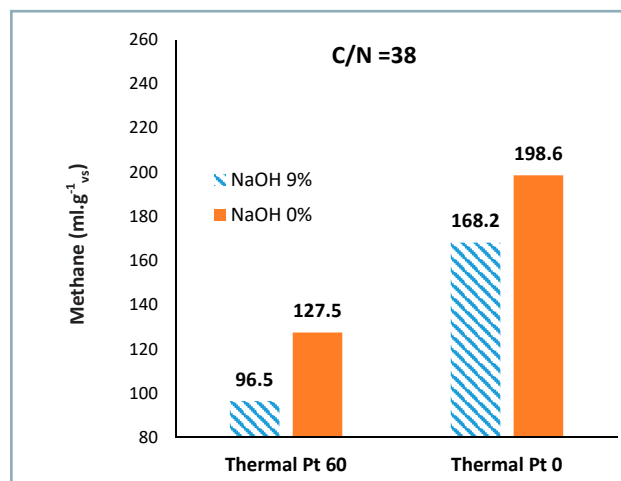


Fig. 4B Cumulative methane production by different samples

Azolla). Moreover, the lowest production rate was showed by steamed Azolla with C/N ratio of 38 and NaOH (9%) application. Based on Table 3, there is a significant difference between methane production of raw and steamed samples. Furthermore, there is a significant difference between the methane production of samples with application of NaOH (9%) and without it (NaOH 0%). Considering the significant differences at 5% level for different C/N ratios, there is a difference between methane production of samples with C/N ratios of 30 and 34, 38. What is more, interactions between C/N ratio and thermal pre-treatment; C/N ratio and chemical pre-treatment; as well as thermal pre-treatment and chemical pre-treatment, are also significant. This implies that there is no clear trend between the main effects. As it can be seen in Fig. 4, both raw and steamed samples with C/N ratio of 30 pre-treated by NaOH (9%) showed decreasing methane production, however, this trend is completely reversed for samples with C/N ratio of 38. Therefore, it is not possible to identify the effective parameter on the methane production prediction by means of Anova analysis method.

To predict each of the output variables, 4 different models were developed. Table 4 presents the structural parameters of the models with their statistical criteria in order to evaluate their performance. According to the

Table 3 Statistical results of Anova for methane production

| Source              | Type III sum of squares | df | Mean square | F           | Sig.  |
|---------------------|-------------------------|----|-------------|-------------|-------|
| Thermal Pt (TPt)    | 29,628.507              | 1  | 29,628.507  | 214,986.714 | .000* |
| Chemical            | 114.640                 | 1  | 114.640     | 831.836     | .000* |
| CN                  | 7,941.973               | 2  | 3,970.986   | 28,813.781  | .000* |
| TPt * chemical      | 657.495                 | 1  | 657.495     | 4,770.834   | .000* |
| TPt * CN            | 6,781.132               | 2  | 3,390.566   | 24,602.207  | .000* |
| Chemical * CN       | 8,168.106               | 2  | 4,084.053   | 29,634.199  | .000* |
| TPt * chemical * CN | 3,484.213               | 2  | 1,742.106   | 12,640.856  | .000* |
| Error               | 3.308                   | 24 | .138        |             |       |
| Total               | 1,081,334.961           | 36 |             |             |       |
| Corrected total     | 56,779.373              | 35 |             |             |       |

**Table 4** Structure characteristics of developed ANFIS architectures for methane production prediction

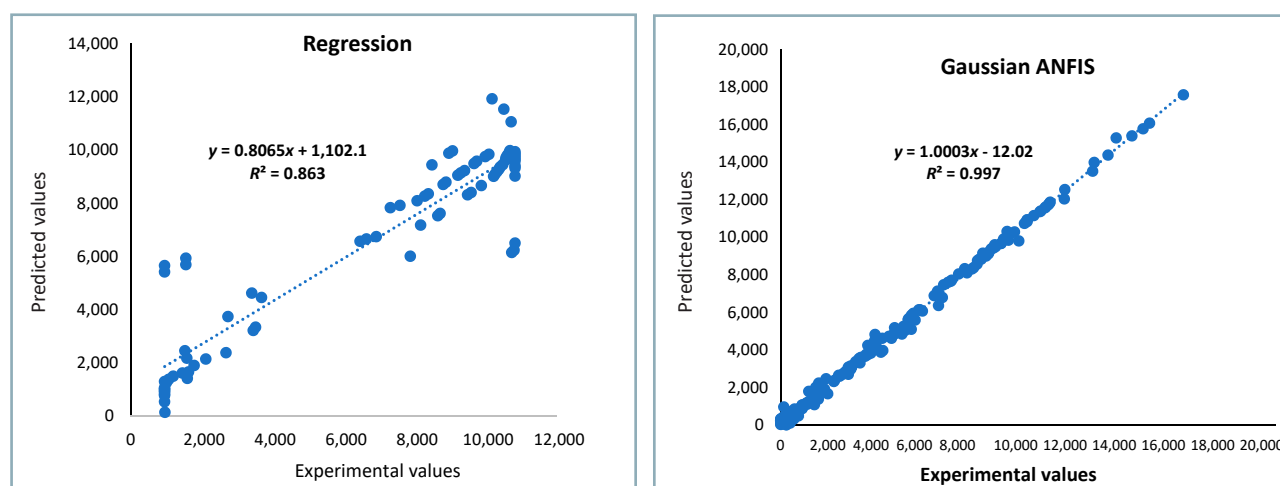
| Model          | Type of MF |        | Number of MF |       | Optimization method | Test           |        |
|----------------|------------|--------|--------------|-------|---------------------|----------------|--------|
|                | input      | output | input        | epoch |                     | $\epsilon$ (%) | $R^2$  |
| Grid partition | trimf      | Linear | 2 2 3 3      | 20    | hybrid              | 2.12           | 0.9959 |
| Grid partition | gaussmf    | Linear | 2 2 3 3      | 20    | hybrid              | 1.32           | 0.9972 |
| Grid partition | trapmf     | Linear | 2 2 3 3      | 20    | hybrid              | 1.19.          | 0.9957 |
| Grid partition | gbellmf    | Linear | 2 2 3 3      | 20    | hybrid              | 1.18           | 0.9967 |

**Table 5** Results of multiple regression analysis for methane production effective parameters

| Model                       | Unstandardized coefficients | Standardized coefficients | t     | sig     |
|-----------------------------|-----------------------------|---------------------------|-------|---------|
|                             | B                           | B                         |       |         |
| Constant                    | -9,040                      | 3,303                     | -2.74 | 0.006ns |
| Thermal pre-treatment (TPt) | 256                         | 227                       | 1.13  | 0.259ns |
| NAOH                        | 144                         | 519                       | 0.28  | 0.782ns |
| Day                         | 428.1                       | 61.7                      | 6.94  | 0.000*  |
| C/N                         | 233.4                       | 96.7                      | 2.41  | 0.016*  |
| TPt*NAOH                    | -92.9                       | 35.6                      | -2.61 | 0.009*  |
| TPt*day                     | 16.38                       | 4.23                      | 3.87  | 0.000*  |
| TPt*C/N                     | -6.57                       | 6.63                      | -0.99 | 0.322ns |
| NAOH*day                    | -28.28                      | 9.69                      | -2.92 | 0.004*  |
| NAOH*C/N                    | 1.8                         | 15.2                      | 0.12  | 0.906ns |
| Day*C/N                     | -9.90                       | 1.81                      | -5.48 | 0.000*  |
| TPt*NAOH*day                | 2.448                       | 0.665                     | 3.68  | 0.000*  |
| TPt*NAOH*C/N                | 2.28                        | 1.04                      | 2.19  | 0.029*  |
| TPt*day*C/N                 | -0.391                      | 0.124                     | -3.15 | 0.002*  |
| NAOH*day*C/N                | 0.752                       | 0.284                     | 2.65  | 0.008*  |
| TPt*NAOH*day*C/N            | -0.0690                     | 0.0195                    | -3.54 | 0.000*  |

results presented, all models have high ability ( $R^2 \geq 0.99$  and  $\epsilon(\%) \leq 2$ ) of prediction. The best model for methane production prediction is a model that uses the Gaussian linear membership function ( $R^2 = 0.997$  and  $\epsilon(\%) = 0.32$ ).

The ANFIS model does not provide a specific relationship for modelling the output variable. In contrast, the regression model directly deals with the impact of each factor and attempts to present a model that clearly identifies the

**Fig. 5** Experimental and predicted methane production by ANFIS and regression models

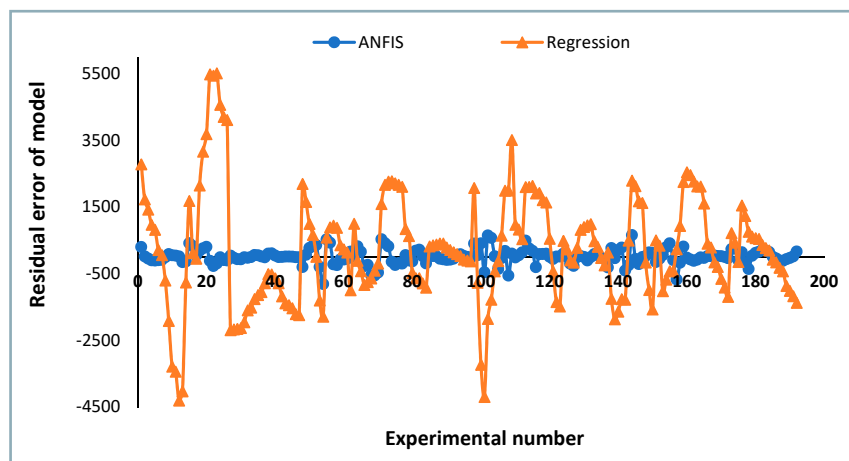


**Fig. 6** Variance of the observed values with the values predicted by ANFIS and regression models

significance and effect of each factor. For this purpose, Table 5 presents the statistical characteristics of the methane production prediction by stepwise regression model.

Regarding the results of the regression model presented in Table 5, it was observed that there is no specific trend between the C/N – TPt and C/N – NaOH variables; for this reason, these two variables cannot be effective in model prediction. However, multiple effects are significant between the other variables and therefore, considering the beta coefficients contained in the table, TPt – NaOH factor is more effective in predicting the model ( $b = 35.6$ ).

Fig. 5 shows the mapping between the experimental and predicted methane productions by the ANFIS and stepwise regression models. As it can be seen, the ANFIS model provides a more accurate mapping between experimental and predicted values in contrast to the regression model.

Fig. 6 shows the deviation of each model from the target value. The zero value of deviation is related to the target value. The blue line indicates the deviations associated with the output of the ANFIS; the red line implies the deviations associated with the output of the regression model. Fig. 6 clearly indicates that the ANFIS output shows a minimum deviation from the target value and the highest performance for predicting the model.

### Conclusion

Based on experimental research, it was observed that the highest methane production was shown by raw Azolla samples with C/N ratio of 30 pre-treated by NaOH (9%). The highest digestion yield was obtained for raw Azolla samples, since steaming the Azolla is expensive and time consuming, therefore, Azolla as a raw material is more economical and cost-effective. Chemical pre-treatment had a significant effect on methane production, with the highest yield obtained by samples pre-treated by NaOH (9%). For further research, it is also recommended to test various percentages of NaOH in order to determine the most suitable one for methane production.

C/N ratio also played a significant role – the highest methane production was obtained at C/N ratio of 30, what is in compliance with results obtained by Shilpakar and Shilpakar (2009). Considering the methane production prediction, the ANFIS model showed better performance in contrast to stepwise regression models.

### References

ABDESHAHIAN, P. – LIM, J. S. – HASHIM, H. – LEE, C. T. 2016. Potential of biogas production from farm animal waste in Malaysia. In *Renewable and Sustainable Energy Reviews*, vol. 60, pp. 714–723.

ADELARD, L. – POULSEN, T. G. – RAKOTONIA, V. 2015. Biogas and methane yield in response to co- and separate digestion of biomass wastes. In *Waste Management and Research*, vol. 33, pp. 55–62.

ANONYMOUS. 2013. World Energy Council. London.

BASRI, M. F. – YACOB, S. – HASSAN, M. A. – SHIRI, Y. – WAKISAKA, M. – ZAKARIA, M. R. 2010. Improved biogas production from palm oil mill effluent by a scaled down anaerobic treatment process. In *World Journal of Microbiology and Biotechnology*, vol. 26, pp. 505–514.

CARMAN, K. 2008. Prediction of soil compaction under pneumatic tires a using fuzzy logic approach. In *Journal of Terramechanics*, vol. 45, pp. 103–107.

DAS, D. – SIKDAR, K. – CHETTERJEE, A. K. 1994. Potential of Azolla pinnata as biogas generator and as a fish feed. In *Indian Journal of Environmental Health*, vol. 36, pp. 186–191.

JANKE, R. – KONG, J. – BRABERG, H. – CANTIN, G. – YATES, J. R. – KROGAN, N. J. – HEYER, W. D. 2016. Nonsense-mediated decay regulates key components of homologous recombination. In *Nucleic Acids Research*, vol. 44, no. 11, pp. 5218–30.

KAŽIMÍROVÁ, V. – GADUŠ, J. – GIERTL, T. 2018. Verification of suitability of substrate composition for production and quality of biogas. In *Acta Technologica Agriculturae*, vol. 21, no. 3, pp. 118–121.

PAUDEL, B. 2009. Suitability of Azolla for biogas slurry enrichment. Thesis in M.S., Kerala Agricultural University, Kerala, India.

PHETYIMA, N. – WANTHONGA, T. – KANNIKAA, P. – SUPNGAMA, A. 2015. Biogas production from vegetable waste by using dog and cattle manure. In *Energy Procedia*, vol. 49, pp. 436–441.

ROY, D. C. – PAKHIRA, M. C. – BERA, S. 2016. A review on biology, cultivation and utilization of Azolla. In *Advances in Life Sciences*, vol. 5, no. 1, pp. 11–15.

SHILPAKAR, P. – SHILPAKAR, D. 2009. Nutrition of rice through Azolla organic material. In *Indian Journal of Agronomy*, vol. 42, no. 4, pp. 626–633.

TASNIM, F. – AKHTAR, S. – CHOWDHURY, A. R. 2017. Biogas production from anaerobic co-digestion of cow manure with kitchen waste and Water Hyacinth. In *Renewable Energy*, vol. 109, pp. 434–439.

WILKIE, A. C. 2000. Reducing dairy manure odor and producing energy. In *Biocycle*, vol. 41, no. 9, pp. 48–57.

YADAVA, L. S. – HESSE, R. P. 1981. The development and use of biogas technology in rural area of Asia. Improving soil fertility through organic recycling. FAO project RAS/75/004, no. 10.

ZHANG, J. – ZHANG, M. – SHAN, S. – WANG, M. 2013. Effect of biogas slurry application on grain yield. In *Journal of Agro-Environmental Science*, vol. 28, no. 10, pp. 2005–2009.



Acta Technologica Agriculturae 3  
Nitra, Slovaca Universitas Agriculturae Nitriae, 2020, pp. 132–136

## ASSESSMENT OF THE EFFECTS OF SUGARCANE STRAW ADDITION TO THE FLOCCULATION/COAGULATION PROCESS ON VINASSE CONCENTRATION

Pietro SICA\*, Renan CARVALHO, Hélder BELTRAME, Antonio Sampaio BAPTISTA

University of Sao Paulo, Piracicaba, Sao Paulo, Brazil

Vinasse is the main by-product of ethanol production. In 2005, its application was regulated in the state of Sao Paulo, so if it is to be applied to the fields, its volume must meet the established concentration regulations. Straw contains one-third of sugarcane calorific value and can be used for cogeneration. For these purposes, the project objective was to assess the effects of straw on the concentration of vinasse solids through physical and chemical processes, so its concentrated form could be used as biomass for cogeneration. For that, different concentrations of straw, ferric sulphate, and ferric chloride were used. Turbidity reduction was the parameter analysed. Both reagents were effective in reducing the turbidity. The 200 ppm of ferric chloride and 0.25% straw content reduced the turbidity by 55.02% and 400 ppm of ferric sulphate and 0.25% of straw reduced it by 57.96%. The addition of straw showed no significant effect in terms of the turbidity reduction, however, both best treatments had 0.25% straw content addition in it. Straw can be used to concentrate vinasse, contributing to the efficiency of the process and increasing the energy potential of the concentrated solids.

**Keywords:** vinasse concentration; biofertilizer; physical and chemical treatments; water recovery; turbidity reduction

Brazil is the world's largest producer of sugarcane ethanol, producing approx. 33 billion litres of ethanol in the 2018/2019 harvest season (Brazilian Sugarcane Industry Association, 2019). Ethanol consists of the same chemical compound, regardless of whether it is produced from starch (e.g. corn), or fermentable sugars (sugarcane) (Božiková and Hlaváč, 2013). Sugarcane ethanol is considered more renewable, cleaner and sustainable than the corn ethanol. By-products generated in sugarcane ethanol production process include vinasse, which is the main liquid by-product of sugar-ethanol industry (Moraes et al., 2015); it is composed of 93% water and 7% minerals (mainly potassium) and organic matter (Laimé et al., 2011; Ferreira et al., 2011) and is 100 times more pollutant than domestic sewage (Freire and Cortez, 2000). For each litre of ethanol produced, 10–15 litres of vinasse are generated (Silva et al., 2013).

The main application of vinasse is as biofertilizer for its high potassium content. However, besides the organic content, it has high pollutant capacity; when applied to the soil, high concentrations of  $K^+$  ions can form chemical complexes, promoting the leaching of anions, such as nitrate, and polluting the groundwaters (Rodella et al., 1983). The state of Sao Paulo produced 16 billion litres of ethanol in the 2018/2019 harvest season (Brazilian Sugarcane Industry Association, 2019) and generated approx. 160–240 billion litres of vinasse for this same period. The Guarani Aquifer System (SAG) is considered one of the most important in the world and 80% of its total exploited yield for drinking and industrial utilization is in the state of Sao Paulo (Foster et al., 2009). Hirata et al. (1991) considered

sugar and ethanol plants to be part of the group classified as high potential contaminant load to the state of Sao Paulo groundwaters. For these reasons, in 2005, the Sao Paulo's State Sanitation Company (CETESB) established the P4.231 technical standard regulating the vinasse application; it disallows the  $K^+$  concentration in the soil to exceed 5% of the cation exchange capacity (CEC) (State of Sao Paulo, 2005). One of the consequences of this regulation is that now the vinasse must be applied to larger areas (Silva et al., 2013), increasing the application and handling costs. Increased machinery traffic over fields causes soils compaction, damaging the soil structure and degrading the soil functions (Galambošová et al., 2020). One of the solutions for this issue is to concentrate the vinasse solids in the industry and take smaller volumes of it to the field. Furthermore, the combustion of vinasse solids or its incineration for the recovery of potassium salts and energy are other alternatives (Freire and Cortez, 2000).

On September 19, 2002, the State of Sao Paulo approved the Act no. 11.241 (State of Sao Paulo, 2002), gradually banning the burning of sugarcane before harvesting, by 2021 (Aguiar et al., 2011). The manual harvesting of sugarcane has been and is gradually being replaced by mechanized harvesting with efficiency of 10–20 tons of dry leaves per hectare in the top of the soil under the system known as green cane management. Sugarcane straw represents approx. one-third of the total primary calorific value of sugarcane in the field (Leal et al., 2013). However, the greatest agronomic and environmental benefits of leaving the straw on the field result from leaving at least

**Contact address:** Pietro Sica, University of Sao Paulo, Food and Nutrition, College of Agriculture "Luiz de Queiroz", Department of Agri-food Industry, 11 Padua Dias Avenue, 13418-900, Piracicaba, Sao Paulo, Brazil, e-mail: [pietros0394@gmail.com](mailto:pietros0394@gmail.com)

7 tons of sugarcane straw per hectare. Consequently, 3–13 tons of straw per hectare can be harvested by power generation purposes (Carvalho et al., 2017). To enhance the sugar-energy sector sustainability, it is necessary to optimize the utilization of sugarcane energy content. In the field, one ton of sugarcane has  $7,188 \times 10^3$  kJ, which is more than one barrel of crude oil has ( $5,799 \times 10^3$  kJ). This one ton of sugarcane provides 276 kg of bagasse with 50% moisture content that has  $2,502 \times 10^3$  kJ, 165 kg of straw with 15% moisture content that has  $2,142 \times 10^3$  kJ, and 153 kg of sugar ( $2,543 \times 10^3$  kJ). Part of the sugar calorific value goes to the sugar production, another part to the ethanol production, and the rest “disappears” in the vinasse (Oliverio, 2016).

This project aims to assess the efficiency of flocculation/coagulation and centrifugation processes to concentrate the vinasse solids together with sugarcane straw in order to increase the calorific power of the concentrated solids, so that they can be used for cogeneration. Moreover, the vinasse water can be recovered and reused for the industrial purposes. For that, different concentrations of ferric chloride and ferric sulphate were added to the vinasse samples (with and without sugarcane straw), which were subsequently centrifuged. The vinasse turbidity was the main parameter used to compare the samples.

## Material and methods

The straw was collected in Bariri, state of São Paulo, using rake and sacks. Subsequently, it was transported to the Sugar and Alcohol Laboratory of the College of Agriculture “Luiz de Queiroz”, University of São Paulo campus in Piracicaba (ESALQ/USP). The straw was shredded and sieved to 0.3 mm particle size.

Vinasse for analysis was obtained by fermentation in 7 l reactors. Sugarcane juice used for fermentation (18 °Bx) was obtained from the dilution of stored syrup (55 °Bx) at the Sugar and Alcohol Laboratory of ESALQ/USP.

Flocculating agents used were ferric sulphate and ferric chloride.

### Turbidity

Turbidity is a physical property of fluids that translates into reduced transparency due to the presence of suspended materials that interfere with the passage of light through the fluid and can be measured based on the difficulty of the light to pass through the liquid (USGS, 2019). The turbidity was used to assess the efficiency of each treatment in terms of reducing the solids content of the vinasse and was determined by using a 2100Q portable turbidimeter by Hach Company. This equipment has two-detector optical system that compensates for colour in the sample, light fluctuation, and stray light. It is calibrated with a standard curve with 6 different turbidity values ranging from 0 to 1000 NTU (nephelometric turbidity units). These suspended materials can be decanted or removed from the liquid with flocculation, coagulation and centrifugation. For this reason, the turbidity was used as the main parameter to determine the efficiency of the treatments in terms of concentrating the suspended vinasse solids. The turbidity reduction was calculated in percentage as follows:

$$\text{turbidity reduction} = \frac{(\text{initial turbidity} - \text{final turbidity}) \times 100}{\text{initial turbidity}} \quad (1)$$

### Experimental design

Three different concentrations of straw were used: 0.0% (S0%), 0.1% (S0.1%), and 0.25% (S0.25%). For all three straw concentrations, 0 ppm, 50 ppm, 100 ppm, and 200 ppm of ferric chloride (FC) and ferric sulphate (FS) were used. For the 0.25% concentration of sugarcane straw, the concentrations of 300 ppm, 400 ppm, and 500 ppm were also used. In total, the following 27 treatments were performed: 1) S0 – no reagent; 2) S1 – no reagent; 3) S2 – no reagent; 4) S0 – FS50; 5) S0 – FS100; 6) S0 – FS200; 7) S0 – FC50; 8) S0 – FC100; 9) S0 – FC200; 10) S1 – FS50; 11) S1 – FS100; 12) S1 – FS200; 13) S1 – FC50; 14) S1 – FC100; 15) S1 – FC200; 16) S2 – FS50; 17) S2 – FS100; 18) S2 – FS200; 19) S2 – FS300; 20) S2 – FS400; 21) S2 – FS500; 22) S2 – FC50; 23) S2 – FC100; 24) S2 – FC200; 25) S2 – FC300; 26) S2 – FC400; 27) S2 – FC500.

Each treatment was replicated 4 times. Vinasse was transferred to 50 ml Falcon tubes and mixed with the straw after mixing with the reagent. Then, it was centrifuged at 4,000 rpm for 5 min. The supernatant was collected, the turbidity after treatment was measured, and the turbidity reduction for each experimental sample was calculated according to Eq. 1. The vinasse used was homogenized and the measured initial turbidity was 936 NTU.

### Statistical analysis

The data obtained were analysed using the software R. First, ANOVA. Utilizing the Tukey HSD test (5%), the effects of ferric sulphate and ferric chloride on the turbidity reduction of vinasse were assessed. Subsequently, the effects of adding straw in different concentrations were evaluated by running ANOVA and Tukey HSD test (5%). The effects of different straw and reagent concentrations were also assessed by using ANOVA and Tukey HSD test (5%).

## Results and discussion

The treatments without straw addition showed an average turbidity reduction of 47.15% and no significant differences in contrast to the treatments with 0.1% ( $p = 0.214$ ) and 0.25% of straw ( $p = 0.695$ ). The treatments with 0.1% straw content showed the lowest turbidity reduction – by 44.87% – which is significantly different from the treatments with 0.25% straw content – 48.25% ( $p = 0.037$ ) (Fig. 1). The straw addition had no influence on the turbidity reduction; however, the process can be influenced by different concentrations of straw. Although the data is not presented in this manuscript, treatments with 0.50% and 1.00% straw contents were also performed in a preliminary study. Such larger straw contents made the centrifugation process difficult, as it was unable to remain at the base of the tubes, rising and bringing the vinasse solids after centrifugation, reducing the final turbidity by less than 28%.

The addition of flocculants showed an effect on the vinasse turbidity reduction. The control treatments (C) with no reagents added reduced the turbidity by 40.14% and were significantly different in comparison to the

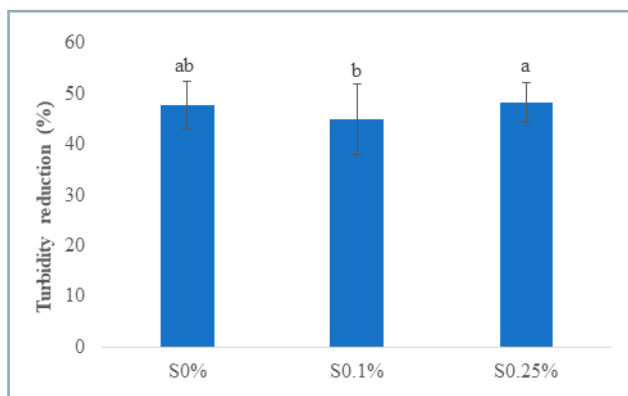


**Fig. 1** Dependency of turbidity reduction on different straw content addition

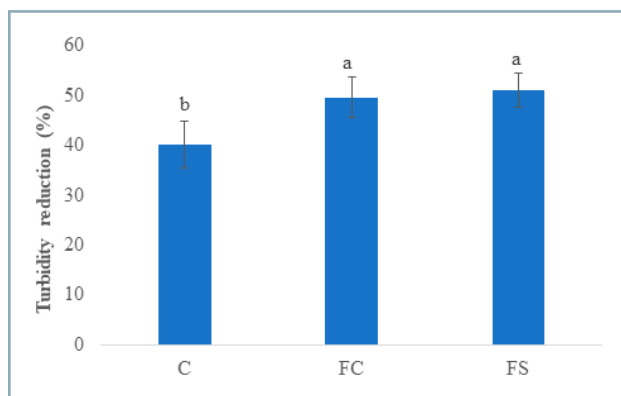


**Fig. 2** Dependency of turbidity reduction on different reagents

treatments with ferric chloride, 49.57% ( $p = 0.000$ ), and with ferric sulphate, 50.97% ( $p = 0.000$ ). There was no significant difference between the treatments with ferric chloride and ferric sulphate ( $p = 0.222$ ) (Fig. 2).

Different straw and flocculant concentrations also influenced the vinasse turbidity reduction. Considering the sole ferric sulphate application, the turbidity reduction significantly increased from 42.55% (0 ppm) to 52.83% (200 ppm) (Table 1).

When 0.1% straw content was added to the process, the treatment with no reagent was also the one with lower value, 33.95%, and the turbidity reduction increased significantly with the addition of 50 ppm (47.30%) of ferric sulphate. The highest significant reduction was observed in treatments with addition of 100 ppm (51.12%) and 200 ppm (50.24%) of ferric sulphate (Table 1).

All in all, the treatments with 0.25% straw content and higher amounts of ferric sulphate showed high turbidity reduction. For those treatments, the increasing of the reagent concentration from 0 ppm to 400 ppm also increased the turbidity reduction – from 43.94% to 57.96%. However, when increasing from 400 ppm to 500 ppm, although there was no significant difference, the turbidity reduction decreased to 55.85%, since addition of the reagent achieved a saturation point, at which adding more reagent does not affect the turbidity reduction positively. The treatment with addition of 400 ppm and 0.25% straw content showed the highest turbidity reduction and had significant difference

in contrast to the treatment with addition of 500 ppm and 0.25% of straw. The latter showed no significant difference in comparison to the treatments with addition of 200 ppm and no straw; 0.1% straw content and 100 ppm and 200 ppm; and 0.25% straw content and 300 ppm and 200 ppm (Table 1).

Different concentrations of ferric chloride also affected the turbidity reduction. Without straw addition, the turbidity reduction increased as the amount of applied ferric chloride increased: from 42.55% at 0 ppm to 52.94% at 200 ppm. The treatment with 200 ppm showed no significant difference in comparison to the treatment with 100 ppm (50.27%) (Table 2).

The turbidity reduction also increased, as the reagent concentration increased with 0.1% straw addition: from 33.95% without any reagent application to 51.98% with application of 200 ppm of ferric chloride. The treatment with 200 ppm was significantly different in contrast to the others. There was no significant difference between the treatments with 50 ppm and 100 ppm, 43.32% and 47.09%, respectively.

Considering the treatments with 0.25% straw, the turbidity reduction increased from 43.94% to 55.02% as the ferric chloride concentration increased from 0 ppm to 200 ppm. The treatment with 200 ppm had no significant difference when compared to the treatment with 300 ppm (52.19%) and 400 ppm (53.63%). The treatment with 500 ppm decreased the turbidity reduction to 49.36%, since addition of the reagent achieved a saturation point, at which

**Table 1** Turbidity reduction showed by treatments with different concentrations of ferric sulphate and straw

| Ferric sulphate | S 0%                    |    | S 0.1%       |      | S 0.25%      |     |
|-----------------|-------------------------|----|--------------|------|--------------|-----|
|                 | turbidity reduction (%) |    |              |      |              |     |
| 0 ppm           | 42.55 ± 0.72            | f  | 33.95 ± 1.75 | g    | 43.94 ± 1.58 | def |
| 50 ppm          | 46.85 ± 0.32            | de | 47.30 ± 1.21 | de   | 47.36 ± 1.90 | de  |
| 100 ppm         | 49.65 ± 1.15            | de | 51.12 ± 0.52 | bcd  | 48.02 ± 0.97 | de  |
| 200 ppm         | 52.83 ± 0.47            | bc | 50.24 ± 0.31 | bcde | 51.47 ± 0.73 | bc  |
| 300 ppm         | –                       | –  | –            | –    | 52.99 ± 0.88 | bc  |
| 400 ppm         | –                       | –  | –            | –    | 57.96 ± 0.49 | a   |
| 500 ppm         | –                       | –  | –            | –    | 55.85 ± 0.47 | ab  |

Different letters indicate that there was a significant difference between treatments at a 5% significance level (Tukey test)

**Table 2** Turbidity reduction of treatments with different concentrations of ferric chloride and straw

| Ferric chloride | S 0%                    |     | S 0.1%      |     | S 0.25%     |     |
|-----------------|-------------------------|-----|-------------|-----|-------------|-----|
|                 | turbidity reduction (%) |     |             |     |             |     |
| 0 ppm           | 42.55 ±0.72             | e   | 33.95 ±1.75 | f   | 43.94 ±1.58 | e   |
| 50 ppm          | 42.84 ±0.93             | e   | 43.32 ±1.47 | e   | 45.51 ±1.60 | e   |
| 100 ppm         | 50.27 ±0.76             | cd  | 47.09 ±1.51 | de  | 50.72 ±0.90 | bc  |
| 200 ppm         | 52.94 ±0.54             | abc | 51.98 ±0.76 | abc | 55.02 ±1.31 | a   |
| 300 ppm         | –                       | –   | –           | –   | 52.19 ±0.39 | abc |
| 400 ppm         | –                       | –   | –           | –   | 53.63 ±0.34 | ab  |
| 500 ppm         | –                       | –   | –           | –   | 49.36 ±1.15 | cd  |

Different letters indicate that there was a significant difference among the treatments at a 5% significance level (Tukey test)

adding more reagent does not affect the turbidity reduction positively.

Based on the results obtained in this study, it is possible to affirm that the ferric chloride and the ferric sulphate can increase the vinasse solids concentration and its water recovery efficiency. Following the methods established by Souza et al. (2013b), Souza et al. (2013a) used a commercial vegetable tannin (TanFloc®) to clarify that by adding 2.5% of tannin to the vinasse, the turbidity fell by 70%. Similarly, Souza et al. (2013b) manage to reduce it by more than 90% in a similar manner. However, Souza et al. (2013b) highlighted that the simple process of coagulation/flocculation without adding toxic components was able to reduce the vinasse turbidity and concentrate its solids. In addition to this, these studies used photocatalytic processes to degrade the remaining vinasse organic content. Ferric chloride and ferric sulphate consist of iron and chlorine, and iron and sulphate, respectively. Taking into account that the concentrated solids contain minerals that are going to be applied to the field, those components added to the vinasse are also going to be applied to the field. Sulphate is a macronutrient, and iron and chlorine are micronutrients essential for the plant development, therefore, utilization of these reagents is not going to be toxic to the sugarcane in the field and will not pose the same toxicity issue of TanFloc® highlighted by Souza et al. (2013b).

Flocculation and coagulation processes were able to reduce the vinasse turbidity and concentrate its solids, however, the supernatant still retains almost half of it. In order to remove these solids completely and recover the water, a process or sequence of processes would be required after this step. Souza et al. (2013a; 2013b) observed that a photocatalytic degradation reduced the organic load of the vinasse by almost 80%. Sica et al. (2017) filtered the supernatant in a sand filter, reducing the turbidity and total solids by more than 90%, reaching final pH of approx. 7.0, thus obtaining treated clear water that could be reused in industrial processes.

### Conclusion

The flocculation/coagulation process to concentrate the vinasse solids is more efficient with application of ferric chloride and ferric sulphate. The best results were obtained with application of 200 ppm ferric chloride and 0.25% of straw, reducing the turbidity by 55.02%. Considering the

ferric sulphate application, the best results were achieved at 400 ppm and 0.25% of straw, reducing the turbidity by 57.96%.

In terms of comparison of treatments with straw addition, the straw content of 0.25% showed no significant difference in contrast to the samples without straw. However, the treatments with ferric sulphate showed higher turbidity reduction with application of 0.25% of straw. Furthermore, addition of 0.1% and 0.25% of straw showed no negative impacts on this process and can increase the calorific power of the concentrated vinasse solids.

Although the proposed treatments were able to concentrate the vinasse solids, the flocculation/coagulation process alone was not enough for these purposes. However, it can be considered as a suitable pre-treatment. Therefore, further studies are necessary to assess different processes that can be added after this pre-treatment and make the vinasse concentration more efficient.

### References

- AGUIAR, D. A. – RUDORFF, B. F. T. – SILVA, W. F. – ADAMI, M. – MELLO, M. P. 2011. Remote sensing images in support of environmental protocol: monitoring the sugarcane harvest in Sao Paulo State, Brazil. In *Remote Sensing*, vol. 3, no. 12, pp. 2682–2703.
- BOŽIKOVÁ, M. – HLAVÁČ, P. 2013. Thermal conductivity and thermal diffusivity of biodiesel and bioethanol samples. In *Acta Technologica Agriculturae*, vol. 16, no. 4, pp. 90–94.
- CARVALHO, J. – NOGUEIROL, R. – MENANDRO, L. – BORDONAL, R. – BORGES, C. – CANTARELLA, H. – FRANCO, H. 2017. Agronomic and environmental implications of sugarcane straw removal: a major review. In *Global Change Biology – Bioenergy*, vol. 9, no. 7, pp. 1181–1195.
- FERREIRA, L. F. R. – AGUIAR, M. M. – MESSIAS, T. G. – POMPEU, G. B. – LOPEZ, A. M. Q. – SILVA, D. P. – MONTEIRO, R. T. 2011. Evaluation of sugar-cane vinasse treated with *Pleurotus sajor-caju* utilizing aquatic organisms as toxicological indicators. In *Ecotoxicology and Environmental Safety*, vol. 74, no. 1, pp. 132–137.
- FOSTER, S. – HIRATA, R. – VIDAL, A. – SCHMIDT, G. – GARDUÑO, H. 2009. The Guarani Aquifer initiative – towards realistic groundwater management in a transboundary context. In *Groundwater Management Advisory Team (GW-MATE) 2009*. Washington: World Bank. Available at: <https://www.un-igrac.org/sites/default/files/resources/files/GWMATE%20case%20profile%20-%20Guarani.pdf>. Accessed on December 03, 2019.

- FREIRE, W. J. – CORTEZ, L. A. B. 2000. Vinasse from sugarcane (in Portuguese). Guaíba (Brazil): Agropecuária, 203 pp.
- GALAMBOŠOVÁ, J. – MACÁK, M. – RATAJ, V. – BARÁT, M. – MISIEWICZ, P. 2020. Determining trafficked areas using soil electrical conductivity – a pilot study. In *Acta Technologica Agriculturae*, vol. 23, no. 1, pp. 1–6.
- HIRATA, R. C. A. – BASTOS, C. R. A. – ROCHA, G. A. – GOMES, D. C. – IRITANI, M. A. 1991. Ground water pollution risk and vulnerability map of the state of Sao Paulo, Brazil. In *Water Science and Technology*, vol. 24, no. 11, pp. 159–169.
- LAIME, E. M. O. – FERNANDES, P. D. – OLIVEIRA, D. C. S. – FREIRE, E. A. 2011. Technological possibilities for the destination of vinasse: a review (in Portuguese). In *Revista Trópica: Ciências Agrárias e Biológicas*, vol. 5, no. 3, pp. 16–29.
- LEAL, M. R. L. V. – GALDOS, M. V. – SCARPARE, F. V. – SEABRA, J. E. A. – WALTER, A. – OLIVEIRA, C. O. 2013. Sugarcane straw availability, quality, recovery and energy use: a literature review. In *Biomass and Bioenergy*, vol. 53, no. 6, pp. 11–19.
- MORAES, B. S. – ZAIAT, M. – BONOMI, A. 2015. Anaerobic digestion of vinasse from sugarcane ethanol production in Brazil: challenges and perspectives. In *Renewable and Sustainable Energy Reviews*, vol. 44, no. 4, pp. 888–903.
- OLIVERIO, J. L. 2016. The Dedini and the private effort during 40 years of Pro-Alcohol, or... from the sugar mill to the sustainable plant (in Portuguese). In FAPESP (Sao Paulo Research Foundation). Available at: <http://www.fapesp.br/eventos/2016/11/proalcool/Dedini.pdf>. Accessed on February 28, 2020.
- RODELLA, A. A. – ZAMBELLO, E. – FRANCISCO, J. O. 1983. Effects of vinasse added to soil on pH and exchangeable aluminum content. In *Congress of the International Society of Sugar Cane Technologists 1983*. Havana: Jose Marti Publishing House, pp. 237–247.
- SICA, P. – BAPTISTA, A. S. – DAS, K. C. – PIOTROVSKI, J. 2017. Development of physical and chemical processes to increase the efficiency of concentration of vinasse's solids. In *Journal of Environmental Sciences and Engineering A*, vol. 6, no. 2, pp. 90–97.
- SILVA, A. – ROSSETTO, R. – BONNECINE, J. – PIEMONTE, M. – MURAOKA, T. 2013. Net and potential nitrogen mineralization in soil with sugarcane vinasse. In *Sugar Technology*, vol. 15, no. 2, pp. 159–164.
- SOUZA, R. P. – FERRARI-LIMA, A. M. – SEIXAS, F. L. – BATISTELA, V. R. – FAVARO, S. L. – HIOKA, N. – FERNANDES-MACHADO, N. R. C. 2013a. Evaluation of ZnO catalyst supported on zeolite NaA in the photocatalytic degradation of vinasse pretreated by coagulation/flocculation. In *Chemical Engineering Transactions*, vol. 32, pp. 823–828.
- SOUZA, R. P. – GIRARDI, F. – SANTANA, V. S. – FERNANDES-MACHADO, N. R. C. – GIMENES, L. M. 2013b. Vinasse treatment using vegetable-tanning coagulant and photocatalysis. In *Acta Scientiarum – Technology*, vol. 35, no. 1, pp. 89–95.
- State of Sao Paulo. Law 11.241 Provides for the gradual elimination of the burning of sugarcane straw and gives related measures (in Portuguese). Available at: <https://www.al.sp.gov.br/repositorio/legislacao/lei/2002/lei-11241-19.09.2002.html>. Accessed on December 3, 2019.
- State of Sao Paulo's Technical Standard P4.231/2005. Silage – Criteria and procedures for agricultural application.
- UNICA (BRAZILIAN SUGARCANE INDUSTRY ASSOCIATION). 2019. Sugarcane, ethanol and sugar production – 2018/2019 harvest season. Available at: <http://www.unica.com.br/historico-de-producao-e-moagem.php?idMn=32&tipoHistorico=4&acao=visualizar&idTabela=2336&safr=2018%2F2019&estado=RS%2CSC%2CPR%2CSP%2CRJ%2CMG%2CES%2CMS%2CMT%2CGO%2CDF%2CBA%2CSE%2CAL%2CPE%2CPB%2CRN%2CCE%2CPI%2CMA%2CTO%2CPA%2CAP%2CRO%2CAM%2CAC%2CRR>. Accessed on December 03, 2019.
- USGS (United States Geological Survey). 2019. Water and Turbidity. Available at: [https://www.usgs.gov/special-topic/water-science-school/science/turbidity-and-water?qt-science\\_center\\_objects=0#qt-science\\_center\\_objects](https://www.usgs.gov/special-topic/water-science-school/science/turbidity-and-water?qt-science_center_objects=0#qt-science_center_objects). Accessed on February 28, 2020.



Acta Technologica Agriculturae 3  
Nitra, Slovaca Universitas Agriculturae Nitriae, 2020, pp. 137–143

## EVALUATION OF PROPERTIES OF PELLETS MADE OF SWINE MANURE

Viera KAŽIMÍROVÁ\*, Ľubomír KUBÍK, Štefan MIHINA

Slovak University of Agriculture in Nitra, Slovakia

This paper deals with assessment of density, moisture content and mechanical properties of pellets made of dry swine manure utilizing pellet production line MGL 200. Pellets were subsequently subjected to compressive loading test. Furthermore, the values obtained were measured by means of device Andilog Stentor 1000 and compression diagrams were plotted. In terms of compressive strength, pellet type 1 showed value of 10.47 MPa; pellet type 2 showed value of 6.24 MPa. Considering the elasticity modulus, pellet type 1 showed value of 122.39 MPa; pellet type 2 showed value of 71.12 MPa. Other observed properties included force necessary for 10% compression strain; force in the first maximum of force-strain curve; force in the inflection point of the force-time curve. Results obtained from compressive loading test provide a basis for innovations in pellet production utilizing materials other than wood biomass.

**Keywords:** compressive loading; deformation; strength; modulus of elasticity

Utilization of biomass made of materials from agricultural production and waste biomass, the potential of which cannot be neglected, comes to the forefront and is very topical. Great attention is currently paid to utilization of wastes from agricultural production not only in the field of science and research (Bappah et al., 2019; Martínez-Guido et al., 2019; Purohit and Chaturvedi, 2018), but also in practice. Alternative pellet production represents one method for utilization of the aforementioned materials, not only in energy sector but also in agriculture. Their utilization is closely tied to the requirements for the pellet quality. Multiple scientists investigate the pellet quality in Slovakia, as well as abroad (Dumitrascu et al., 2018; Jiang et al., 2016; Lee et al., 2019; Spirchez et al., 2019; Zamorano et al., 2011), who evaluated the pellet quality on the basis of their composition, density, moisture content, durability, etc. Zafari and Kianmehr (2012) have dealt with the issue of effects of temperature, pressure and moisture on durability of cattle manure pellets.

Pellet mechanical properties assessment by compressive loading test began to receive increased attention in the last decade. Testing utilizes the experience achieved by other researchers, obtained from evaluation of other materials of biological origin (Kubík and Kažimírová, 2015; Olosu and Clarke, 1993; Vursavuş and Özgüven, 2004). Hardness (compression strength) is one of the significant properties of commercial pellets, which reflects the mechanical strength of single pellet during handling, transportation, and storage (Jiang et al., 2014). Compression strength is defined as the maximum compressive force that a pellet can withstand before breaking when exposed to a diametrical compressive force between two horizontal metal plates. In general, there are no limits for pellet hardness established

by standards. According to the literature, the hardness value of different biomass materials reached 25 kgf and the ideal value that ensures high-quality pellets was found to be 22 kgf (Carroll and Finnan, 2012; García-Maraver et al., 2015; Said et al., 2015). Assessment of such pellet values proved to play a significant role in terms of handling, storage and subsequent industrial and agricultural pellet exploitation.

### Material and methods

The work aimed to conduct an analysis of the mechanical properties of pellets made of alternative materials based on pellet behaviour observation during compressive loading test by means of the Stentor Andilog 1000 device (Andilog Technologies, Vitrolles, France). Pellets were made of separated and dried swine manure (Fig. 1) from local pig farm. Pellets were produced by means of production line MGL 200 (Kovo Novak, Czech Republic) and their final form was achieved by employing the water as binding agent.



**Fig. 1** Dried swine manure and swine manure pellet type 1

**Contact address:** Viera Kažimírová, Slovak University of Agriculture in Nitra, Slovakia, e-mail: [viera.kazimirova@uniag.sk](mailto:viera.kazimirova@uniag.sk)

Swine manure pellet type 1 was produced from dried swine manure by adding 10% of water. Swine manure pellet type 2 was produced from dried swine manure by adding 20% of water.

#### Parameters and pellet density

Pellet density was measured in accordance with the STN EN ISO 18847 Solid biofuels – Determination of particle density of pellets and briquettes, which is aimed at evaluation of pellet density produced from wood as well as waste of agricultural production origins. It is necessary to let the pellets to stabilize. The diameter, length and weight of the pellet are continuously measured throughout the entire process. Only when the pellet weight changes by a maximum of 0.1% within 24 hours, it is possible to consider the pellets stabilized. In relation to determination of pellet density, the specimen diameter and length with an accuracy of  $\pm 0.05$  mm was determined according to the STN EN ISO 17829 Solid biofuels – Determination of length and diameter of pellets. Pellet weight was measured by means of laboratory scales Explorer Pro (Ohaus Corporation, USA) with an accuracy of  $\pm 0.0001$  mg. The final pellet weight was calculated on the basis of obtained data.

#### Pellet moisture content

In order to determine the pellet moisture content, gravimetric furnace Nabertherm L9/11/SW (Nabertherm GmbH, Germany) with digital scales Kern ew 420-3NM (with accuracy of  $\pm 0.001$  g) was used, since it allows heating of analysed samples up to  $1,100$  °C while recording the weight of the samples.

Pellet moisture was determined in accordance with STN EN ISO 18134 Solid biofuels – Determination of moisture content. The sample is heated to  $105$ – $110$  °C and is dried until the difference in sample mass between two consecutive measurements, conducted 30 minutes apart, is lower than 0.1% of the sample mass observed at the previous measuring.

#### Measurement of pellet mechanical properties

Pellet mechanical properties are assessed by means of a quasi-static compressive loading test. For the purposes of measurement, only undamaged pellet samples with modified contact surfaces – these must be straight – can be used. The pellet is placed on a solid plane in the axis of the testing device. Subsequently, the pellet is compressed between two planes, while the upper plane of testing device is of circular shape with 20 mm diameter; the lower plane is of rectangular shape. Movement speed of upper circular plane is set to  $10$  mm·min<sup>-1</sup>. The maximal loading force applied to sample is 500 N. The device records loading force values with accuracy of 0.05 N.

#### Measurement evaluation

The results of pellet compressive loading test include values of force  $F$  and movement of upper plane of measuring device  $\Delta L_0$ . In order to plot the compression diagram  $F(\varepsilon)$ , it is firstly necessary to calculate the pellet deformation according to the relation:

$$\varepsilon = \frac{\Delta L_0}{L_0} \quad (1)$$

where:

$\varepsilon$  – deformation (mm·mm<sup>-1</sup>);  $L_0$  – initial pellet length (mm);  $\Delta L_0$  – distance between the device planes (mm)

Furthermore, for the purposes of plotting the compression diagram, it is vital to determine the compressive stress on the basis of the following relation:

$$\sigma = \frac{F}{S} \quad (2)$$

where:

$\sigma$  – compressive stress (MPa);  $F$  – force acting on the pellet (N);  $S$  – cross-sectional area of the pellet (mm<sup>2</sup>)

The pellet elasticity modulus is determined using linear regression method, the result of which is as follows:

$$\sigma = E\varepsilon + m \quad (3)$$

where:

$\sigma$  – compressive stress (MPa);  $E$  – elasticity modulus (MPa);  $\varepsilon$  – deformation (mm·mm<sup>-1</sup>);  $m$  – regression coefficient (MPa)

Subsequently, the force in the first maximum of the loading curve  $F_m$  and deformation in the first maximum are determined:

$$\varepsilon_m = \frac{vt_m}{L_0} \quad (4)$$

where:

$\varepsilon_m$  – deformation at the first maximum of force (mm·mm<sup>-1</sup>);  $v$  – deformation rate (mm·s<sup>-1</sup>);  $t_m$  – time at the first maximum of force (s);  $L_0$  – initial pellet length (mm)

Time  $t_m$  is determined on the basis of the first maximum of the loading curve  $F(t)$ . Deformation rate is calculated on the basis of values of movement course and rate of upper loading plane. Deformation  $\varepsilon_{mp}$  is subtracted from dependence  $F(\varepsilon)$ .

Compressive stress in the first maximum of loading curve is calculated as follows:

$$\sigma_m = \frac{4F_m}{\pi d^2}(1 - \varepsilon_m) \quad (5)$$

where:

$\sigma_m$  – compressive stress in the first maximum (MPa);  $F_m$  – force at the first maximum (N);  $d$  – pellet diameter (mm);  $\varepsilon_m$  – deformation at the first maximum of force (mm·mm<sup>-1</sup>)

Compressive stress  $\sigma_{mp}$  is subtracted from dependence  $\sigma(\varepsilon)$ .

Initial pellet strength  $F_{10}$  is determined as force necessary for 10% compression strain. Value  $F_{10}$  is subtracted from dependence  $F(\varepsilon)$ .

Another evaluated pellet property is loading force in the inflection point  $F_{inf}$ , deformation in the inflection point  $\varepsilon_{inf}$  and compressive stress in the inflection point  $\sigma_{inf}$ . Inflection point lies between the beginning and the first maximum of the loading curve. Dependence gradient changes its increasing tendency to decreasing in the inflection point.

In order to obtain these properties, it is necessary to plot a cubic regression curve in compression diagram within the interval  $(0, F_m)$ . Following regression formula are the results:

$$F = a\varepsilon^3 + b\varepsilon^2 + c\varepsilon + d \quad (6a)$$

where:

$F$  – compression force (N);  $\varepsilon$  – deformation ( $\text{mm}\cdot\text{mm}^{-1}$ );  $a$  – regression coefficient ( $\text{N}\cdot(\text{mm}\cdot\text{mm}^{-1})^{-3}$ );  $b$  – regression coefficient ( $\text{N}\cdot(\text{mm}\cdot\text{mm}^{-1})^{-2}$ );  $c$  – regression coefficient ( $\text{N}\cdot(\text{mm}\cdot\text{mm}^{-1})$ );  $d$  – regression coefficient (N)

$$F = et^3 + ft^2 + gt + h \quad (6b)$$

where:

$F$  – compression force (N);  $t$  – compression time (s);  $e$  – regression coefficient ( $\text{N}\cdot\text{s}^{-3}$ );  $f$  – regression coefficient ( $\text{N}\cdot\text{s}^{-2}$ );  $g$  – regression coefficient ( $\text{N}\cdot\text{s}^{-1}$ );  $h$  – regression coefficient (N)

Accuracy of the regression formula is expressed by determination coefficient  $R^2$ .

Deformation in the inflection point of the compression diagram is calculated as follows:

$$\varepsilon_{inf} = \frac{vt_{inf}}{L_0} \quad (7)$$

where:

$\varepsilon_{inf}$  – deformation in the inflection point ( $\text{mm}\cdot\text{mm}^{-1}$ );  $v$  – deformation rate ( $\text{mm}\cdot\text{s}^{-1}$ );  $t_{inf}$  – time in the inflection point (s);  $L_0$  – original pellet length (mm)

Compressive stress in the inflection point can be calculated according to the following formula:

$$\sigma_{inf} = \frac{4F_{inf}}{\pi d^2} (1 - \varepsilon_{inf}) \quad (8)$$

where:

$\sigma_{inf}$  – compressive stress in the inflection point (MPa);  $F_{inf}$  – force in the inflection point (N);  $d$  – pellet diameter (mm);  $\varepsilon_{inf}$  – deformation in the inflection point ( $\text{mm}\cdot\text{mm}^{-1}$ )

Time and force in the inflection point were subtracted from dependence  $F(t)$ .

Statistical indicators – arithmetic mean; standard deviation; variation coefficient – are utilized for the purposes of assessment of recorded and calculated values. In terms of pellet properties evaluation, correlation coefficient is also determined.

## Results and discussion

Table 1 shows geometrical properties, density and moisture content of pellet types 1 and 2.

**Table 1** Properties of pellet types 1 and 2

|  | Pellets   | 1        | 2        |
|--|-----------|----------|----------|
| Diameter $d$ (mm)                                | $\bar{x}$ | 6.21     | 5.82     |
|  | $S$       | 0.08     | 0.09     |
|  | $s$ (%)   | 1.32     | 1.54     |
| Length $L_0$ (mm)                                | $\bar{x}$ | 14.36    | 13.03    |
|  | $S$       | 1.51     | 1.02     |
|  | $s$ (%)   | 10.52    | 7.8      |
| Density $\rho$ ( $\text{kg}\cdot\text{m}^{-3}$ ) | $\bar{x}$ | 1,407.23 | 1,363.04 |
|  | $S$       | 9        | 10.88    |
|  | $s$ (%)   | 0.64     | 0.8      |
| Moisture $W$ (%)                                 | $\bar{x}$ | 8.46     | 8.46     |
|  | $S$       | 0.14     | 0.13     |
|  | $s$ (%)   | 1.63     | 1.48     |

Mean density is  $1,407.23 \text{ kg}\cdot\text{m}^{-3}$  for pellet type 1 and  $1,363.04 \text{ kg}\cdot\text{m}^{-3}$  for pellet type 2. The standard deviation for density is low. Pampuro et al. (2013) reported that it is possible to increase the pellet density made of swine manure from an initial value of  $<200 \text{ kg}\cdot\text{m}^{-3}$  to a final value  $>1,000 \text{ kg}\cdot\text{m}^{-3}$  by compression of dry fraction. The density of the pellet type 2 is lower in contrast to pellet type 1, however, mean moisture contents of both types are identical – 8.46% – despite the fact that different amounts of water were used for their production. This does not influence the moisture content of stabilized pellets, what is also indicated by standard deviation, as well as low variation coefficient.

Fig. 2 illustrates the dependences  $F(\varepsilon)$  and  $F(t)$  obtained from compressive loading test of pellets made of swine manure 1. Behaviour of all pellets during compression process is very similar. Compression diagrams are largely almost linear. Pampuro et al. (2017) reported similar course of compressive loading test in their investigation of pellets made of swine manure.

Values of  $F_m$  ranged from 215.77 to 418.18 N. Deformation values are low, mere 10–15%, suggesting the low pellet compressibility. The time necessary for reaching the first maximum is relatively balanced and ranges from 8.6 to 12 s.

Fig. 3 illustrates the dependences  $F(\varepsilon)$  and  $F(t)$  obtained from compressive loading test of pellets made of swine manure 2. Similarly to pellet type 1, compression diagram of all pellets is largely linear. Furthermore, almost all curves show a steep gradient. Values of  $F_m$  ranges from 105.4 to 217.36 N; Zhai et al. (2018) – who investigated pellets made of hydrochar with molasses as a binder and subjected them to compressive loading test – observed similar values for  $F_m$ . The time, necessary for reaching the first maximum, ranges from 8.8 to 16.1 s.

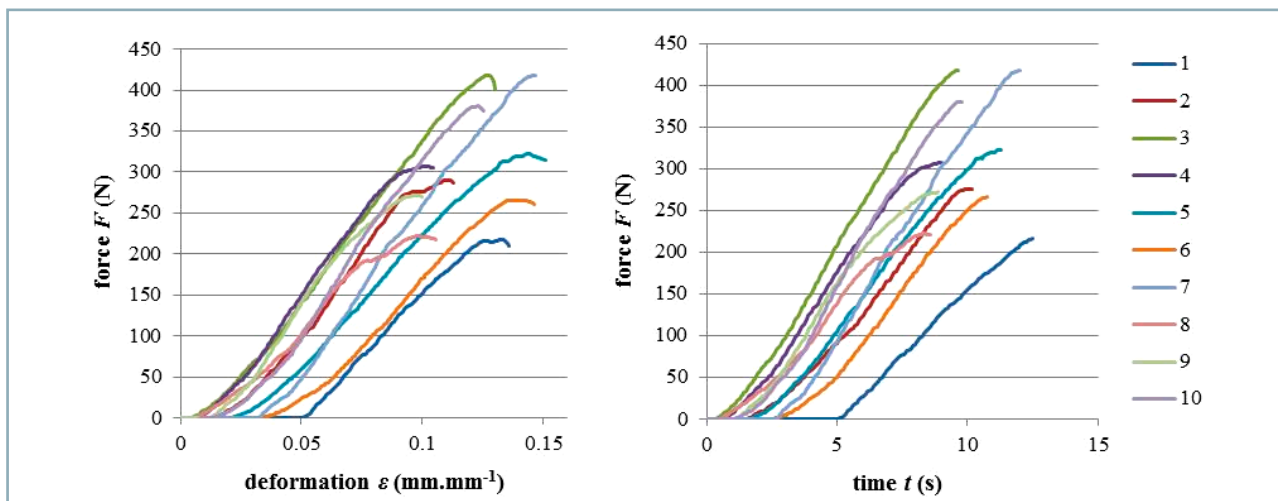


Fig. 2 Compression diagrams of pellet type 1 – dependences  $F(\varepsilon)$  and  $F(t)$

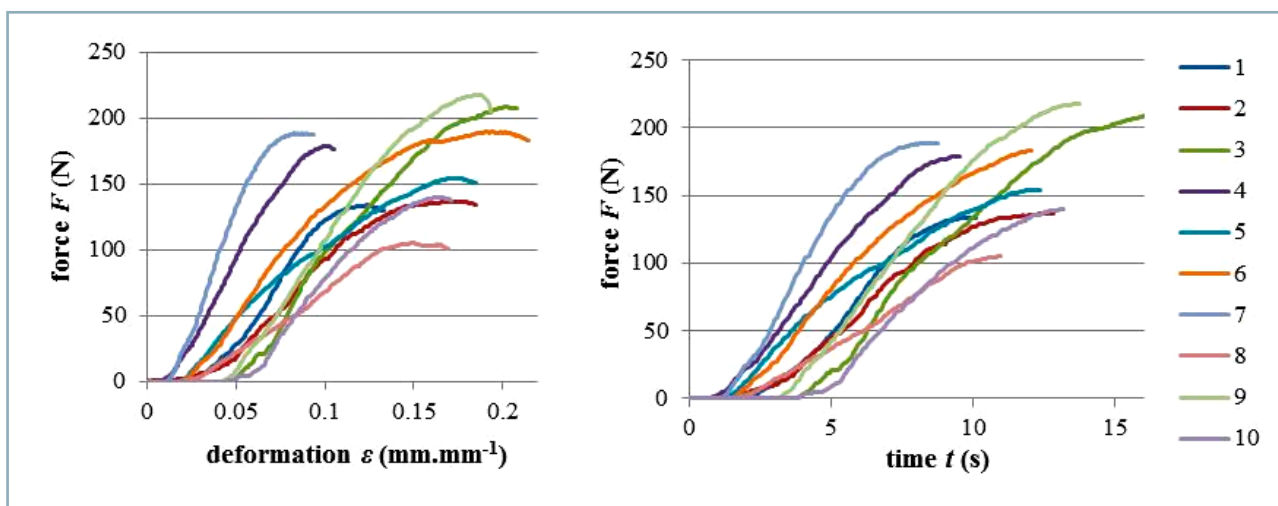


Fig. 3 Compression diagrams of pellet type 2 – dependences  $F(\varepsilon)$  and  $F(t)$

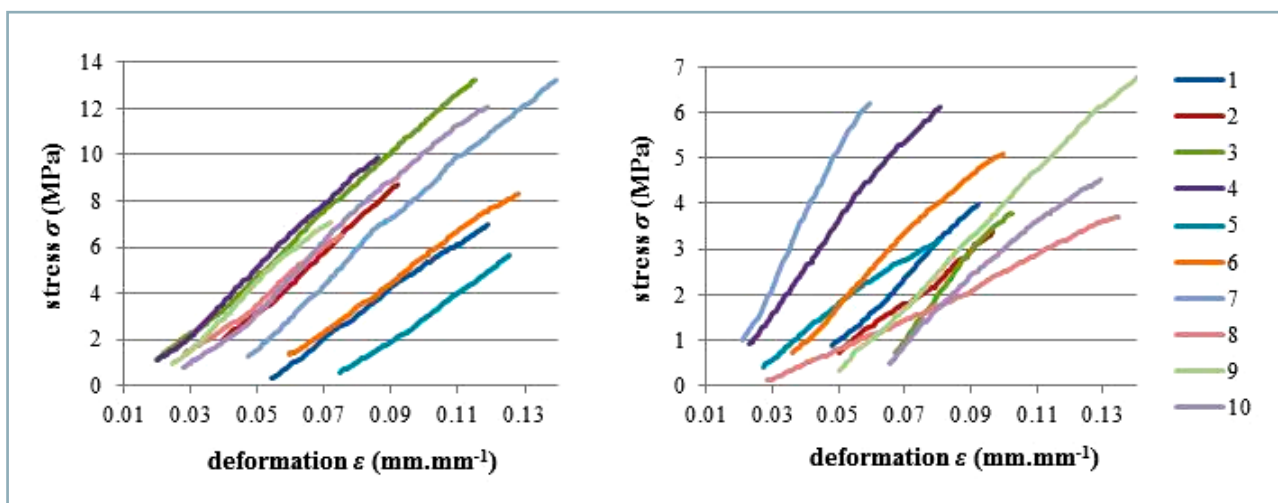


Fig. 4 Linear parts of dependence  $\sigma(\varepsilon)$

Course of compressive loading test indicates that majority of pellets of both types is fragile.

Pellet modulus of elasticity is determined from linear part of dependence  $\sigma(\epsilon)$  (Fig. 4). Gradient of all curves obtained from testing of pellet type 1 is uniform. Values of modulus of elasticity of pellet type 1 ranges from 102.58 to 139.05 MPa. It is possible to divide the pellet type 2 into two groups on the basis of the gradient of curves. Values of modulus of elasticity of pellet type 2 ranges from 34.77 to 140.63 MPa.

Each determination coefficient  $R^2$  shows value close to 1, indicating that their regressive curves showing the course of compressive loading test are almost identical with compression diagrams.

Table 2 shows the mechanical properties of the pellets made of swine manure (types 1 and 2). The results show that mechanical properties of these pellets are not the same. Values of  $F_m$ ,  $\sigma_m$ ,  $E$ ,  $F_{10}$ ,  $F_{inf}$  and  $\sigma_{inf}$  are higher in pellet type 1;  $\epsilon_m$  shows higher values in pellet type 2 and values of  $\epsilon_{inf}$  are the same for both pellet types. Values of  $F_m$  and  $F_{10}$  show the highest standard deviation.

The results indicate that addition of different amounts of water for the binding purposes in pellet production has an impact on the mechanical properties of the final products. Moreover, Jandačka et al. (2013) and Zhai et al. (2018) also confirmed that addition of liquid binder directly influences the final pellet mechanical properties.

Mean value of the elasticity modulus of pellet type 2 is 1.7 times lower in contrast to pellet type 1 that is made with addition of smaller amount of water. Furthermore, pellet type 1 showed mean strength of 10.47 MPa; pellet type 2 – produced with twice as much water as pellet type 1 – showed mean strength of 6.24 MPa. In addition to this, moisture content of final pellets after their stabilization was 8.46% for both types.

However, not only the final moisture content but also the amount of water or other liquid used during pellet production process for the binding purposes is of great significance, as confirmed by Huang et al. (2017). This means that the input material moisture influences the quality characteristics of the final products. Amount of added water is particularly important in cases when input resource contains water-soluble components, which subsequently form solid bridges that usually result in pellet strength enhancement after their drying. By adding more water than the optimal amount, the pellet material passes through the compression die holes more easily and compression level and density of pellets are lower. This fact is also confirmed by the results of assessment of mechanical properties of pellets made of swine manure.

Table 3 shows correlation coefficients of properties of pellet type 1 and Table 4 provides correlation coefficients for pellet type 2. Correlation coefficients with value exceeding 0.8 indicate significant linear dependence between properties and are highlighted in the tables. Mechanical pellet properties do not show significant dependence on geometric parameters.

**Table 2** Mechanical properties of pellets

|   | Pellets   | 1      | 2      |
|---|-----------|--------|--------|
| $F_m$ (N)                               | $\bar{x}$ | 309.65 | 164.69 |
|   | S         | 70.54  | 34.32  |
|   | s (%)     | 22.78  | 20.84  |
| $\epsilon_{mp}$ (mm·mm <sup>-1</sup> )  | $\bar{x}$ | 0.12   | 0.15   |
|   | S         | 0.02   | 0.04   |
|   | s (%)     | 15.44  | 23.32  |
| $\sigma_{mp}$ (MPa)                     | $\bar{x}$ | 10.22  | 6.21   |
|   | S         | 2.27   | 1.36   |
|   | s (%)     | 22.24  | 21.92  |
| $\epsilon_m$ (mm·mm <sup>-1</sup> )     | $\bar{x}$ | 0.12   | 0.16   |
|   | S         | 0.02   | 0.03   |
|   | s (%)     | 15.24  | 21.31  |
| $\sigma_m$ (MPa)                        | $\bar{x}$ | 8.98   | 4.1    |
|   | S         | 1.91   | 0.88   |
|   | s (%)     | 21.24  | 21.45  |
| $E$ (MPa)                               | $\bar{x}$ | 122.39 | 71.12  |
|   | S         | 13.35  | 27.34  |
|   | s (%)     | 10.91  | 38.44  |
| $F_{10}$ (N)                            | $\bar{x}$ | 253.91 | 116.43 |
|   | S         | 57.76  | 37.82  |
|   | s (%)     | 22.75  | 32.48  |
| $F_{inf}$ (N)                           | $\bar{x}$ | 165.37 | 71.65  |
|   | S         | 34.48  | 27.34  |
|   | s (%)     | 20.85  | 38.16  |
| $\epsilon_{inf}$ (mm·mm <sup>-1</sup> ) | $\bar{x}$ | 0.07   | 0.07   |
|   | S         | 0.02   | 0.03   |
|   | s (%)     | 23.9   | 34.09  |
| $\sigma_{inf}$ (MPa)                    | $\bar{x}$ | 5.07   | 2.49   |
|   | S         | 1.01   | 0.95   |
|   | s (%)     | 19.9   | 38.15  |
| $\sigma_p$ (MPa)                        | $\bar{x}$ | 10.47  | 6.24   |
|   | S         | 2.19   | 1.38   |
|   | s (%)     | 20.93  | 22.15  |

**Table 3** Correlation coefficients of properties of pellet type 1

|                     | $d$  | $L_0$ | $F_{10}$ | $F_m$ | $\varepsilon_{mp}$ | $\sigma_{mp}$ | $\varepsilon_m$ | $\sigma_m$ | $E$   | $F_{inf}$ | $\varepsilon_{inf}$ | $\sigma_{inf}$ |
|---------------------|------|-------|----------|-------|--------------------|---------------|-----------------|------------|-------|-----------|---------------------|----------------|
| $d$                 | 1    |       |          |       |                    |               |                 |            |       |           |                     |                |
| $L_0$               | 0.01 | 1     |          |       |                    |               |                 |            |       |           |                     |                |
| $F_{10}$            | 0.27 | -0.2  | 1        |       |                    |               |                 |            |       |           |                     |                |
| $F_m$               | 0.33 | -0.57 | 0.69     | 1     |                    |               |                 |            |       |           |                     |                |
| $\varepsilon_{mp}$  | 0.06 | -0.53 | -0.32    | 0.46  | 1                  |               |                 |            |       |           |                     |                |
| $\sigma_{mp}$       | 0.23 | -0.6  | 0.69     | 0.99  | 0.46               | 1             |                 |            |       |           |                     |                |
| $\varepsilon_m$     | 0.09 | -0.54 | -0.32    | 0.44  | 0.99               | 0.44          | 1               |            |       |           |                     |                |
| $\sigma_m$          | 0.23 | -0.56 | 0.75     | 0.99  | 0.38               | 1             | 0.36            | 1          |       |           |                     |                |
| $E$                 | 0.27 | 0.06  | 0.83     | 0.48  | -0.45              | 0.47          | -0.49           | 0.53       | 1     |           |                     |                |
| $F_{inf}$           | 0.34 | -0.37 | 0.58     | 0.94  | 0.53               | 0.93          | 0.49            | 0.92       | 0.37  | 1         |                     |                |
| $\varepsilon_{inf}$ | 0.03 | -0.03 | -0.56    | 0.1   | 0.83               | 0.09          | 0.81            | 0.02       | -0.59 | 0.33      | 1                   |                |
| $\sigma_{inf}$      | 0.23 | -0.38 | 0.63     | 0.94  | 0.47               | 0.94          | 0.43            | 0.94       | 0.41  | 0.99      | 0.26                | 1              |

**Table 4** Correlation coefficients of properties of pellet type 2

|                     | $d$   | $L_0$ | $F_{10}$ | $F_m$ | $\varepsilon_{mp}$ | $\sigma_{mp}$ | $\varepsilon_m$ | $\sigma_m$ | $E$   | $F_{inf}$ | $\varepsilon_{inf}$ | $\sigma_{inf}$ |
|---------------------|-------|-------|----------|-------|--------------------|---------------|-----------------|------------|-------|-----------|---------------------|----------------|
| $d$                 | 1     |       |          |       |                    |               |                 |            |       |           |                     |                |
| $L_0$               | -0.25 | 1     |          |       |                    |               |                 |            |       |           |                     |                |
| $F_{10}$            | -0.5  | 0.6   | 1        |       |                    |               |                 |            |       |           |                     |                |
| $F_m$               | -0.42 | 0.14  | 0.48     | 1     |                    |               |                 |            |       |           |                     |                |
| $\varepsilon_{mp}$  | 0.24  | -0.65 | -0.74    | 0.18  | 1                  |               |                 |            |       |           |                     |                |
| $\sigma_{mp}$       | -0.53 | 0.17  | 0.53     | 0.99  | 0.12               | 1             |                 |            |       |           |                     |                |
| $\varepsilon_m$     | 0.05  | -0.7  | -0.63    | 0.27  | 0.96               | 0.24          | 1               |            |       |           |                     |                |
| $\sigma_m$          | -0.57 | 0.31  | 0.67     | 0.96  | -0.08              | 0.98          | 0.04            | 1          |       |           |                     |                |
| $E$                 | -0.51 | 0.48  | 0.89     | 0.48  | -0.7               | 0.53          | -0.59           | 0.68       | 1     |           |                     |                |
| $F_{inf}$           | 0.03  | 0.35  | 0.23     | 0.53  | -0.03              | 0.49          | -0.15           | 0.53       | 0.43  | 1         |                     |                |
| $\varepsilon_{inf}$ | 0.48  | -0.15 | -0.64    | 0.01  | 0.54               | -0.07         | 0.36            | -0.16      | -0.41 | 0.57      | 1                   |                |
| $\sigma_{inf}$      | -0.07 | 0.4   | 0.33     | 0.55  | -0.13              | 0.52          | -0.24           | 0.58       | 0.52  | 0.99      | 0.47                | 1              |

### Conclusion

The presented research was aimed at evaluation of the selected properties of alternative pellets made from dried swine manure, i.e. density, moisture, and mechanical properties.

The density values of the two observed pellet types are 1,407.23 kg·m<sup>-3</sup> and 1,363.04 kg·m<sup>-3</sup>, respectively. It can be concluded that, from the density standpoint, the observed pellets are comparable to pellets commonly used for heat production by direct combustion.

Mean moisture value of both pellet types is 8.46%, satisfying the standards for solid biofuels.

Static compressive loading test was used for evaluation of the pellet mechanical properties. Results show that the observed pellets do not differ from each other significantly in this regard. Additionally, the observed values are comparable to those of pellets made from other types of biomass. In pellet type 1, which used 10% vol. water as a binder, compressive strength was higher than in type 2. The same is true for other

observed properties, with the exception of deformation properties, which were lower than in type 2.

### Acknowledgement

This publication was supported by the operational programme Research and Innovation for the project: Support of Energetics Research Activities at SUA Nitra, 313011X029, co-funded with resources of European Regional Development Fund.

### References

- BAPPAH, M. – BRADNA, J. – VELEBIL, J. – MALAŤÁK, J. 2019. The potential of energy recovery from by-products of small agricultural farms in Nigeria. In *Agronomy Research*, vol. 17, no. 6, pp. 2180–2186.
- CARROLL, J. P. – FINNAN, J. 2012. Physical and chemical properties of pellets from energy crops and cereal straws. In *Biosystem Engineering*, vol. 112, no. 2, pp. 151–159.

- DUMITRASCU, R. – LUNGULEASA, A. – SPIRCHEZ, C. 2018. Renewable pellets obtained from aspen and birch bark. In *BioResources*, vol. 13, no. 3, pp. 6985–7001.
- GARCÍA-MARAVÉ, A. – RODRIGUEZ, M. L. – SERRANO-BERNARDO, F. – DIAZ, L. F. – ZAMORANO, M. 2015. Factors affecting the quality of pellets made from residual biomass of olive trees. In *Fuel Processing Technology*, vol. 129, pp. 1–7.
- HUANG, Y. – FINELL, M. – LARSSON, S. – WANG, X. – ZHANG, J. – WEI, R. – LIU, L. 2017. Biofuel pellets made at low moisture content – Influence of water in the binding mechanism of densified biomass. In *Biomass and Bioenergy*, vol. 98, pp. 8–14.
- JANDAČKA, J. – HOLUBČÍK, M. – MALCHO, M. – NOSEK, R. 2013. Modification of wood pellets parameters by using of organic compounds from defibration. In *Acta Facultatis Xylogologiae Zvolen*, vol. 55, no. 2, pp. 105–115. (In Slovak: Modifikácia vlastností drevných peliet aplikáciou koncentráту organických látok z defibrácie).
- JIANG, L. B. – LIANG, J. – YUAN, X. Z. – LI, H. – LI, C. – XIAO, Z. H. – HUANG, H. – WANG, H. – ZENG, G. M. 2014. Co-pelletization of sewage sludge and biomass: The density and hardness of pellet. In *Bioresource Technology*, vol. 166, pp. 435–443.
- JIANG, L. B. – YUAN, X. Z. – LI, H. – CHEN, X. H. – XIAO, Z. H. – LIANG, J. – LENG, L. J. – GUO, Z. – ZENG, G. M. 2016. Co-pelletization of sewage sludge and biomass: Thermogravimetric analysis and ash deposits. In *Fuel Processing Technology*, vol. 145, pp. 109–115.
- KUBÍK, Ľ. – KAŽIMÍROVÁ, V. 2015. Determination of mechanical properties of apple cultivar Golden Delicious. In *Journal on Processing and Energy in Agriculture*, vol. 19, no. 1, pp. 17–20.
- LEE, Y. L. – AHMED, O. H. – WAHID, S. A. – AB AZIZ, Z. F. 2019. Characterization of tablets made from mixture of charred agricultural residues with and without embedded fertilizer. In *Acta Technologica Agriculturae*, vol. 22, no. 3, pp. 70–74.
- MARTÍNEZ-GUIDO, S. I. – RÍOS-BADRÁN, I. M. – GUTIÉRREZ-ANTONIO, C. – PONCE-ORTEGA, J. M. 2019. Strategic planning for the use of waste biomass pellets in Mexican power plants. In *Renewable energy*, vol. 130, pp. 622–632.
- OLOSÓ, A. O. – CLARKE, B. 1993. Some aspects of strength properties of cashew nuts. In *Journal of Agricultural Engineering Research*, vol. 55, no. 1, pp. 27–43.
- PAMPURO, N. – BAGAGIOLO, G. – PRIARONE, P. C. – CAVALLO, E. 2017. Effects of pelletizing pressure and the addition of woody bulking agents on the physical and mechanical properties of pellets made from composted pig solid fraction. In *Powder Technology*, vol. 311, pp. 112–119.
- PAMPURO, N. – FACELLO, A. – CAVALLO, E. 2013. Pressure and specific energy requirements for densification of compost derived from swine solid fraction. In *Spanish Journal of Agricultural Research*, vol. 11, no. 3, pp. 678–684.
- PUROHIT, P. – CHATURVEDI, V. 2018. Biomass pellets for power generation in India: a techno-economic evaluation. In *Environmental Science and Pollution Research*, vol. 25, no. 29, pp. 29614–29632.
- SAID, N. – ABDEL DAIEM, M. M. – GARCÍA-MARAVÉ, A. – ZAMORANO, M. 2015. Influence of densification parameters on quality properties of rice straw pellets. In *Fuel Processing Technology*, vol. 138, pp. 56–64.
- SPIRCHEZ, C. – LUNGULEASA, A. – GACEU, L. 2019. Researches on grape husk waste obtained from the winery and its use as pellets for combustion. In *Wood Research*, vol. 64, no. 3, pp. 557–564.
- VURSAVUŞ, K. – ÖZGÜVEN, F. 2004. Mechanical behaviour of apricot pit under compression loading. In *Journal of Food Engineering*, vol. 65, no. 2, pp. 255–261.
- ZAFARI, A. – KIANMEHR, M. H. 2012. Effect of temperature, pressure and moisture content on durability of cattle manure pellet in open-end die method. In *Journal of Agricultural Science*, vol. 4, no. 5, pp. 203–208.
- ZAMORANO, M. – POPOV, V. – RODRÍGUES, M. L. – GARCÍA-MARAVÉ, A. 2011. A comparative study of quality properties of pelletized agricultural and forestry lopping residues. In *Renewable Energy*, vol. 36, pp. 3133–3140.
- ZHAI, Y. – WANG, T. – ZHU, Y. – PENG, C. – WANG, B. – LI, X. – LI, C. – ZENG, G. 2018. Production of fuel pellets via hydrothermal carbonization of food waste using molasses as a binder. In *Waste Management*, vol. 77, pp. 185–194.



Acta Technologica Agriculturae 3  
Nitra, Slovaca Universitas Agriculturae Nitriae, 2020, pp. 144–149

## THE EFFECT OF FERTILIZATION ON TIME DOMAIN REFLECTOMETRY PROBE MEASUREMENT ACCURACY IN THE FIELD EXPERIMENT IN SLOVAKIA

Lucia TOKOVÁ, Dušan IGAZ\*, Elena AYDIN, Ján ČIMO, Ján HORÁK

Slovak University of Agriculture in Nitra, Slovakia

The paper presents evaluation of the calibration method using side-by-side direct gravimetric and indirect time domain reflectometry (TDR) for soil moisture measurements to improve TDR measurement accuracy. Measurements were carried out at the experimental site Dolná Malanta (Slovakia) in 2017. Two non-fertilized treatments – without biochar (B0 + N0) and with biochar at 20 t·ha<sup>-1</sup> (B20 + N0) – and two fertilized treatments – with biochar at 20 t·ha<sup>-1</sup> and N fertilizer at dosages of 160 kg·ha<sup>-1</sup> (B20 + N160) and 240 kg·ha<sup>-1</sup> (B20 + N240) – were used in this study. The study also investigates the relationship between both used methods of soil water content determination. A strong correlation between both methods was observed. In case of (B0 + N0); (B20 + N0); (B20 + N160); and (B20 + N240), it was 0.93; 0.97; 0.97; and 0.98, respectively. However, it is assumed that the TDR probe may show errors in the results without prior calibration. It was observed that the accuracy of TDR device was lower for fertilized treatments in contrast to the gravimetric method and non-fertilized treatments. It is assumed that the higher measurement inaccuracy might be increased by salt concentration in the soil as a result of applied N fertilizer.

**Keywords:** soil moisture; fertilizer; time domain reflectometry; gravimetric method

Accurate measurement of soil moisture is essential for many investigations in agriculture, horticulture, ecology, forestry, hydrology, civil engineering, waste management and other environmental fields (Smith and Mullins, 2001; Chandler et al., 2014; Susha et al., 2014; Shaikh et al., 2019; Abbaspour-Gilandeh et al., 2018). Methods used for determination of the soil moisture content are divided into direct gravimetric methods, relying on the principle of determining the amount of water in the soil, and the indirect methods, relying on the principle of measuring the specific soil property which is dependent on soil moisture (Quinones and Nemeth, 2003; Antal and Igaz, 2012). Gravimetric method can be performed on both disturbed and undisturbed soil samples and it is not affected by the soil type and salinity and is easily computable. It is the standard reference method, on the basis of which the other techniques are usually calibrated. However, this method has also certain disadvantages. It is rather time-consuming in terms of soil sampling and subsequent drying in the oven until the constant weight is reached and it does not allow repetition of the measurement at the same site. Furthermore, the topsoil is severely disrupted during the soil sampling, indicating destructive aspects (Susha et al., 2014; Antal et al., 2014; Tanriverdi et al., 2016). On the contrary, indirect soil water content determination using probes is much faster than soil sampling for gravimetric method (Shukla et al., 2014). The most commonly used indirect methods of soil moisture measurement in the soil hydrology include: tensiometric method, electrical methods, dielectric methods and neutron probe method (Antal et al.,

2014). The most common dielectric method used is time domain reflectometry (TDR) method. TDR is nowadays well-established method that determines the soil moisture content using the frequency in the range from 10 MHz to 12 GHz. Application of TDR principles for determination of soil moisture has been widely accepted as an alternative method proposing an empirical relationship between the dielectric constant of soil and soil water content (Smith and Mullins, 2001; Quinones and Nemeth, 2003). Considering the saline soils, in certain cases, the imaginary part of the dielectric constant can also affect the TDR reading. When the electrical conductivity of the pore water is higher than 8–10 dS·m<sup>-1</sup>, the TDR overestimates volumetric water content. In such a manner, TDR values can be bias-free, and simultaneously underestimated, overestimated, or both underestimated and overestimated in relation to values determined by the gravimetric method. The influence of high electrical conductivity on TDR measurements seems to be soil specific (Bonnell et al., 1991; Wyseure et al., 1997; Hook et al., 2004).

The nitrogen fertilization affects the soil chemical properties, which can be followed by the lower accuracy of TDR measurements. Therefore, the aim of this study was to analyse the impacts of fertilization by inorganic nitrogen (N) at doses of 160 and 240 kg·ha<sup>-1</sup> on soil moisture content measurement using HydroSense II probe on the basis of the TDR method.

**Contact address:** Dušan Igaz, Slovak University of Agriculture in Nitra, Department of Biometeorology and Hydrology, Hospodárska 7, 949 01 Nitra, Slovakia, e-mail: [dušan.igaz@gmail.com](mailto:dušan.igaz@gmail.com)

## Material and methods

### Experimental site

Field experiment was established on March 2014 at the experimental site of the Slovak University of Agriculture in Nitra located in Dolná Malanta (48° 19' 00'' N; 18° 09' 00'' E) in the Nitra region of Slovakia. The experimental site was used for agricultural production and research purposes in order to examine the effect of biochar application at different application doses on greenhouse gas emissions, soil chemical and physical properties and crop yields (Horák et al., 2017; Kondrlová et al., 2017; Vitková et al., 2017; Kondrlová et al., 2018; Igaz et al., 2018; Juriga et al., 2018; Šimanský et al., 2018). The biochar used for the experiment was produced from the mixture of paper fibre sludge and cereal husks using pyrolysis process at 550 °C for 30 min in a Pyreg reactor (Pyreg GmbH, Dörhe, Germany) and applied at doses of 0, 10 and 20 t·ha<sup>-1</sup> to trial plots and incorporated into the top layer of soil (0–10 cm) in 2014. The N fertilizer was manually applied twice (May 9<sup>th</sup> and August 14<sup>th</sup>) during 2017 at doses of 160 and 240 kg·ha<sup>-1</sup> in the form of calcium ammonium nitrate. The lower applied rate of N was calculated according to the requirements of each crop using the balance method; the higher rate of N included 50% more N-fertilizers than the lower rate of N. The soil is classified as Haplic Luvisol according to the Soil Taxonomy (IUSS Working Group WRB, 2014) with 9.13 g·kg<sup>-1</sup> of soil organic carbon, 5.71 pH and silty loam texture (content of sand 15.2%, silt 59.9% and clay 24.9%). The area is characterized by warm lowland climate with long, warm and dry summers, short, dry winters and only a very short duration of snow cover (Igaz et al., 2018). The mean annual air temperature at the Dolná Malanta site in 2017 was 7.9 °C and the annual rainfall was 489 mm.

### Soil moisture measurement

Soil moisture measurements were conducted during the corn growing season (GS) in 2017. The measurements by means of both gravimetric and TDR methods were conducted at the following treatments: B0 + N0 – control treatment (biochar 0 t·ha<sup>-1</sup>, nitrogen 0 kg·ha<sup>-1</sup>), B20 + N0 (biochar 20 t·ha<sup>-1</sup>, nitrogen 0 kg·ha<sup>-1</sup>), B20 + N160 (biochar 20 t·ha<sup>-1</sup>, nitrogen 160 kg·ha<sup>-1</sup>) and B20 + N240 (biochar 20 t·ha<sup>-1</sup>, nitrogen 240 kg·ha<sup>-1</sup>). The volumetric water content (VWC) measurements were conducted weekly from April to May and on monthly basis during the rest of the corn GS (June to October 2017). Undisturbed soil samples were taken from the topsoil (10 cm depth) with a special coring tool with a fixed volume of 100 cm<sup>3</sup>. Soil sampling was performed at 3 randomly selected locations at plots representing each of 4 treatments for VWC determination. Volumetric water content in the soil samples was calculated as follows:

$$VWC = \frac{V_w}{V_t} \quad (1)$$

where:

$V_w$  – volume of soil water phase (cm<sup>3</sup>);  $V_t$  – total volume of the soil sample (cm<sup>3</sup>) (Antal and Igaz, 2012; Shukla et al., 2014; Lima et al., 2018)

Simultaneously, TDR equipment was used for the purposes of performing the measurements at the same time and location of soil sampling. The TDR measurements were performed using HydroSense II system – model CS659 (Campbell Scientific, Inc.®). It uses a proprietary technique to determine the water content in widely varying soils with corrections for a range of bulk electrical conductivities. A display (sensor with two 12 cm long rods) and processing software belong to the major system components. The HS2 presents measured VWC as volumetric water content (% vol.). In order to achieve the accurate repeatable measurements, the sensor rods must be fully inserted into the soil during the measurement. If the water content over a large area is to be determined, several measurements may be required to establish a representative measurement. The calibration coefficients used by the HS2 were determined for typical soil types under laboratory conditions by the manufacturer. The device accuracy is ±3% VWC for typical mineral soils with solution electric conductivity ≤6.5 dS·m<sup>-1</sup>. When measuring atypical soils, user-determined coefficients can be applied. Soil-specific calibration can be performed using an independent measurement of water content such as by gravimetric analysis (Product Manual HS2 and HSP2, 2019).

## Results and discussion

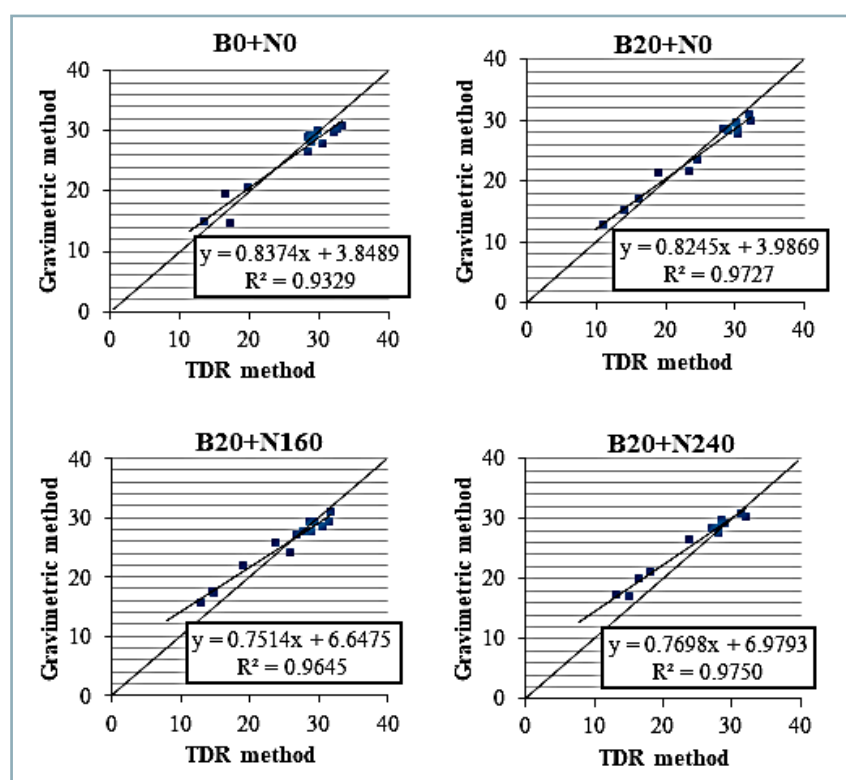
The calibration of TDR probes is sensitive to variations in soil properties, such as soil texture. Gravimetric method is a standard method that can be applied to calibration of all indirect methods (Chandler et al., 2014; Tanriverdi et al., 2016). Shukla et al. (2014) as well as Holzman et al. (2017) by comparison of values obtained by standard gravimetric method with values measured by soil moisture sensors calculated linear regression equations for each soil type. The field comparison of gravimetric and TDR water content measurements gives a good confidence in the TDR calibration relationships. In the research of Tanriverdi et al. (2016), TDR calibration was found to fit the gravimetrically determined volumetric water content data very well (with  $R^2 = 0.995$ ). In the case presented, the CS659 sensor used was calibrated for 4 different treatments: B0 + N0; B20 + N0; B20 + N160; and B20 + N240. The mean soil volumetric water content values determined by drying of soil samples and measured by the TDR in the field are provided in Table 1.

The regression relationship between gravimetric and TDR methods expressed by calibration equations is shown in Fig. 1. These equations were used to recalculate (calibrate) values of soil volumetric water content determined by TDR method, which are also listed in Table 1 (as a mean).

The Pearson correlation coefficient showed a very high correlation between TDR and gravimetric method. The determined correlation coefficients ( $R^2$ ) for B0 + N0; B20 + N0; B20 + N160; and B20 + N240 were 0.93; 0.97; 0.97; and 0.98, respectively. Table 2 presents a comparison of the number of measured and calibrated values to the total number of measurements that are within ±10% threshold of the values obtained utilizing gravimetric method (Igaz et al., 2008). Before TDR device calibration, only 67% of all measured values were within ±10% threshold when compared to

**Table 1** Measured values of VWC (%) by the gravimetric and TDR methods and calibrated TDR values

|            |                               | April |      |      |      | May  |      |      |      |      | June | July | August | September | October |
|------------|-------------------------------|-------|------|------|------|------|------|------|------|------|------|------|--------|-----------|---------|
|            |                               | 03    | 10   | 21   | 24   | 03   | 09   | 15   | 22   | 29   | 29   | 18   | 14     | 05        | 10      |
| B0 + N0    | measured values (gravimetric) | 28.2  | 30.2 | 29.1 | 29.3 | 30.8 | 29.9 | 30.2 | 28.1 | 26.7 | 19.5 | 20.8 | 15.1   | 14.7      | 29.2    |
|            | measured values (TDR)         | 28.8  | 29.6 | 28.3 | 28.6 | 33.3 | 32.0 | 32.6 | 30.4 | 28.3 | 16.4 | 19.6 | 13.4   | 17.2      | 29.3    |
|            | calibrated values (TDR)       | 27.9  | 28.6 | 27.5 | 27.8 | 31.8 | 30.7 | 31.2 | 29.3 | 27.5 | 17.6 | 20.3 | 15.0   | 15.0      | 28.4    |
| B20 + N0   | measured values (gravimetric) | 28.6  | 28.5 | 28.4 | 29.7 | 30.9 | 30.0 | 27.7 | 23.5 | 21.5 | 17.0 | 21.4 | 15.2   | 12.9      | 28.3    |
|            | measured values (TDR)         | 28.3  | 28.9 | 30.3 | 30.2 | 32.0 | 32.2 | 30.5 | 24.5 | 23.4 | 16.0 | 19.0 | 13.9   | 10.9      | 28.9    |
|            | calibrated values (TDR)       | 27.3  | 27.8 | 28.9 | 28.9 | 30.4 | 30.5 | 29.2 | 24.2 | 23.3 | 17.2 | 19.7 | 15.4   | 13.0      | 27.8    |
| B20 + N160 | measured values (gravimetric) | 27.7  | 29.4 | 27.8 | 29.2 | 30.9 | 29.4 | 28.4 | 24.1 | 25.8 | 17.2 | 21.9 | 17.7   | 15.6      | 27.3    |
|            | measured values (TDR)         | 27.6  | 29.2 | 28.9 | 28.7 | 31.7 | 31.4 | 30.5 | 25.8 | 23.7 | 14.7 | 18.9 | 14.4   | 12.9      | 26.8    |
|            | calibrated values (TDR)       | 27.4  | 28.6 | 28.4 | 28.2 | 30.5 | 30.3 | 29.6 | 26.0 | 24.5 | 17.7 | 20.8 | 17.4   | 16.3      | 26.8    |
| B20 + N240 | measured values (gravimetric) | 27.7  | 29.9 | 28.6 | 28.4 | 30.8 | 30.5 | 29.4 | 28.4 | 26.5 | 20.0 | 21.1 | 17.3   | 17.0      | 28.3    |
|            | measured values (TDR)         | 28.1  | 28.5 | 27.2 | 28.0 | 31.4 | 32.0 | 28.9 | 27.9 | 23.8 | 16.4 | 18.1 | 13.1   | 15.0      | 27.1    |
|            | calibrated values (TDR)       | 28.6  | 28.9 | 27.9 | 28.5 | 31.2 | 31.6 | 29.2 | 28.5 | 25.3 | 19.6 | 20.9 | 17.1   | 18.5      | 27.9    |

**Fig. 1** Linear relationship between gravimetric and TDR methods and calibration equations

gravimetric method used for B0 + N0, B20 + N0 and B20+N160. In case of B20 + N240, it was only 62%. After calibration, this amount increased for all four treatments to 81%; 86%; 83%; and 81% for B0 + N0, B20 + N0, B20 + N160 and B20 + N240, respectively. The correlation coefficients between the gravimetric and TDR methods are also shown in Table 2.

As it can be seen, the correlation coefficients did not change after calibration of the TDR device. Considering the trend of correlation equations (Fig. 1), effect of applied N fertilizer in combination with biochar was observed in TDR measurements. The difference between the soil moisture measured by the TDR and the gravimetric methods was more pronounced with increasing dose of N fertilizer. When comparing the treatments without fertilization (B0 + N0 and B20 + N0), no substantial differences between the TDR measurement and the gravimetric method were observed. Figs. 2 and 3 show the course of daily precipitation and volumetric water content measured by both gravimetric and TDR methods for non-fertilized and fertilized treatments.

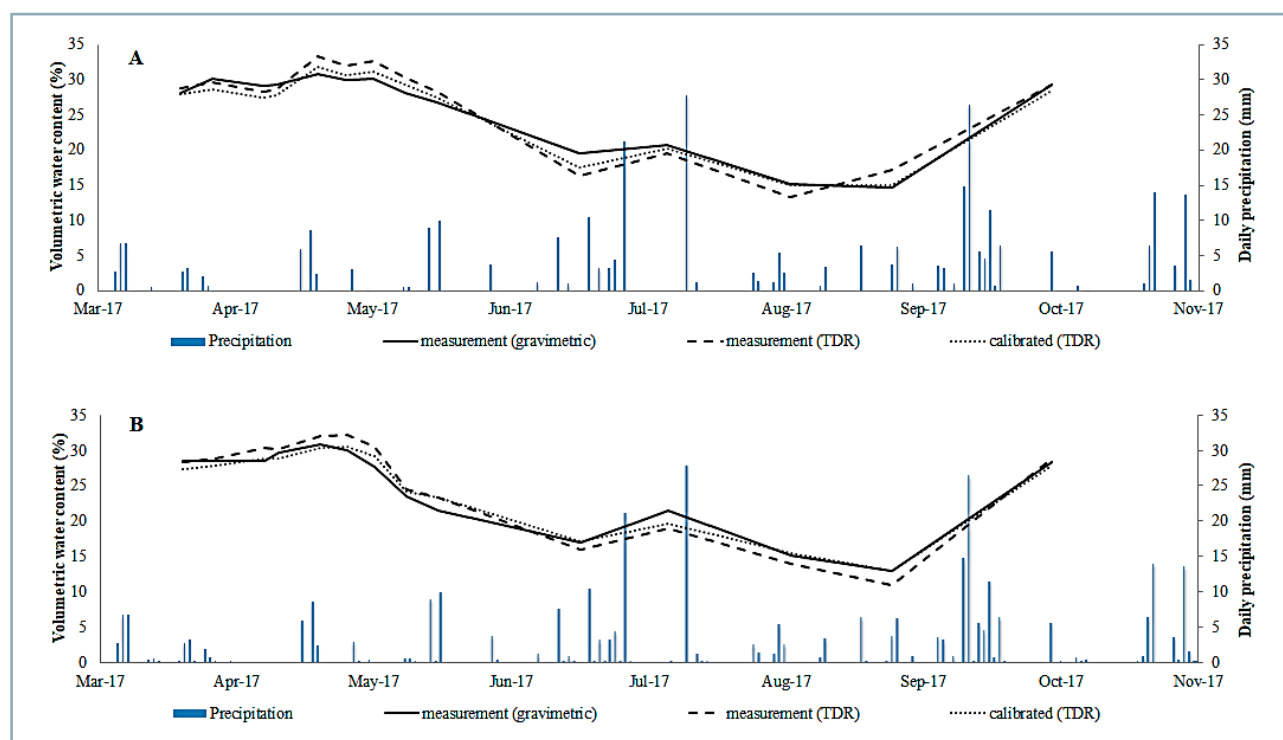
**Table 2** Comparison of the TDR measured and calibrated values within  $\pm 10\%$  with gravimetric measurement and the obtained correlation coefficients

|                   | Total number of measurements | No. of measurements within difference of $\pm 10\%$ |                         | Percentage within difference of $\pm 10\%$ |                         | Correlation coefficient ( $R^2$ ) |                         |
|-------------------|------------------------------|---|-------------------------|--|-------------------------|-----------------------------------|-------------------------|
|                   |                              | measured values (TDR)                               | calibrated values (TDR) | measured values (TDR)                      | calibrated values (TDR) | measured values (TDR)             | calibrated values (TDR) |
| <b>B0 + N0</b>    | 42                           | 28  | 34                      | 66.67%                                     | 80.95%                  | 0.93                              | 0.93                    |
| <b>B20 + N0</b>   | 42                           | 28  | 36                      | 66.67%                                     | 85.71%                  | 0.97                              | 0.97                    |
| <b>B20 + N160</b> | 42                           | 28  | 35                      | 66.67%                                     | 83.33%                  | 0.97                              | 0.97                    |
| <b>B20 + N240</b> | 42                           | 26  | 34                      | 61.90%                                     | 80.95%                  | 0.98                              | 0.98                    |

According to the trend of volumetric water content for non-fertilized treatments (Fig. 2), the differences between the moisture measured by TDR device and gravimetric method were small (0 up to 3% vol.). Such a variability might be caused by TDR device measurement inaccuracy. Following the trend of the volumetric water content for fertilized treatments (Fig. 3), lower values (from 0 up to 5% vol.) measured by TDR were observed in comparison to the gravimetric method. The greatest differences can be observed especially during the dry summer season (June – September 2017) in case of both fertilized treatments. On the basis of the results, the differences between the gravimetric method and the TDR method were considerable. It is also interesting to note that there were observed not only higher correlation coefficients ( $R^2$ ) – 0.97 and 0.98 – for fertilized treatments (B20 + N160 and B20 + N240, respectively) but also even larger differences in volumetric water content in contrast to the values obtained by gravimetric method. In the case of the control variant (B0 + N0), the correlation

coefficient was the lowest ( $R^2 = 0.93$ ), however, the difference between the water content measured by both methods was negligible. Non-fertilized treatment B20 + N0 resulted in small differences and a high correlation coefficient ( $R^2 = 0.97$ ). Using soil moisture values obtained by the CS659 sensor without prior calibration may lead to errors in the results. After applying the calibration equations obtained from the linear relationship between the gravimetric and TDR methods for the four experimental treatments, the accuracy of the measured TDR values throughout the vegetation period visibly improved, what can also be seen in Fig. 2 and Fig. 3. The soil water content values have been improved in all treatments to a range of 0 up to 2% vol. when compared to the gravimetric method. After the calibration, the values of volumetric water content measured by TDR are comparable with values determined by the gravimetric method.

Soil electrical conductivity, and thus also soil salinity, are affected by application of soil amendments such as fertilizers,

**Fig. 2** Graphical trends of VWC measured by gravimetric and TDR methods and calibrated TDR values for non-fertilized treatments A) B0 + N0 and B) B20 + N0

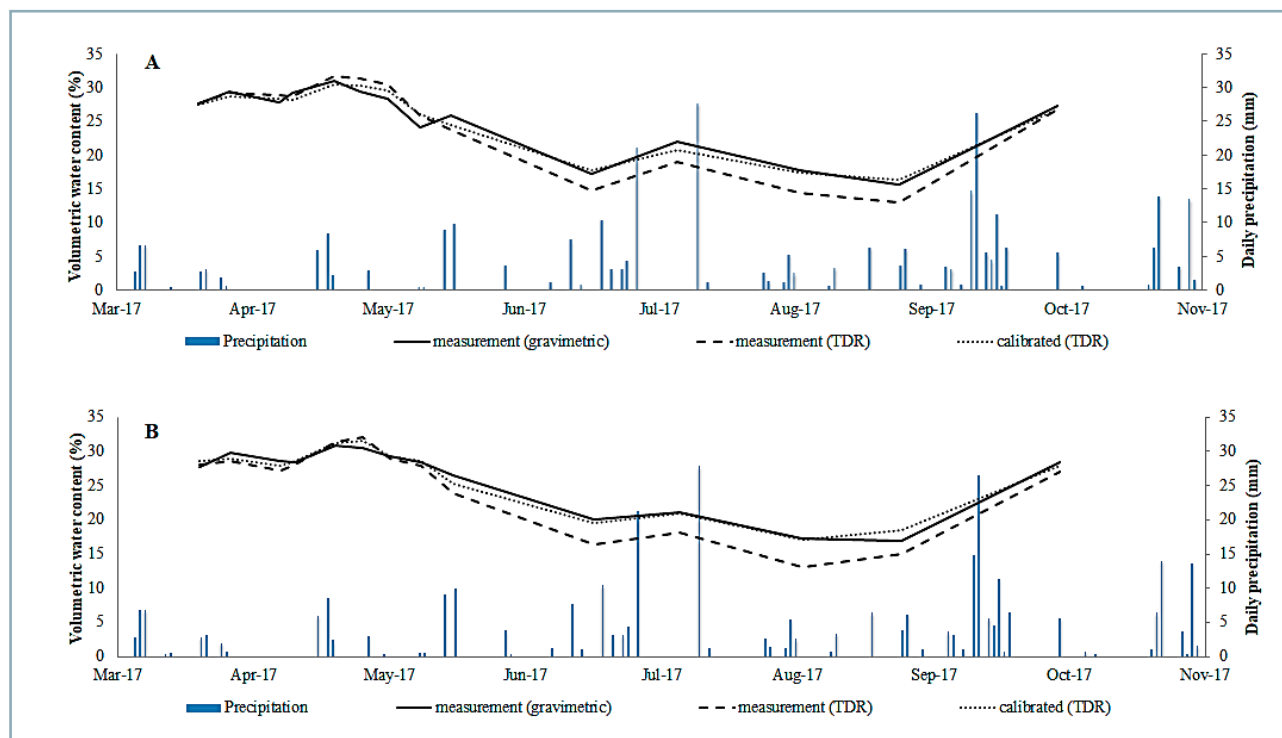


**Fig. 3** Graphical trends of VWC measured by gravimetric and TDR methods and calibrated TDR values for fertilized treatments A) B20 + N160 and B) B20 + N240

manure and composts. Nitrogen fertilizer application can increase salinity and should be monitored closely on sites with potential salinity concerns. Salinity of soil solution can be increased significantly by addition of nitrogen, because nitrogen salts are generally quite soluble with little resultant effect on the solubility of other salts that may already be present in the soil solution. Therefore, dissolved nitrogen fertilizers are additional to the total salt in solution (Yaron, 1981). Several authors, including Jiangpei et al. (2015), have investigated the impact of N fertilizers on increasing soil salinity. In their particular study, nitrogen was applied at high doses of 600 and 1,200 kg·ha<sup>-1</sup>. The authors stated that salinity had increased significantly after N addition. The increase in soil salinity was attributed to the nitrification of excess N fertilizer. Similarly, Bryla et al. (2010) pointed out that increasing N application had effect on soil electrical conductivity. The application of granular N fertilizer may increase the electrical conductivity of the soil solution. One of the disadvantages of TDR devices is their inaccurate measurement in soils with higher salinity. There is a lack of information on the soil salinity or electrical conductivity at our experimental site, however, the results show that, in treatments with added nitrogen fertilizer at doses of 160 and 240 kg·ha<sup>-1</sup>, TDR measurements were performed with better inaccuracy in contrast to non-fertilized treatments. Using the information observed by Jiangpei et al. (2015) and Bryla et al. (2010), we assume that one of the reasons of differences in the obtained values might be due to the N fertilizer application.

### Conclusion

The paper presents evaluation of the effect of applied N fertilizer at doses of 160 and 240 kg·ha<sup>-1</sup> on the accuracy

of soil moisture measurement with a HydroSense II device operating under the principle of TDR method. The measurements using TDR devices can result in errors when there is a high salt concentration in the soil. It is assumed that N fertilization increased salinity in the soil, which in turn led to measurement inaccuracies in fertilized treatments. Values on soil volumetric water content obtained by TDR for fertilized treatments (B20 + N160 and B20 + N240) differed by up to 5% vol. in comparison to gravimetric method. In case of non-fertilized treatments (B0 + N0 and B20 + N0), the differences were negligible. After application of calibration equations for each treatment, the differences in obtained values dropped to 0 up to 2% vol. during the whole crop vegetation period.

### Acknowledgement

This study was financially supported by the projects APVV-15-0160, KEGA 019SPU-4/2020, 026SPU-4/2020 and VEGA 1/0064/19, 1/0747/20.

### References

- ABBASPOUR-GILANDEH, Y. – HASANKHANI-GHAVAM, F. – SHAHGOLI, G. – SHRABIAN, V. R. – ABBASPOUR-GILANDEH, M. 2018. Investigation of the effect of soil moisture content, contact surface material and soil texture on soil friction and soil adhesion coefficients. In *Acta Technologica Agriculturae*, vol. 21, no. 2, pp. 44–50.
- ANTAL, J. – IGAZ, D. 2012. *Applied Agrohydrology*. Nitra : Slovak University of Agriculture in Nitra, 210 pp. ISBN 978-80-552-0731-5. (In Slovak: Aplikovaná agrohydrologia).
- ANTAL, J. – BÁREK, V. – ČIMO, J. – HALAJ, P. – HALÁSZOVÁ, K. – HORÁK, J. – IGAZ, D. – JURÍK, Ľ. – MUCHOVÁ, Z. – NOVOTNÁ, B. –

- ŠINKA, K. 2014. Hydrology of Agriculture Landscape. Nitra : Slovak University of Agriculture in Nitra, 371 pp. ISBN 978-80-552-1257-9. (In Slovak: Hydrológia poľnohospodárskej krajiny).
- BONNELL, R. B. – BROUGHTON, R. S. – ENRIGHT, P. 1991. The measurement of soil moisture and bulk soil salinity using time domain reflectometry. In Canadian Agricultural Engineering, vol. 33, no. 2, pp. 225–229.
- BRYLA, D. R. – SHIREMAN, A. D. – MACHADO, R. M. A. 2010. Effects of method and level of nitrogen fertilizer application on soil pH, electrical conductivity, and availability of ammonium and nitrate in blueberry. In Acta Horticulturae, vol. 868, pp. 95–102.
- CHANDLER, D. G. – SEYFRIED, M. – MURDOCK, M. – MCNAMARA, J. 2014. Field calibration of water content reflectometers. In Soil Science, vol. 68, no. 5, pp. 1501–1507.
- HOLZMAN, M. – RIVAS, R. – CARMONA, F. – NICLÒS, R. A. 2017. A method for soil moisture probes calibration and validation of satellite estimates. In MethodsX, vol. 4, pp. 243–249.
- HOOK, W. R. – FERRÉ, T. P. A. – LIVINGSTON, N. J. 2004. The effects of salinity on the accuracy and uncertainty of water measurement. In Soil Science of America Journal, vol. 68, pp. 47–56.
- HORÁK, J. – KONDRLOVÁ, E. – IGAZ, D. – ŠIMANSKÝ, V. – FELBER, R. – LUKÁČ, M. – BALASHOV, E. V. – BUCHKINA, N. P. – RIŽIJA, E. – JANKOWSKI, M. 2017. Biochar and biochar with N-fertilizer affected soil N<sub>2</sub>O emission in Haplic Luvisol. In Biologia, vol. 72, no. 9, pp. 995–1001.
- IGAZ, D. – BÁREK, V. – HALAJ, P. – TAKÁČ, J. – ČIMO, J. 2008. A comparison of measured soil moisture with simulated results obtained by selected models for Danubian lowland. In Cereal Research Communication, vol. 36, pp. 1619–1622.
- IGAZ, D. – ŠIMANSKÝ, V. – HORÁK, J. – KONDRLOVÁ, E. – DOMANOVÁ, J. – RODNÝ, M. – BUCHKINA, N. P. 2018. Can a single dose of biochar affect selected soil physical and chemical characteristics? In Journal of Hydrology and Hydromechanics, vol. 66, no. 4, pp. 421–428.
- IUSS Working Group WRB. 2014. World reference base for soil resources 2014. Update 2015. International soil classification system for naming soils and creating legends for soil maps. World Soil Resources Reports No. 106, FAO, Rome.
- JIANGPEI, H. – JIACHUN, S. – LINGZAO, Z. – JIANMING, X. – LAOSHENG, W. 2015. Effects of nitrogen fertilization on the acidity and salinity of greenhouse soils. In Environmental Science and Pollution Research, vol. 22, no. 4, pp. 2976–2986.
- JURIGA, M. – ŠIMANSKÝ, V. – HORÁK, J. – KONDRLOVÁ, E. – IGAZ, D. – POLLÁKOVÁ, N. – BUCHKINA, N. P. – BALASHOV, E. V. 2018. The effect of different rates of biochar and biochar in combination with N fertilizer on the parameters of soil organic matter and soil structure. In Journal of Ecological Engineering, vol. 19, no. 6, pp. 153–161.
- KONDRLOVÁ, E. – HORÁK, J. – IGAZ, D. – DOBIÁŠOVÁ, D. 2017. The possibility of using digital images in assessment of plant canopy development and weed spread. In Acta Horticulturae et Regiotecturae, vol. 20, no. 2, pp. 35–39.
- KONDRLOVÁ, E. – HORÁK, J. – IGAZ, D. 2018. Effect of biochar and nutrient amendment on vegetative growth of spring barley (*Hordeum vulgare* L. var Malz). In Australian Journal of Crop Science, vol. 12, no. 2, pp. 178–184.
- LIMA, J. G. A. – OLIVEIRA, A. S. – SOUZA, L. S. – SILVA, N. D. – VIANA, P. C. 2018. Calibration of a soil moisture sensor with disturbed and undisturbed soil samples from Bahia. In Revista Brasileira de Engenharia Agrícola e Ambiental, vol. 22, no. 10, pp. 696–701.
- PRODUCT MANUAL HS2 and HSP2 (HydroSense II). 2019. © 2011–2019. Available online: <https://s.campbellsci.com/documents/au/manuals/hs2.pdf>
- QUINONES, H. – NEMETH, I. 2003. Comparison of three calibration procedures for TDR soil moisture sensors. In Irrigation and Drainage, vol. 52, pp. 203–207.
- SHAIKH, J. – YAMSANI, S. K. – SEKHARAN, S. – RAKESH, R. R. 2019. Performance evaluation of 5TM sensor for real-time monitoring of volumetric water content in landfill cover system. In Civil Engineering Materials, vol. 8, no. 1, pp. 322–335.
- SHUKLA, A. – PANCHAL, H. – MISHRA, M. – PATEL, P. R. – SRIVASTAVA, H. S. – PATEL, P. – SHUKLA, A. K. 2014. Soil moisture estimation using gravimetric technique and FDR probe technique: A comparative analysis. In American International Journal of Research in Formal Applied & Natural Sciences, vol. 8, no. 1, pp. 89–92.
- SMITH, K. A. – MULLINS, CH. E. 2001. Soil water content. In Soil Environmental Analysis, 2<sup>nd</sup> ed. New York : Marcel Dekker, Inc., 637 pp. ISBN 0-8247-0414-2.
- SUSHA, L. S. U. – SINGH, S. N. – BAGHINI, M. S. 2014. A critical review of soil moisture measurement. In Measurement, vol. 54, pp. 92–105.
- ŠIMANSKÝ, V. – HORÁK, J. – IGAZ, D. – BALASHOV, E. V. – JONCZAK, J. 2018. Biochar and biochar with N fertilizer as a potential tool for improving soil sorption of nutrients. In Journal of Soil Sediments, vol. 18, no. 4, pp. 1432–1440.
- TANRIVERDI, C. – DEGIRMENCI, H. – GONEN, E. – BOYACI, S. 2016. A comparison of the gravimetric and TDR methods in terms of determining the soil water content of the corn plant. In Scientific Papers. Series A. Agronomy, vol. 59, pp. 153–158.
- VITKOVÁ, J. – ŠURDA, P. – KONDRLOVÁ, E. – HORÁK, J. – RODNÝ, M. 2017. Analysis of soil water content and crop yield after biochar application in field conditions. In Plant Soil and Environment, vol. 63, no. 12, pp. 569–573.
- WYSEURE, G. C. L. – MOJID, M. A. – MALIK, M. A. 1997. Measurement of volumetric water content by TDR in saline soils. In European Journal of Soil Science, vol. 48, pp. 347–354.
- YARON, D. 1981. Salinity in Irrigation and Water Resources. New York : Marcel Dekker, Inc., 448 pp. ISBN 0-8247-6741-1.



Acta Technologica Agriculturae 3  
Nitra, Slovaca Universitas Agriculturae Nitriae, 2020, pp. 150–154

## USING ACOUSTIC EMISSION FOR MEASURING SURFACE ROUGHNESS

Jakub ROZLIVKA<sup>1</sup>, Václav KAŠPAR<sup>1</sup>, Petr DOSTÁL<sup>1</sup>, Michal ČERNÝ<sup>1</sup>,  
Benjamín HAJTMAN<sup>1</sup>, Jozef ŽARNOVSKÝ<sup>2\*</sup>

<sup>1</sup>Mendel University in Brno, Czech Republic

<sup>2</sup>Slovak University of Agriculture in Nitra, Slovakia

This paper is focused on exploring and utilizing the acoustic emission and its behaviour during surface roughness measurement. Surface quality or coating properties significantly affect the reliability and durability of operations. Three samples were selected for an experiment to demonstrate the possibility of measuring the roughness of surface textures by means of acoustic emission method (AE). These samples were made of the following materials: sample A2 – EN 54SiCr6 steel formed in water, austenitized at 850 °C for 20 minutes, sample A3 – non-heat-treated spheroidal graphite cast iron, and sample B5 – abrasion resistant austenitic manganese steel. The surfaces were subjected to the same surface treatments (roughness  $Ra = 1.6\text{--}3.2\ \mu\text{m}$ ) and measured under the same conditions. All possible measurements were measured on both x- and y-axes. Final results are presented graphically. The measured AE values showed a visible effect in the AE signals due to the lack of surface roughness.

**Keywords:** acoustic emission; surface roughness; surface quality; surface texture; acoustic waves

Evaluation of the surface properties of the parts is a result of a specific technological process depending on specific operational conditions of the surface in operation. This surface rating is frequently referred to as surface integrity. According to Dias et al. (2016) and Barényi et al. (2019), the concept of surface integrity can be defined as all properties of a functional surface, which have direct impact on its performance under operation and result from technological methods used for its manufacturing; these are also reflected in the quality of the machined surface manufactured components. The most frequently evaluated surface integrity parameters include microgeometry (surface structure); surface hardening layer after machining; and structural changes in coating (Junki et al., 2018; Gong et al., 2018; Dobrocký and Kusmič, 2015; Barényi et al., 2019).

Surface represents a border separating objects or substances from each other. One can subdivide the surface into three groups (nominal, real and measured) (Bhushan, 2001).

Nominal surface (ideal surface) represents the intended surface without any surface irregularities. Its profile and dimensions are usually shown in a drawing. The nominal or ideal surface structure does not consider the intended surface roughness (Bhushan, 2001).

Real surface is the real shape of an object and actual boundary of an object. It differs from the nominal surface due to the surface-shaping processes taking place. Differences also come from the properties, composition and structure of the body material (Bhushan, 2001).

Measured surface is shown using a measuring device that obtains values by measuring the actual surface. The

real and measured surfaces differ, because no measuring method is capable of perfect interpretation of the actual surface (Bhushan, 2001).

Surface parameters are repeated or irregular deviations from the ideal surface and form a surface texture. Surface texture includes (a) roughness (nano-roughness and micro-roughness); (b) waviness (macro-roughness); (c) lay; and (d) flaws.

Nano-roughness and micro-roughness are shaped by fluctuations of short wavelengths on the surface, indicated by ridges (asperities) (local maxima) and valleys (local minima) of changeable amplitudes and distances. Their size can be described as large in contrast to the molecular dimensions (Bhushan, 2013). Within the roughness sampling length, nano-roughness and micro-roughness are considered to include traverse feed marks and other errors (Votava et al., 2020; Ohtsu, 1995; Miller et al., 2005). Amplitude parameters are considered to be the most important indicators for surface texture assessment. Measurements of vertical surface deviations are described herein (Machek, 2013).

Waviness is a surface irregularity formed by surface layers of longer wavelength; it can be a result of device deflection, vibration, heat treatment, and uneven pressure of the work tool on the material. Irregularities are associated with waviness, the length of which exceeds the roughness sampling length but does not exceed the waviness sampling length (Votava et al., 2020; Ohtsu, 1995; Miller et al., 2005).

Lay is determined by the main direction of the predominant surface pattern, which is usually defined by the manufacturing process (Poláková and Dostál, 2019; Ohtsu, 1995)

**Contact address:** Jozef Žarnovský, Slovak University of Agriculture in Nitra, Department of Quality and Engineering Technologies, Tr. Andreja Hlinku 2, 949 76 Nitra, Slovak Republic, e-mail: [jozef.zarnovsky@uniag.sk](mailto:jozef.zarnovsky@uniag.sk)

Flaws are unintentional, unexpected and undesirable surface texture errors. Furthermore, the surface may contain significant deviations from the nominal shape due to a very long wavelength, resulting in shape errors. They are generally not considered to be part of the surface (Ohtsu, 1995).

Acoustic emission (AE) is a promising and challenging subject of modern technology and science. It is defined as the generation of sound and ultrasound waves in materials subjected to deformation forces. At the time of fracture, cracking occurs with the release of stored stress energy. Due to microcracking, some of the stored energy is released in the form of elastic waves – acoustic emissions. As illustrated in Fig. 7, AE waves spread through an object and can be recorded by an AE sensor on the surface, which transforms the vibrations into electric signals (Ohtsu, 1995, Miller et al., 2005).

The propagation of fracture sound in materials was originally marked as AE because they are both acoustic and audible. It has been explained, on the basis of the elastodynamics, that AE waves may be synthesized as elastic waves due to dislocation movement. The latter part of the AE waveform is generally the result of the AE sensor resonance vibration (Junki et al., 2018; Gong et al., 2018; Dobrocký et al., 2019).

The volume and characteristics of generated AE waves are based on the source characteristics: initial significance; current state; local metallurgical structure; and current environments. There is a couple of factors which effect the propagation of the wave in the material. Surface waves are created by reflections that are caused by macro-discontinuities and micro-discontinuities. Grain boundaries, inclusion, etc. lead to reflection and diffraction. The anisotropic properties of the medium cause the wave to change its speed and disperse in different directions with different speeds, showing the non-ideal elastic behaviour of the medium (Ohtsu, 1995; Miller et al., 2005).

The paper aims to show the diversity of acoustic emission utilization and possibilities of its use in practice. A new method of surface roughness measurement using acoustic emission is proposed and AE surface scanning procedure was designed. This procedure was subsequently tested using the surfaces of various types of materials.

## Material and methods

Three samples made of different materials were selected to demonstrate the ability to measure surface texture roughness using the designed method. The surfaces were subjected to the same surface treatment (roughness  $Ra = 1.6\text{--}3.2\ \mu\text{m}$ ) and measured under the identical conditions (Tulka, 2005). Each sample was marked with a combination of letter and number for simplification:

- A2 – Steel EN 54SiCr6 hardened in water, austenitized at 850 °C for 20 minutes (Fig. 1);
- A3 – Spheroidal graphite cast iron without heat treatment;
- B5 – Abrasion resistant austenitic manganese steel (EN X53CrMnNiN21 9), especially resistant to dynamic abrasive wear (so-called 13% Mn “HADFELD steel”).



Fig. 1 Measured samples

An AE Xedo analyser manufactured by Dakel was used for the purposes of measuring the acoustic signal. Amount of released energy during the measurements was recorded utilizing an IDK 09 sensor produced by Dakel; this sensor transferred the released energy to the acoustic signal. Recorded signal was then sent to Xedo analyser and subsequently to PC with DaeShow software, by means of which the measurement plots were created.

Diamond tip was used to produce acoustic signals. Gauge for the tip was tailored specifically to order and was made of stainless steel. A diamond tip with a diameter of approx.  $0.75\ \mu\text{m}$ , with an angle of  $60^\circ$ , was embedded to a stainless steel cylinder and fastened with silver solder (Fig. 2).

For accurate measuring, optimal conditions were provided by isolating the ambient conditions from ambient noise in order not to distort the measurement results. An IDK-09 sensor was attached to each sample using a plastic clamp (a special binding medium was added between the meter and the sensor). Several measurements were performed before the measurement. Pen tests were conducted to tune ambient noise, which would distort the entire measurement. DaeShow software was set up to provide the clearest results with almost no noise, following the Pen test.

The distance was measured simultaneously in the x-axis and y-axis in the sample. The sample was supported with an anti-vibration pad to prevent the propagation of vibrations from the surroundings.



**Fig. 2** Diamond tipped gauge used for surface roughness measurement

The measurement record was started when the gauge diamond tip was placed on the sample surface and pulled along the indicated path. The track length was 50 mm. Recording stopped at the end of the track. The measurement was repeated five times and then continued on the y-axis.

### Results and discussion

The acoustic surface response of selected materials was measured. For this purpose, a special tool equipped with a diamond tip and a piezoelectric sensor connected to the evaluation device was produced. Samples of three types of material were tested, all with surface roughness in the range  $R_a$  1.6–3.2  $\mu\text{m}$ . The following materials were investigated: steel EN 54SiCr6; spheroidal graphite cast iron without heat treatment; and steel EN X53CrMnNiN21 9, resistant to abrasion. Diamond specimen cross-sections were measured in samples in both the x-axis and y-axis.

Following graphs show data on the observed sample surfaces obtained by means of IDK-09 sensor fixed on the gauge. On the basis of the obtained results, it is clear that the values measured by AE method differ significantly in various materials.

In relation to testing of EN 54SiCr6 hard steel, a large difference in acoustic response was observed between the x and y measurements. This was due to the directionality of the roughness of the surface created by the defending tool. The recording was performed in the direction and perpendicular direction of the tool track. In the x-axis direction, one can see a regular mark of the instrument. On the y-axis, the track is irregular, which is caused by the gauge moving along the track (Figs. 3 and 4).

The surface analysis of a spheroidal graphite cast iron material shows a similar signal in the AE record in both measured directions. However, its course was influenced by the graphite contained in the alloy and the presence of graphite in the material affected the recording. After the measurement, there remained a visible trace in the material (Figs. 5 and 6). Moreover, record of the cast iron was distorted despite using less sensitive sensor. The

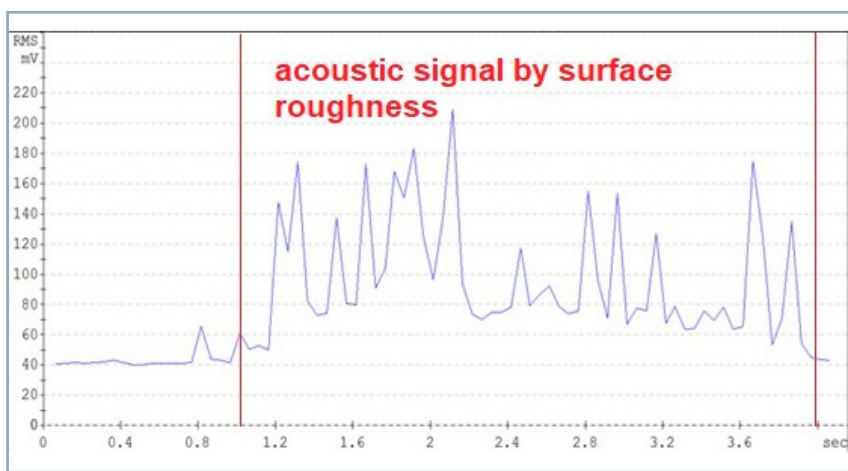


**Fig. 3** Sample A2 measured using IDK-09 sensor on the x-axis

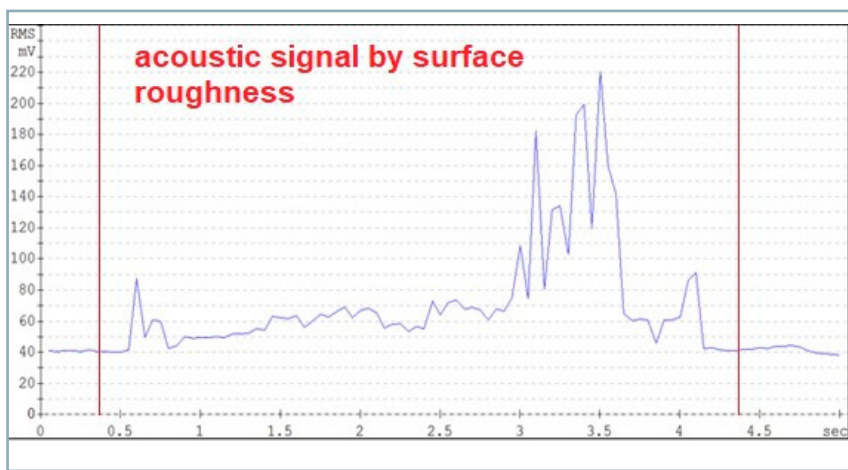


**Fig. 4** Sample A2 measured using IDK-09 sensor on the y-axis

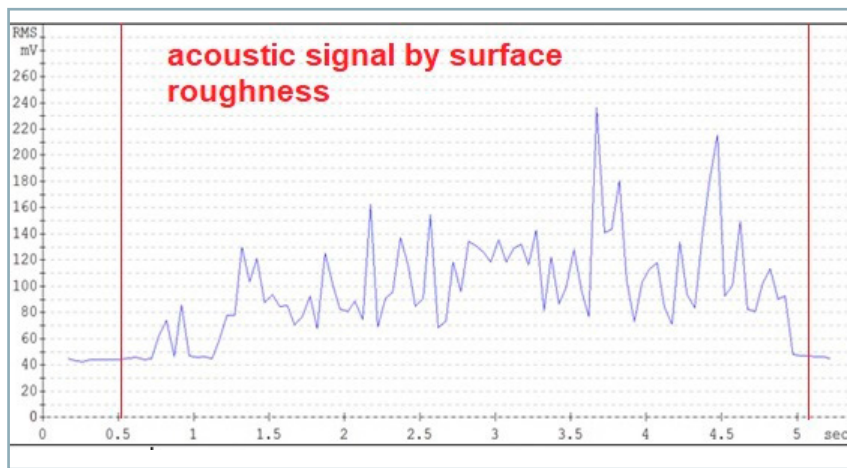


**Fig. 5** Sample A3 measured using IDK-09 sensor on the x-axis

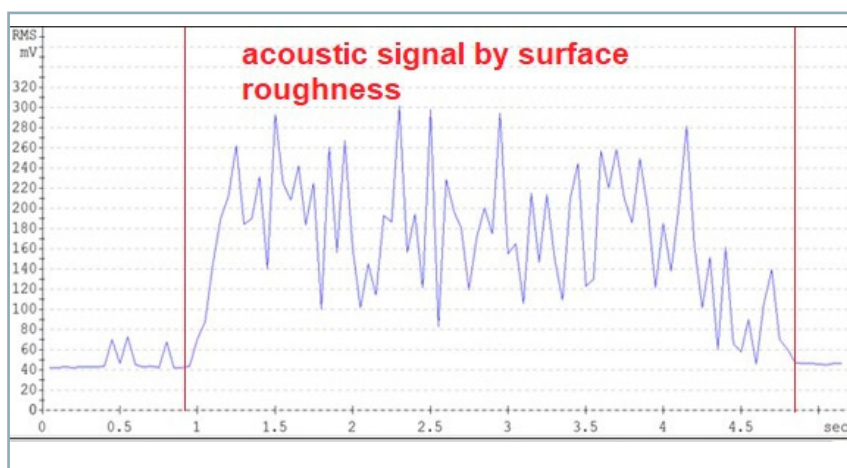


**Fig. 6** Sample A3 measured using IDK-09 sensor on the y-axis

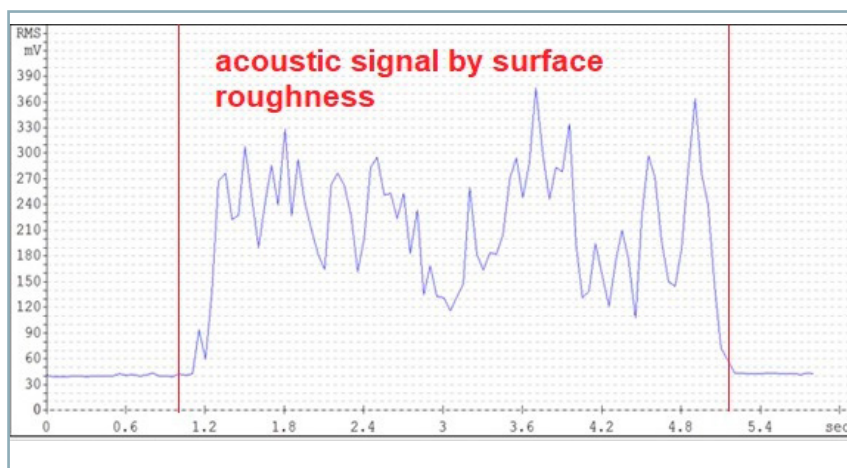


**Fig. 7** Sample B5 measured using IDK-09 sensor on the x-axis

diamond tip did not copy the surface, indicating that it is an inappropriate method for cast iron roughness measurements. The issue can be probably solved by using a diamond tip with a larger angle.

The last observed material was abrasion-resistant steel EN X53CrMnNiN21 9. The emission of acoustic waves is noticeable in both transverse and longitudinal directions with similar RMS values. It showed a suitable signal in regard to the measured voltage level on the sensor, as well as the shape, in both directions. This might have been caused by the surface finish of the material, which was performed by diamond grinding. This signal can be further processed and evaluated.

It is thus evident from the experimental results that hard materials with less rough surface are the most suitable materials for surface analysis using the AE method. Considering the softer materials and alloys, it is advisable to adjust the measuring diamond tip to avoid damaging the sample and prevent the influences on the measurement at the same time.

For the purposes of the experiment presented, a diamond cone with an angle of  $60^\circ$  was selected to measure the surface roughness. Utilization of this apex angle on hard materials is considered appropriate, since the tip traces the surface more precisely and provides a more accurate picture of the surface. However, for surfaces with lower hardness, a diamond tip with a greater apex angle of  $90^\circ$  would be more efficient. A larger apex angle should prevent the formation of a deep trace on the material surface and distorting the measurement results. In order to achieve the accurate results, gauge tip is made of diamond, because it shows high durability and also ensures low abrasion wear on surfaces with higher hardness. In the case of measuring the materials with lower hardness, it is also possible to use a cheaper alternative in the form of hardened steel.

The surface roughness  $R_a$  of specimens ranged from  $1.6$  to  $3.2 \mu\text{m}$ . However, the voltage generated on the membrane differed considerably in observed materials. These deviations were caused by the hardness and

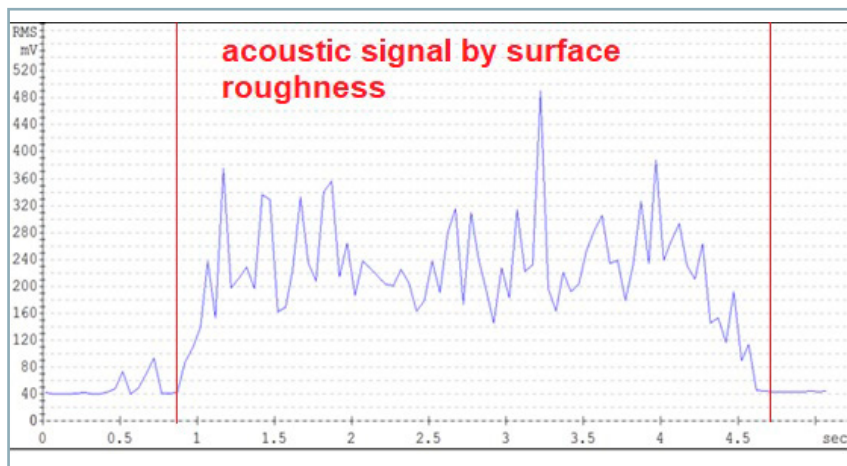


**Fig. 8** Sample B5 measured using IDK-09 sensor on the y-axis

structure of the material. For example, the difference of the values in the particular axes is best seen in the A3 sample (spheroidal graphite cast iron) where the voltage is at 130 mV on the y-axis and at approx. 230 mV on the x-axis.

### Conclusion

The aim of this work was to investigate the suitability of the acoustic emission method for surface roughness measurement. The acoustic surface response of selected materials was observed. Diamond cone with apex angle 60° was selected for the surface roughness measurement; utilization of this angle on hard materials is considered appropriate, because the tip follows the surface more accurately and provides a more accurate surface description. For surfaces with lower hardness, usage of a diamond tip with apex angle of at least 90° would be more effective. A larger apex angle should prevent the formation of deep traces on the material surface and distorting the measurement results. For accurate results, the tip of the gauge uses a diamond that exhibits high durability and also ensures low wear on surfaces with higher hardness. In the case of materials with lower hardness, it is also possible to use a cheaper alternative in the form of hardened steel.

Surface roughness  $R_a$  ranged from 1.6 to 3.2  $\mu\text{m}$ . However, the stress generated on the diaphragm varied widely between materials. These variations were a result of differences in the hardness and structure of materials, e.g. the difference in values

in specific axes can be best seen in sample A3 (spheroidal graphite cast iron), in which the y-axis showed a voltage of 130 mV and the x-axis approx. 230 mV.

This method is less suitable for hard materials with a surface roughness reaching  $R_a = 3.2 \mu\text{m}$ . Furthermore, the measurements presented were greatly influenced by the directionality of the surface structure.

### Acknowledgements

The research has been supported by the project IP 018/2019: Use of inorganic corrosion coatings for heterogeneous weldments protection; financed by IGA FA MENDELU.

### References

- BARÉNYI, I. – MAJERÍK, J. – POKORNÝ, Z. – SEDLÁK, J. – BEZECNÝ, J. – DOBROCKÝ, D. – JAROŠ, A. – ECKERT, M. – JAMBOR, J. – KUSENDA, R. 2019 Material and technological investigation of machined surfaces of the OCHN3MFA steel. In *Kovové Materiály*, vol. 57, no. 2, pp. 131–142.
- BHUSHAN, B. 2001. Chapter 2. Surface Roughness Analysis and Measurement Techniques, In *BHUSHAN, B. Modern Tribology Handbook*. New York : CRC Press, pp. 77. ISBN 0849384036.
- BHUSHAN, B. 2013. Principles and Application of Tribology. John Wiley & Sons, Ltd., 1006 pp. ISBN 978-1119944546.
- DIAS, T. – PAULO, N. – QUEIJO, L. – LOPES, H. R. – CÉSAR, M. B. – RIBEIRO, J. E. 2016. Milling parameters optimization for surface quality. In *CONTROLO 2016. Portuguese Conference in Automatic Control*. Springer International Publishing Switzerland 2017, pp. 583–592. ISBN 9783319436715.

DOBROCKÝ, D. – KUSMIČ, D. 2015. The influence of the nitride layer depth in the root of V-notch to notch toughness of 30CRMOV9 steel. In *Solid State Phenomena*, vol. 258, pp. 242–245.

GONG, Y. – XU, J. – BUCHANAN, R. C. 2018. Surface roughness: A review of its measurement at micro-/nano-scale. In *Physical Sciences Reviews*, vol. 3, no. 1, pp. 1–10.

JUNKI, J. – THOULESS, M. D. – BARBER, J. R. 2018. Effect of roughness on the adhesive tractions between contacting bodies. In *Journal of the Mechanics and Physics of Solids*, vol. 118, pp. 365–373.

OHTSU, M. 1995. The history and development of acoustic emission in concrete engineering. In *Concrete Library JSCE*, no. 25, pp. 121–134.

MACHEK, V. 2013. Metal Materials 1: Structure of Metal Materials. 1st ed. Praha : České vysoké učení technické, 168 pp. ISBN 9788001052488. (In Czech: *Kovové materiály 1: Struktury kovových materiálů*).

MILLER, R. – HILL, E. – MOORE, P. 2005. *Nondestructive Testing Handbook: Acoustic Emission Testing:5*. Columbus : American Society for Nondestructive, 603 pp. ISBN 9780931403026.

POLÁKOVÁ, N. – DOSTÁL, P. 2019. Titanium and stainless steel MIG LSC welding. In *Acta Technologica Agriculturae*, vol. 22, no. 2, pp. 56–59.

TULKA, J. 2005. *Surface Treatment of Materials*. 1<sup>st</sup> ed. Brno : VUT, Fakulta chemická, 136 pp. ISBN 8021430621. (In Czech: *Povrchové úpravy materiálů*).

VOTAVA, J. – KUMBÁR, V. – POLCAR, A. – FAJMAN, M. 2020. Change of mechanical properties of zinc coating after heat treatment. In *Acta Technologica Agriculturae*, vol. 23, no. 1, pp. 7–11.

